NASA CR-112197

Study of the Technique of Stellar Occultation

by

P. B. Hays
M. E. Graves
R. G. Roble
A. N. Shah

prepared for

NATIONAL AERONAUTICS AND SPACE ADMINISTRATION
Contract No. NAS 1 9958

November 30, 1973

THE UNIVERSITY OF MICHIGAN
High Altitude Engineering Laboratory
Departments of Aerospace Engineering
Atmospheric & Oceanic Science
Ann Arbor, Michigan

NASA CR-112197

STUDY OF THE TECHNIQUE OF STELLAR OCCULTATION

By P. B. Hays, M. E. Graves, R. G. Roble and A. N. Shah

Prepared under Contract No. NAS 1 9958 by
The University of Michigan
High Altitude Engineering Laboratory
Departments of Aerospace Engineering
Atmospheric & Oceanic Science
Ann Arbor, Michigan 48105

for

NATIONAL AERONAUTICS AND SPACE ADMINISTRATION

November 30, 1973

TABLE OF CONTENTS

Figure Captions

Figure 1. Oxygen and ozone cross sections with OAO filters transmission functions shown.

Figure 2. Schematic view of occultation.

Figure 3. Typical occultation row data.

Figure 4. Geometry of occutation for any stellar object.

Figure Captions Appendix IV.

Figure 1. Tangent ray height error as a function of satellite height error and altitude.

Figure 2. Tangent ray height error as a function of satellite latitude error.

Figure 3. Tangent point longitude error as a function of satellite latitude error.

Figure 4. Satellite tangent ray height error as a function of satellite longitude error.

1. Introduction

This report describes the results of a study of the stellar occultation technique for measuring the composition of the atmosphere. The work reported here was supported by NASA Contract NAS 1 9958.

The stellar occultation technique is based upon classical absorption spectroscopy, utilizing spacecraft-borne photometers as the detector and a star as the light source. During occultation the ultraviolet stellar spectrum of the star shows absorption features which are uniquely related to various atmospheric constituents. In particular, the spectral region between 1200Å and 2000Å is related to absorption by molecular oxygen and the region between 2000Å and 3500Å is related primarily to absorption by ozone. This is illustrated in Figure 1 where the photo absorption cross sections of both molecular oxygen and ozone are shown.

The intensity of starlight was monitored during the occultation using the Wisconsin stellar ultraviolet photometers aboard the Orbiting Astonomical Observatory (OAO-A2). A schematic diagram of an occultation is shown in Figure 2 where the change in intensity at a given wavelength is illustrated. The vertical projection of the attenuation region is typically 60 km. deep for molecular oxygen and 30 km. deep for ozone.

Intensity profiles obtained during various occultations were analyzed by first determining the tangential column density of the absorbing gases, and then Abel inverting the column densities to obtain the number density profile. Errors are associated with each step in the inversion scheme and have been considered as an integral part of this study.

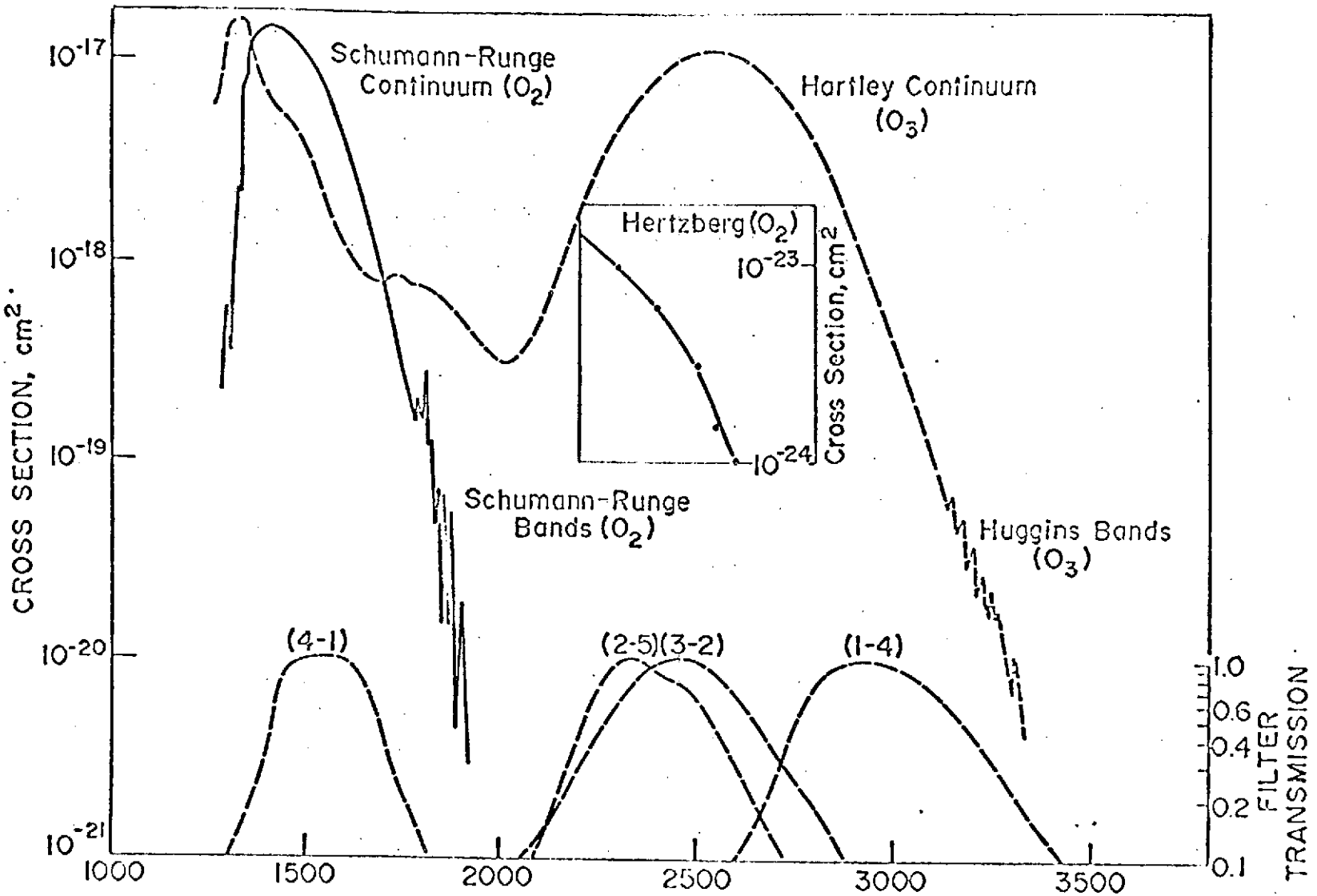

Figure 1. Oxygen and ozone cross sections with OAO filters transmission functions shown.

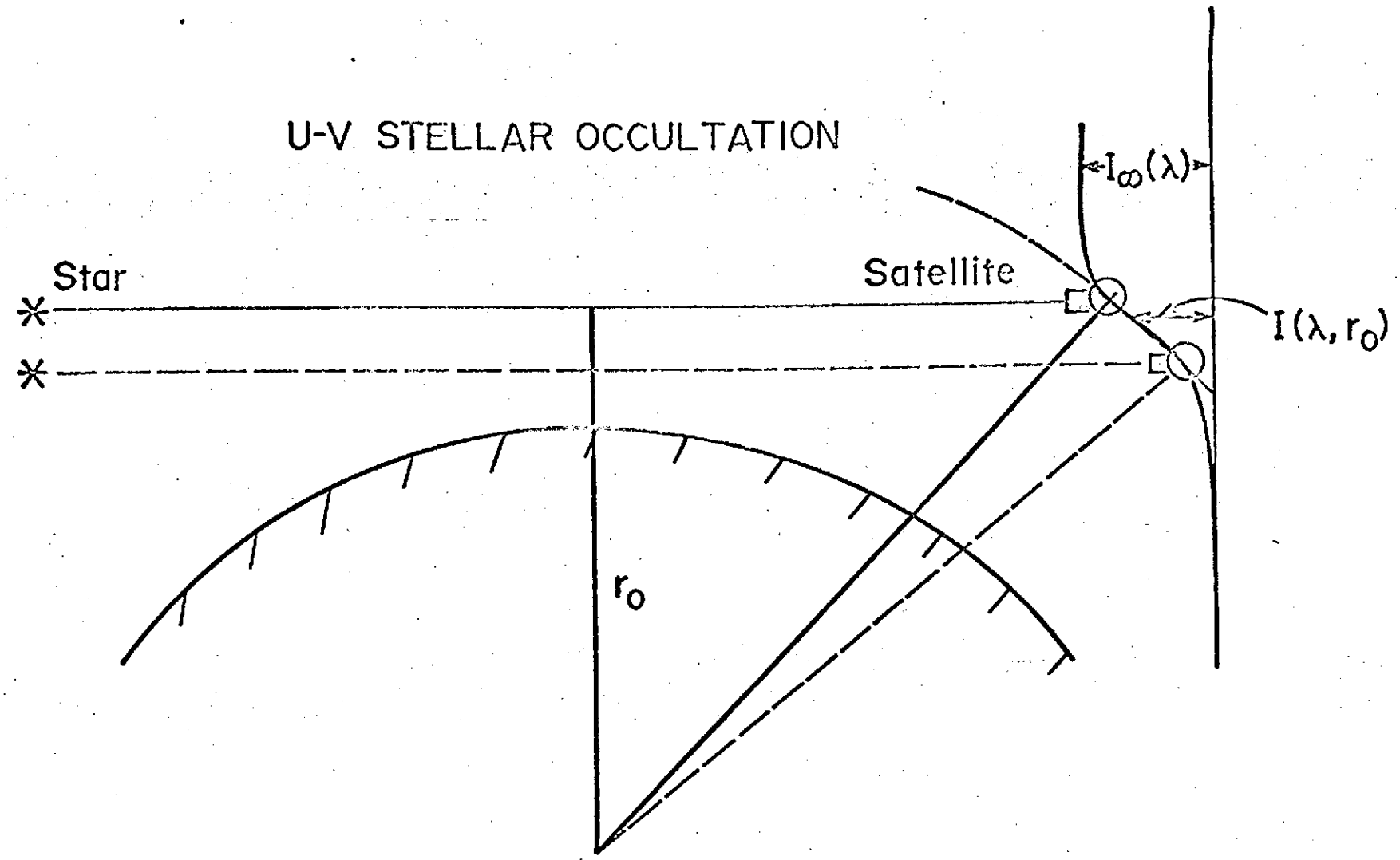

Figure 2. Schematic view of occultation.

Most of the work carried out under this contract has been published in the open literature, thus, we include these papers in this report where appropriate. A general description of this study and the results were published by Hays et al. (1972) and is included as Appendix I of this report.

2. Data Procurement

The data used in this study were obtained through the courtesy of the O. A. O. Wisconsin Experimenters and N. A. S. A. Goddard Space Flight Center. The principle difficulty associated with the data procurement centered on obtaining intensity information at high rates. It was possible to sample the stellar photometer accumulator at high frequency, but only bits 7 through 14 of this register were available in this mode of operation. During this procedure the photometers continued to accumulate for 128 periods of 0.54080 seconds. Upon completion of this process the register was locked until a new command was received, at which time the cycle was repeated. Unfortunately, a finite period of time was required for the new command to be sent and a gap appears in the data every 128 samples. This caused many occultations to be rejected due to re-set blanks appearing in the middle of the attenuation period.

A typical data record is shown in Figure 3, we note that the bottom of each record corresponds to 64 accumulated counts and the top to 16, 384 accumulated counts. The overflow within this sub-set is obvious. The data analyses utilized differences between individual samples and a smooth interpolation to determine the overflow and count accumulated during a sample period. The record labeled Channel 44 in Figure 3 is from the 1500Å filter used to measure molecular oxygen.

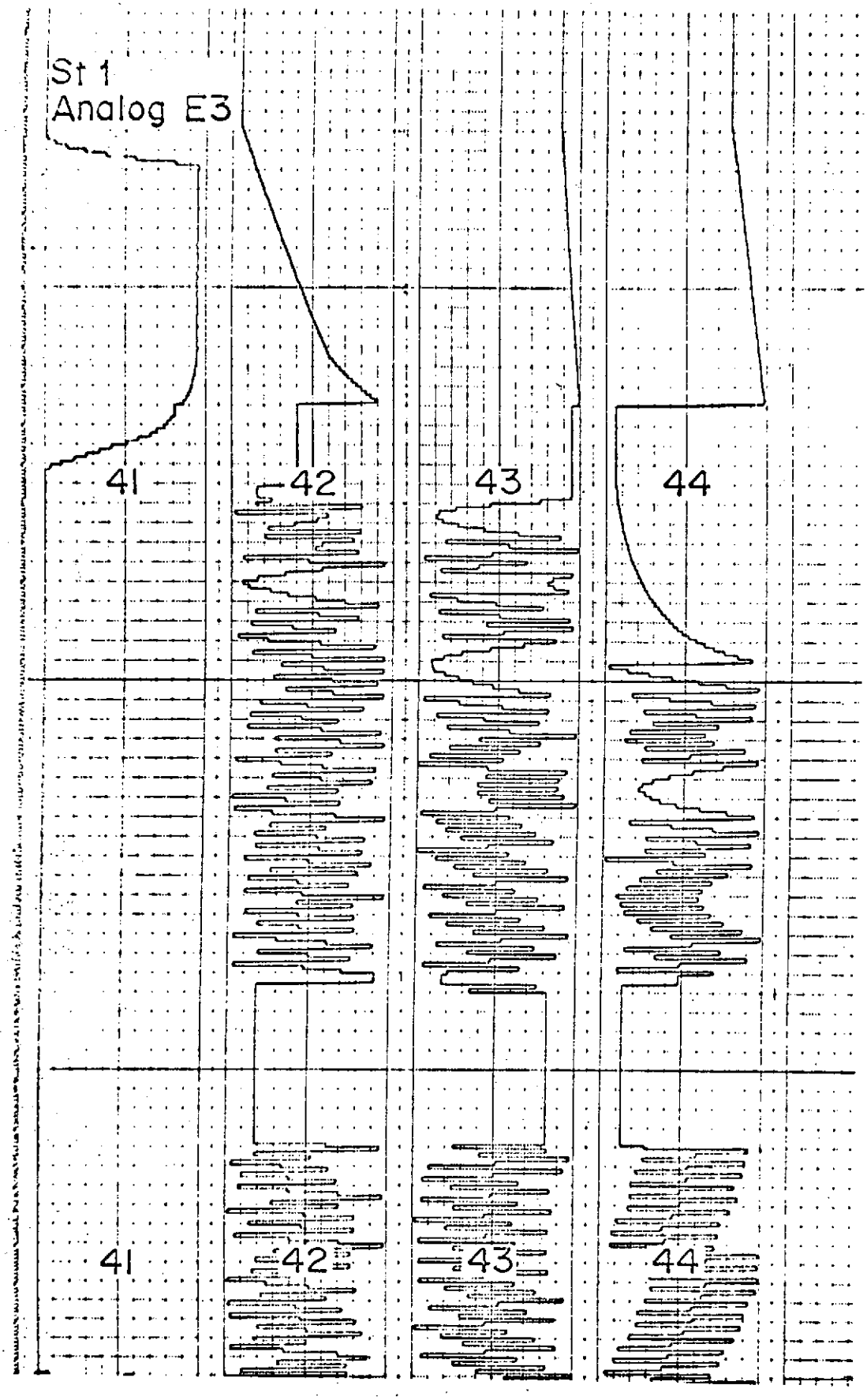

Figure 3. Typical occultation row data.

The stellar photometers have broad band filters which typically cover a 200Å wide region in the spectrum. The relative transmission of these filters are shown at the bottom of Figure 1. Due to the broad spectral band of these filters it was necessary to measure the spectrum of all stars used in the study. This was done prior to the occultation using the O. A. O. spectrometer.

In addition to intensity and spectral information it was necessary to determine the altitude of the tangent ray. This requires an accurate knowledge of the spacecraft positions as well as the coordinates of the star. We acknowledge the considerable effort of the NASA Goddard Space Flight Center who carefully re-checked the satellite ephemeris in order to achieve the accuracy required for our study.

3. Tangent Ray Geometry

Throughout an occultation period, the tangent ray point follows a curved path above the surface of the earth. The coordinates used to describe this path are shown in Figure 4. In this system, the x-axis points toward the First Point of Aries, the y-axis is also in the equatorial plane pointing 90° east of Aries, and the z-axis points toward the North Pole. The time of scan enters into the coordinate system through the Greenwich hour angle of the x-axis, λ_g.

To obtain the height of the tangent point, the angle β at the spacecraft between rays to the star and to the center of the earth must be evaluated in terms of the direction numbers of the star,

$$l = \cos\alpha \cos\delta$$

$$m = \sin\alpha \cos\delta$$

$$n = \sin\delta$$

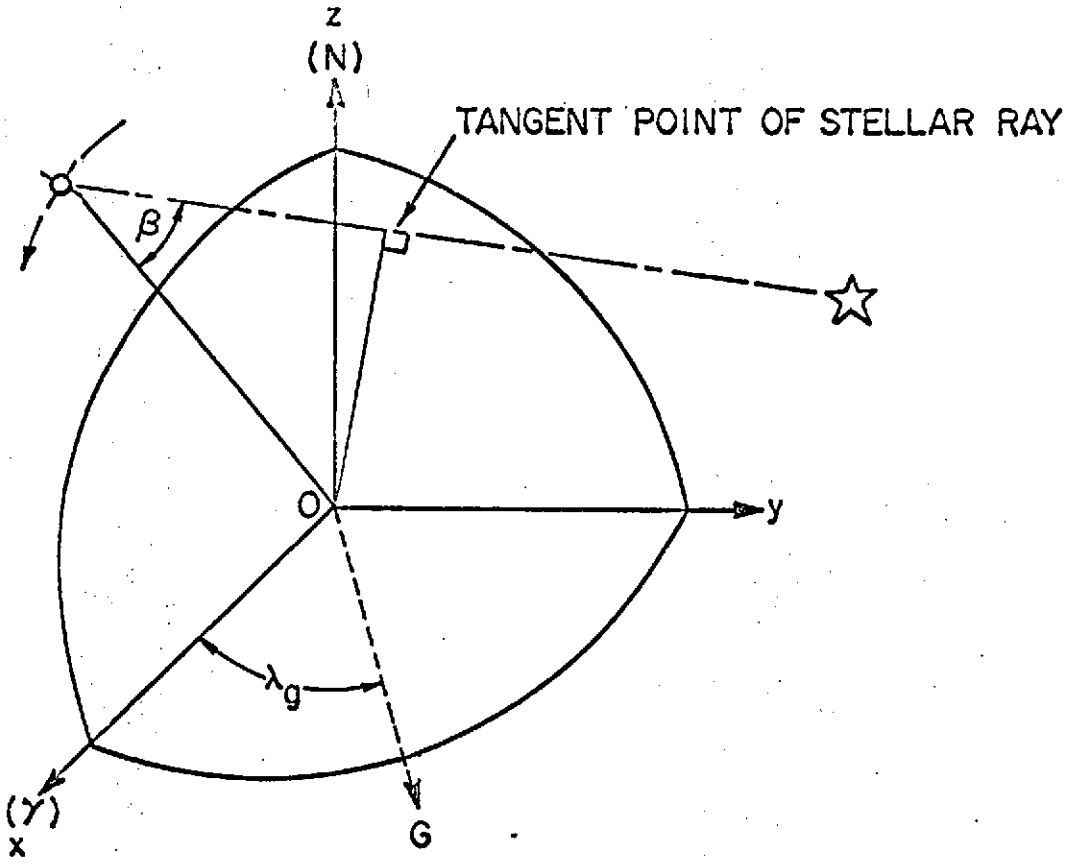

Figure 4. Geometry of occultation for any stellar object.

and the direction cosines of the satellite position,

$$a = \cos \lambda_s \cos \phi_s \cos \lambda_g - \sin \lambda_s \cos \phi_s \sin \lambda_g$$

$$b = \sin \lambda_s \cos \phi_s \cos \lambda_g + \cos \lambda_s \cos \phi_s \sin \lambda_g$$

$$c = \sin \phi_s$$

where α = right ascension

δ = declination

λ = longitude

ϕ = latitude

Subscripts s refers to the spacecraft and subscript o will refer to the tangent ray point. Then utilizing the above quantities,

$$r_o = r_s \sin \beta \tag{1}$$

where $\beta = \pi - \cos^{-1} [\, al+bm+cn \,]$,

$$\phi_o = \tan^{-1} \left[z_o (x_o^2 + y_o^2)^{-\frac{1}{2}} \right] , \tag{2}$$

$$\lambda_o = \cos^{-1} \left[x_o (x_o^2 + y_o^2)^{-\frac{1}{2}} \right] - \lambda_g . \tag{3}$$

If $y_o > o$, $o \leq \lambda_o \leq 180$; if $y_o < o$, $180 \leq \lambda_o \leq 360$.

The additional formulae needed to evaluate Equations 1-3 are

$$x_o = r_s (a+l \cos \beta)$$

$$y_o = r_s (b+m \cos \beta)$$

$$z_o = r_s (c+n \cos \beta)$$

Stellar refraction is neglected in our analysis due to the low index of refraction at the altitudes considered in this study.

4. Data Processing and Error Analysis

The technique of data processing and the analysis of resulting errors has been reported during this study by Roble and Hays (1972). This paper is included as Appendix II and is a complete description of the

results of this study. A complete description of the computer routine used to evaluate the occultation results obtained in this study is included as Appendix III of this report. The reader is referred to these detailed appendices for further information on the results of our study. A separate discussion of influence of orbital errors is included in Appendix IV.

5. Data Analysis

A very large number of scans have been reduced in the course of this contract period. Table I summarizes these results and includes all orbits which have yielded at least a partial result e.g., a molecular oxygen profile or an ozone profile. To provide information on quality in the individual channels, the following code is used

c = processing completed

+ = resulting number density profile, $n(r_o)$, acceptable

- = $n(r_o)$ not acceptable

? = $n(r_o)$ questionable

Other information in the table refers to the starting time (GMT and local) of the scan, the location of the ray tangent point, the target star, and the nature of some of the difficulties. Starting times are only approximate, as they vary up to 20 seconds from channel to channel and they must be entered to the nearest half-second for acceptable accuracy in height of ray tangent point.

These results have been analyzed from the point of view of their geophysical information and are to be published in journals during the next few months. All papers are in press at this time. Detailed computer output containing tabular input data and results are available to the contracting agency on request, but are too lengthly to include in this report.

Table I

orbit	date	GMT hr	GMT min	local hr	local min	Long. (deg)	Lat. (deg)	star	ozone 2390Å	ozone 2460Å	O_2	remarks on data loss
5778	1/13/70	5	28	23	52	-84	48	γ Peg	-		+	O_3 filter
5779	1/13/70	7	8	23	51	-109	48	γ Peg	-		+	O_3 filter
8884	8/17/70	4	55	5	55	15	4	α Lup			+	O_3 reset
8898	8/18/70	4	19	5	51	23	9	β Lup	?	?	?	Height
8899	8/18/70	5	59	5	51	-2	9	β Lup	?	?		Height, O_2 enevenness
8913	8/19/70	5	22	5	54	8	11	β Lup			+	O_3 reset
8942	8/21/70	5	55	4	27	-22	24	τ Sco	+	-	?	O_3 data cutoff, O_2 reset
8943	8/21/70	7	35	4	23	-48	24	τ Sco			+	
8956	8/22/70	5	18	4	26	-14	24	τ Sco	+			O_2 reset
8957	8/22/70	6	58	4	22	-39	25	τ Sco	+	-	+	Height
8971	8/23/70	6	20	4	44	-24	27	δ Sco	+	+	-	O_2 reset
8985	8/24/70	5	45	4	13	-23	24	τ Sco		+	+	
8986	8/24/70	7	25	4	13	-48	24	τ Sco		+	+	
9000	8/25/70	6	47	5	17	-32	27	δ Sco	+	+	+	
9014	8/26/70	6	10	4	30	-25	26	δ Sco	+	+		
10795	12/28/70	2	31	21	55	-69	42	ι Her			+	ϵ Aur spectrum used
10796	12/28/70	4	12	22	12	-91	43	ι Her	-	-	-	ϵ Aur spectrum used Height
10902	1/4/71	13	29	22	38	-223	-16	α And	+		+	
11795	3/7/71	15	59	0	33	128	-34	δ Ori	+		+	
12178	4/3/71	6	8	22	33	-114	36	ι Ori		+	+	
14579	9/17/71	5	42	2	51	-43	26	Θ Oph	+		-	O_2 reset
14580	9/17/71	6	22	1	50	-68	26	Θ Oph	?		+	O_3 values high in bulge

In addition, orbits 13161, 13187, 13189, and 13195 of June 10 and June 12, 1971, provided high quality data which are awaiting accurate satellite position reports.

6. Geophysical Results

Interpretations of the results obtained under this contract have been presented in papers published in the open literature. Molecular oxygen results were compared with theory and previous measurements by Hays and Roble (1972b). Ozone results were discussed by Hays and Roble (1972c), Roble and Hays (1972b) and Roble and Hays (1972c). These papers are included as Appendices V through VIII.

7. Summary of Study

The present study of the stellar occultation technique of recovering atmospheric composition has led to the following conclusions:

a) Any constituent which causes significant absorption in a stellar spectrum can be monitored by using the ultraviolet occultation technique.

b) The error associated with the inversion of occultation data limits the altitude region for which results of high quality can be obtained. In most cases the high quality data results from regions where the intensity lies between 10% to 90% of the unattenuated flux. Finite difference errors are responsible for limiting the structural detail which can be recovered. Orbital errors are serious and are reflected in the altitude scale of the recovered density profiles.

c) Serious geophysical studies can be carried out using as principal data the density profiles of molecular oxygen and ozone obtained from stellar occultation. The following major geophysical features have been identified during this study:

(1) Molecular oxygen shows a strong solar cycle variation in the lower thermosphere. This probably results from changes in

the constant pressure level surfaces at the base of the thermosphere.

(2) Molecular oxygen in equatorial regions shows strong magnetic storm variations due to large scale dynamic motions resulting from polar region heating.

(3) Ozone in the mesopause region is controlled by wet chemistry and supports modern photochemical theories.

APPENDIX I.

Terrestrial Atmospheric Composition from Stellar Occultations

Reprinted from
19 May 1972, volume 176, pages 793-794

SCIENCE

Terrestrial Atmospheric Composition from Stellar Occultations

Abstract. *Stellar ultraviolet light transmitted through the earth's upper atmosphere is strongly absorbed by ozone and molecular oxygen. The stellar ultraviolet photometers aboard the Orbiting Astronomical Observatory (OAO-2) satellite have measured the intensity changes of several stars during occultation of the star by the earth's atmosphere. From the occultation data the nighttime vertical number density profiles of molecular oxygen at altitudes from 120 to 200 kilometers and of ozone at altitudes from 60 to 100 kilometers have been obtained.*

In the earth's upper atmosphere, stellar ultraviolet light is strongly absorbed in the Schumann-Runge continuum of O_2 and the Hartley continuum of O_3. By monitoring the intensity of ultraviolet starlight in these continuum regions from a satellite as the star is occulted by the earth's atmosphere, we are able to obtain information on the number density profile of O_2 in the lower thermosphere and O_3 in the upper mesophere (*1*, *2*). In this report we describe the technique used to obtain the number density profiles from stellar occultation measurements. The data were obtained by the University of Wisconsin stellar photometers aboard the Orbiting Astronomical Observatory (OAO-2) satellite. We discuss here the inversion process and also show the O_2 and O_3 distributions determined from a typical occultation scan.

In the occultation technique classical absorption spectroscopy is used to determine the number density profile of the absorbing species in the upper atmosphere. The star is the source of ultraviolet light, the OAO stellar photometers are the detectors, and the atmosphere between them is the absorption cell. During the occultation process, the ultraviolet light is selectively absorbed in spectral regions for which O_2 and O_3 have large absorption cross sections. The intensity of the transmitted ultraviolet light is related to the number density along a tangential column of the absorbing species (N_i) by Beer's law

$$I(\lambda,r_0) = I_\infty(\lambda) \exp\left[-\sum_i \sigma_i(\lambda) \cdot N_i(r_0)\right] \quad (1)$$

where $I_\infty(\lambda)$ is the unattenuated intensity above the atmosphere of the star at wavelength λ, $\sigma_i(\lambda)$ is the absorption cross section of the ith absorbing species, and $N_i(r_0)$ is the tangential column number density of the ith absorbing species at a tangent ray height r_0. The star's spectrum is measured above the atmosphere by the OAO ultraviolet spectrometer. By also knowing the absorption cross section, one can relate $N_i(r_0)$ to the intensity of the transmitted ultraviolet light. In practice, Eq. 1 must be integrated with respect to wavelength because of the finite passband of the ultraviolet filter. The best

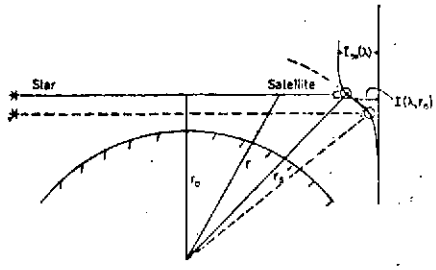

Fig. 1. Geometry of ultraviolet stellar occultation.

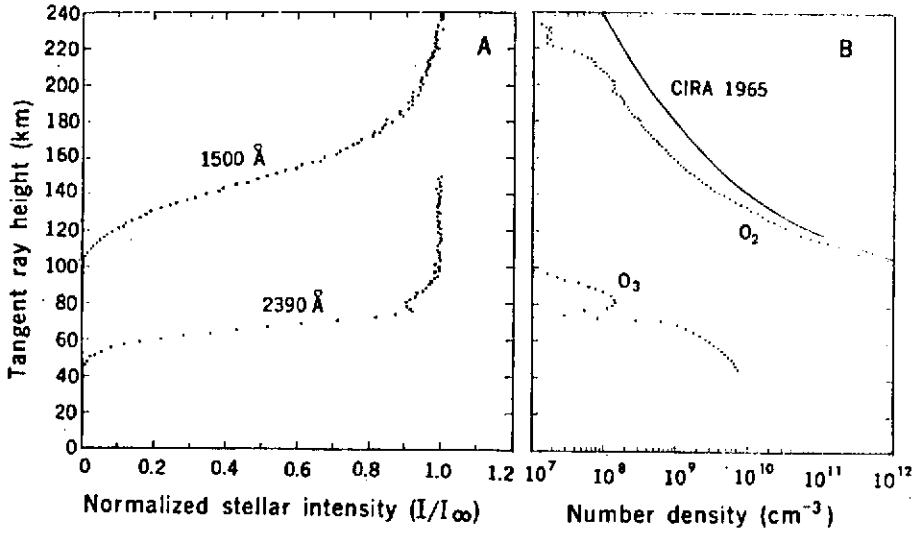

Fig. 2. (A) Normalized intensity of a star as a function of the tangent ray height during occultation of the star by the earth. The curves correspond to the intensity measured in the 1500-Å and 2390-Å channels of the University of Wisconsin stellar photometers aboard the OAO-2 satellite [22 August 1970, 04 hours 22 minutes (local time), 25°N, 39°E]. (B) Number densities of O_2 and O_3 as a function of tangent ray height determined from the occultation measurements. The solid line is the O_2 number density from the CIRA 1965 model atmosphere.

results are thus obtained when a single species dominates the absorption process, and the OAO filters were, therefore, selected accordingly.

Once $N_i(r_0)$ is known, it is a simple matter to invert the data and obtain the vertical number density profile of the absorbing species at the occultation tangent point. A simple geometrical argument (Fig. 1) shows that $N_i(r_0)$ along the ray path for a spherically stratified atmosphere can be written as

$$N_i(r_0) = 2\int_{r_0}^{\infty} \frac{n_i(r)\, r\, dr}{(r^2 - r_0^2)^{1/2}} \qquad (2)$$

where $n_i(r)$ is the number density of the ith absorbing species at radius r. Equation 2, the Abel integral equation (*1*, *2*), is easily inverted to give the number density of the absorbing species at a tangent ray height r

$$n_i(r) = \frac{d}{dr}\left[-\frac{1}{\pi}\int_r^{\infty} \frac{N_i(r_0)\, dr_0}{(r_0^2 - r^2)^{1/2}}\right] \qquad (3)$$

Thus, the stellar occultation technique can be used to obtain the vertical density profile of any absorbing atmospheric species which can be spectrally isolated.

Hays and Roble (*2*) have calculated the tangential ultraviolet transmission of the earth's upper atmosphere. Their results show that both the strong atmospheric absorption of O_2 in the Schumann-Runge continuum near 1500 Å and the strong atmospheric absorption of O_3 in the Hartley continuum near 2500 Å occur in spectrally isolated regions in which the stellar ultraviolet absorption is primarily due to a single species. The absorption cross sections of O_2 and O_3 at these wavelengths have a peak around 10^{-17} cm^2. Therefore, we are able to determine the distribution of these species near altitudes at which N_i is approximately 10^{17} cm^{-2}. If a spectral region away from the peak cross section is utilized, one is able to observe higher tangential column number densities or, equivalently, to measure the number density at lower altitudes within the atmosphere. The ultraviolet light in the wavelength interval from 1400 to 1600 Å is absorbed primarily by O_2 at altitudes from 130 to 230 km. In the wavelength interval from 2400 to 2600 Å, the ultraviolet light is absorbed primarily by O_3 at altitudes from 60 to 100 km (*2*).

The normalized intensity data obtained during one of the many occultations are shown in Fig. 2A for two stellar photometers having filters centered at 1500 and 2390 Å. The normalized intensity is obtained as a function of time; however, by knowing the star's position and the orbital elements of the satellite, we are able to relate time to the tangent ray height of the occulting star. Because of high-altitude absorption, the normalized intensity in the O_2 channel at 1500 Å decays first. Then the intensity in the 2390-Å channel decays rapidly at altitudes where O_3 absorption becomes important. The excellent quality of the data obtained by the OAO-2 stellar photometers allows determination of detailed structure. The data in the 1500-Å channel were inverted, and the results are shown in Fig. 2B where the O_2 number density profile is shown as a function of height. For comparison, the O_2 profile of the Committee on Space Research (COSPAR) CIRA 1965 (*3*) model atmosphere is shown also. These data are only a sample of the approximately 20 stellar occultation scans that have been reduced thus far, but they illustrate the quality of the data obtained from the occultation measurements.

Most of the O_3 scans obtained with the 2390-Å and 2460-Å filters aboard the OAO-2 satellite have a normalized intensity scan similar to the one shown in Fig. 2A. The intensity of the occulting star decreases as the starlight penetrates into the atmosphere until a slight increase in the intensity curve occurs at a tangent ray height near 70 km. These data, when inverted, give the number density profile of O_3 shown in Fig. 2B. The structure in the measured intensity curve is caused by a bulge in the nighttime O_3 number density profile, with the peak occurring near 82 km and a minimum near 75 km for this particular scan. The stellar occultation measurements clearly define the structure of the nighttime O_3 profile at high altitudes where no previous measurements had been made.

The occultation technique has also been used with the sun as the light source. The measurements, however, are restricted to sunrise and sunset, and a general review of the subject has been given by Link (*4*).

P. B. Hays
University of Michigan, Ann Arbor 48105

R. G. Roble
National Center for Atmospheric Research, Boulder, Colorado 80302

A. N. Shah
University of Michigan, Ann Arbor

References and Notes

1. P. B. Hays and R. G. Roble, *Planet. Space Sci.* **16**, 1197 (1968).
2. ———, *J. Atmos. Sci.* **25**, 1141 (1968).
3. *COSPAR International Reference Atmosphere* (North-Holland, Amsterdam, 1965).
4. F. Link, *Eclipse Phenomena in Astronomy* (Springer-Verlag, New York, 1969).
5. The National Center for Atmospheric Research is sponsored by the National Science Foundation.

10 January 1972

APPENDIX II.

A Technique for Recovering the Vertical Number Density Profile of Atmospheric Gases from Planetary Occultation Data

Planet. Space Sci. 1972, Vol. 20, pp. 1727 to 1744. Pergamon Press. Printed in Northern Ireland

A TECHNIQUE FOR RECOVERING THE VERTICAL NUMBER DENSITY PROFILE OF ATMOSPHERIC GASES FROM PLANETARY OCCULTATION DATA

R. G. ROBLE
National Center for Atmospheric Research,* Boulder, Colorado 80302, U.S.A
and
P. B. HAYS
Department of Aerospace Engineering, University of Michigan,
Ann Arbor, Michigan 48104, U.S.A

(*Received* 29 *March* 1972)

Abstract—The occultation technique of determining the properties of the atmosphere using absorption spectroscopy is examined. The intensity of a star, in certain atmospheric absorption bands, is monitored by a satellite tracking the star during occultation by the Earth's atmosphere. The intensity data in certain wavelength intervals, where absorption is attributed to a single species, are related to the tangential column number density of the absorbing species through Beer's law. The equation for the tangential column number density is the Abel integral equation which is inverted to obtain the number density profile of the absorbing species at the occultation tangent ray point. Two numerical schemes for inverting the Abel integral equation for signals of low intensity with statistical noise superimposed are presented; one for determining the number density profile of atmospheric species that decrease exponentially with height, and the second for determining the profile of constituents having a more complex vertical structure, such as ozone. The accuracy of retrieving the number density distribution from planetary occultation data is examined. A theoretical analysis of the errors in determining the number density from occultation data of very low signal intensity is also presented. The errors in retrieving the number density profile are related to the intensity of the source, the number of data points per scan, and the degree of data smoothing required before inversion. As a specific example, calculations are made of the errors in retrieving the molecular oxygen and ozone number density profiles from occultation intensity data in the Schumann–Runge continuum of molecular oxygen at 1450 Å and the Hartley continuum of ozone at 2450 Å.

1. INTRODUCTION

Absorption spectroscopy is an important technique for determining the composition and number density profiles of constituents in the upper atmosphere (Watanabe, 1958; Hinteregger, 1962). Most of the measurements have been made from rockets monitoring the absorption of the solar u.v. flux in certain atmospheric bands (Johnson *et al.*, 1951; Bryam *et al.*, 1957; Kupperian *et al.*, 1959; Jursa *et al.*, 1963, 1965; Carver *et al.*, 1964, 1966; Weeks and Smith, 1968; Opal and Moos, 1969; Wildman *et al.*, 1969; Quessette, 1970; Brannon and Hoffman, 1971). Satellites have also been used to measure the intensity of certain u.v. sources (i.e., Sun, Moon, stars) during occultation of the source by the Earth's atmosphere (Fig. 1). The intensity data measured during occultation are then used to obtain information about the absorbing species in the upper atmosphere (Venkateswaran *et al.*, 1961; Rawcliffe *et al.*, 1963; Miller and Stewart, 1965; Thomas *et al.*, 1965; Fesenkov, 1967; Thomas and Norton, 1967; Norton and Warnock, 1968; Stewart and Wildman, 1969; Hinteregger and Hall, 1969; Lockey *et al.*, 1969; Link, 1969; Reid and Withbroe, 1970; May, 1971; Reid, 1971; Roble and Norton, 1972; Hays *et al.*, 1972).

Basically, the occultation technique is similar to the classical technique of absorption spectroscopy. The Sun, Moon, or a star are used as a source of light and the satellite

* The National Center for Atmospheric Research is sponsored by the National Science Foundation.

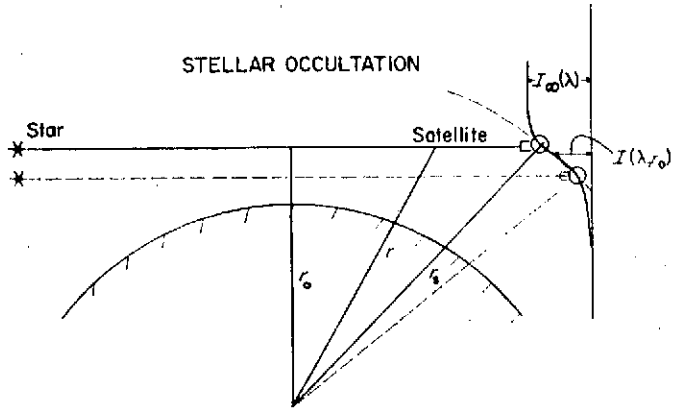

FIG. 1. GEOMETRY OF STELLAR OCCULTATION. $I_\infty(\lambda)$ IS THE INTENSITY OF THE UNATTENUATED STAR ABOVE THE ATMOSPHERE AND $I(\lambda, r_0)$ IS THE MEASURED INTENSITY OF THE STAR AT TANGENT RAY HEIGHT r_0.

photometers as a detector, with the atmosphere between acting as the absorption cell. As the satellite moves in its orbit, the source ultimately is occulted by the Earth. During the occultation process, the intervening atmosphere absorbs progressively more of the light due to the strong photo-absorption features of the atmospheric gases. The occultation intensity data can be related to the tangential column number density of the absorbing species if the absorption cross-sections are known. The equation for the tangential column number density of the absorbing species is the Abel integral equation which is easily inverted to give the number density profile at the occultation tangent point. The occultation technique works best for a point source, such as a star, where the vertical resolution at the tangent point is very sharp (Hays and Roble, 1968b). For a finite-size source, such as the Sun, the light rays emitted from the upper and lower limb can have tangent ray heights separated by about 26 km when observed from normal satellite altitudes. This complicates the problem of relating the transmitted solar intensity to the tangential column number density (May, 1971; Roble and Norton, 1972). However, once the tangential column number density is obtained, it again becomes easy to invert the Abel integral equation and obtain the local number density at the tangent ray point. For simplicity, we therefore assume that the light source is small, such as a star (Hays *et al.*, 1972) or a small portion of the solar disk (Hinteregger and Hall, 1969; Reid and Withbroe, 1970; Reid, 1971).

In the present paper, we describe a technique for retrieving the number density profile of the absorbing species from occultation intensity data. The data-reduction procedure is similar to the method of computing the radial emission distribution of a cylindrical plasma source, as treated by the plasma physicists. The similarity exists because both techniques reduce to the problem of solving the Abel integral equation (Hays and Roble, 1968a, b; Barr, 1962).

In practice, the numerical solution of the Abel integral equation requires special handling because of its sensitivity to small random errors in the data. Therefore, we develop two separate techniques of numerically inverting the Abel integral equation to obtain the number density distribution of the absorbing species. The first utilizes an exponential approximation for atmospheric species which decrease nearly exponentially with altitude; the second, a quadratic approximation which works better for atmospheric species having a more complex vertical distribution such as atmospheric ozone (Hays *et al.*,

1972). The retrieval accuracy of both schemes is examined, and a theoretical analysis of errors is presented which enables us to determine the accuracy of the measurement in the presence of random statistical errors inherent in light sources of very low intensity. The inversion technique and analysis of errors, although examined with respect to molecular oxygen and ozone, are general and can be used to determine the accuracy of any occultation measurement if the signal level and data-acquisition rate are known.

2. OCCULTATION TECHNIQUE

The intensity of a star, as measured by a telescope aboard a satellite, during occultation of the star by the Earth's atmosphere (Fig. 1) is expressed as

$$F^*(r_0) = \varphi \int_0^\infty T(\lambda) I(\lambda, r_0)\, \mathrm{d}\lambda \tag{1}$$

where r_0 is the tangent ray height of the light ray passing tangentially to the Earth's surface, $\varphi = AQ_eT_0$, A is the aperture area of the telescope, Q_e is the quantum efficiency of the photo-multiplier, T_0 is the optical transmission of the system, $T(\lambda)$ is the broadening function or transmission of the dispersive element at wavelength λ and $I(\lambda, r_0)$ is the intensity of the star at wavelength λ and tangent ray height r_0.

The intensity of starlight passing through the Earth's upper atmosphere is determined by considering the combined attenuation of all of the absorbing species along the ray path (Beer's law).

$$I(\lambda, r_0) = I_\infty(\lambda) \exp\left(-\sum_i \sigma_i(\lambda) N_i(r_0)\right) \tag{2}$$

where $I_\infty(\lambda)$ is the stellar intensity above the atmosphere and $\sigma_i(\lambda)$ is the absorption cross-section of the ith atmospheric species. In the case of a spherically stratified atmosphere, the tangential column number density $N_i(r_0)$ is

$$N_i(r_0) = 2\int_{r_0}^\infty \frac{n_i(r) r\, \mathrm{d}r}{\sqrt{r^2 - r_0^2}} \tag{3}$$

where $n_i(r)$ is the number density of the ith absorbing species at a distance r from the center of the Earth.

Hays and Roble (1968b) calculated the tangential u.v. transmission for the mesosphere and the lower thermosphere. They show that in certain specific wavelength intervals the u.v. starlight is absorbed by a single species. These include a broadband region near 1500 Å where molecular oxygen acts as a single absorber in the lower thermosphere and also a region near 2500 Å where ozone is a single absorber in the mesosphere. In both of these regions, Hays and Roble (1968b) show that refractive attenuation, Rayleigh scattering, and absorption by other minor atmospheric constituents are negligible over most of the altitude range where absorption occurs. In addition, they point out that only the relative intensity is important for the occultation measurement. The stellar occultation data are therefore normalized as

$$F(r_0) = \frac{\int_0^\infty T(\lambda) I_\infty(\lambda) \exp\left(-\sigma(\lambda) N(r_0)\right) \mathrm{d}\lambda}{\int_0^\infty T(\lambda) I_\infty(\lambda)\, \mathrm{d}\lambda}. \tag{4}$$

The interference filter used in the occultation measurements is selected so that $T(\lambda)$ includes only a wavelength region where absorption is caused by the single species of

interest. By knowing the filter-broadening function, the stellar spectra above the atmosphere, and the absorption cross-section, the normalized signal is then only a function of the tangential column number density $F(r_0) = F(N(r_0))$. The intensity data can be inverted to give the tangential column number density $N(r_0) = N(F(r_0))$. Equation (3) for the tangential column number density is the Abel integral equation (c.f. Hays and Roble, 1968a, b) which is directly inverted to give the number density of the absorbing species at radius r

$$n_s(r) = -\frac{1}{\pi}\int_r^\infty \frac{[\mathrm{d}N(r_0)/\mathrm{d}r_0]\,\mathrm{d}r_0}{\sqrt{r_0^2 - r^2}}. \tag{5}$$

In the next sections, we develop two separate numerical inversion schemes; one applicable for determining the number density profile of atmospheric species decreasing nearly exponentially with altitude, such as molecular oxygen; and the second for atmospheric species having a more complex number density profile, such as ozone.

3. DATA REDUCTION

(a) *Exponential form.* The intensity of a star measured by photometers aboard a satellite during occultation is generally weak and usually obtained in digital form (Hays *et al.*, 1972). At low intensities, pulse-counting systems are used with a finite integration time between data points. Therefore, the intensity data are obtained at a series of discrete tangent ray heights $F(r_0)$. The normalized intensities are converted to the tangential column number density of the absorbing species along the ray path $N(r_0)$ as described in the previous section. Thus, a set of discrete values of the tangential column number density is obtained as a function of tangent ray height during occultation. We approximate the tangential column number density between data points in the interval $r_i < r < r_{i+1}$ by

$$N(r) = \alpha_i \exp(-\beta_i(r - r_i)) \tag{6}$$

where r_i and r_{i+1} are the i and $i+1$ tangent ray heights of the data points, respectively. The coefficients α_i and β_i are determined from a least squares fit to the data in the vicinity of the ith data point by minimizing the variance of Equation (6) with the data and smoothing M adjacent points (c.f. Roble and Norton, 1972).

$$\delta_i = \sum_{j=K_1}^{K_2} (N_j - \alpha_i \exp(-\beta_i(r_j - r_i)))^2 \tag{7}$$

where $K_1 = i - M/2$, $K_2 = i + M/2$, N_j is the tangential column number density at the jth data point. Then by differentiating Equation (6) and replacing the integral in Equation (5) by a finite sum, we obtain

$$n(r_l) = \frac{1}{\pi}\sum_{i=l}^{\infty} \alpha_i\beta_i \int_{r_i}^{r_{i+1}} \frac{\exp(-\beta_i(r - r_i))}{\sqrt{r^2 - r_l^2}}\,\mathrm{d}r. \tag{8}$$

Expanding the denominator and integrating, we obtain

$$\begin{aligned} n(r_l) = \frac{1}{\pi}\sum_{i=l}^{\infty} \frac{\alpha_i\beta_i}{(r_i + r_l)^{1/2}} \Bigg\{ & \left(1 + \frac{1}{2}\frac{(r_i - r_l)}{(r_i + r_l)} - \frac{1}{4\beta_i}\frac{1}{(r_i + r_l)}\right)\left(\frac{\pi}{\beta_i}\right)^{1/2} \\ & \times [\mathrm{erf}(\beta_i(r_{i+1} - r_l))^{1/2} - \mathrm{erf}(\beta_i(r_i - r_l))^{1/2}] \exp(\beta_i(r_i - r_l)) \\ & + \frac{1}{2\beta_i(r_i + r_l)} [(r_{i+1} - r_l)^{1/2} \exp(-\beta_i(r_{i+1} - r_i)) - (r_i - r_l)^{1/2}] \Bigg\} \end{aligned} \tag{9}$$

where $\mathrm{erf}(x)$ is the error function of x.

Thus, the number density of the absorbing species at radius r_i is determined directly from Equation (9) using the calculated values of α_i and β_i.

(b) *Quadratic form.* When the absorbing constituent has a number density height profile which is not exponentially decreasing with altitude, but varies over the scan altitude, such as for ozone (Fig. 2), then the exponential scheme developed in the previous section may not be

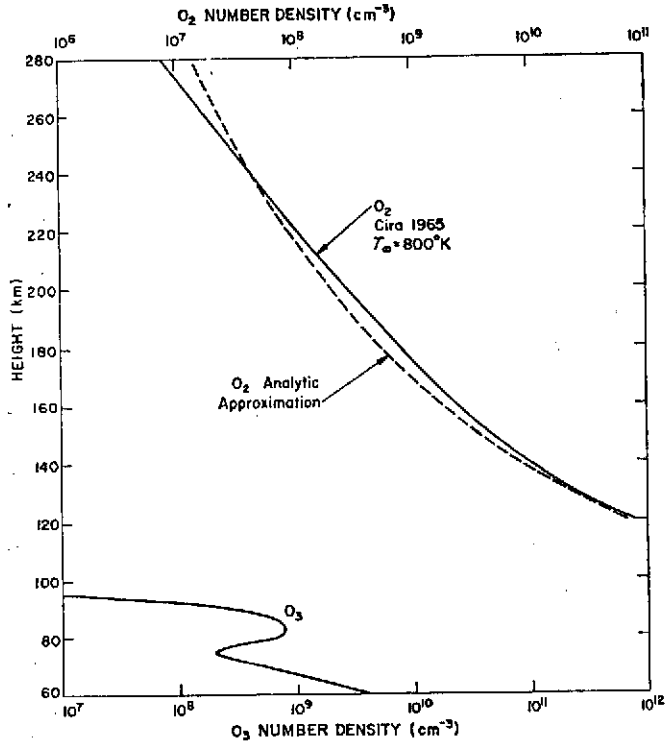

FIG. 2. THE MOLECULAR OXYGEN AND OZONE NUMBER DENSITY AS A FUNCTION OF HEIGHT. THE SOLID CURVE FOR O_2 IS THE NUMBER DENSITY DISTRIBUTION FROM THE MEAN CIRA 1965 MODEL ATMOSPHERE AND THE DASHED CURVE IS AN ANALYTIC APPROXIMATION TO THE DISTRIBUTION. THE O_3 NUMBER DENSITY DISTRIBUTION IS AN ANALYTIC APPROXIMATION OF A NIGHT-TIME PROFILE AND IT IS GIVEN BY EQUATION (17).

best suited for the data-reduction process. In this case, we approximate the tangential column number density in the altitude region $z_i < z < z_{i+1}$ by the quadratic relationship

$$N(z) = Az^2 + Bz + C \tag{10}$$

where $z = r - r_e$ and r_e is the radius of the Earth, 6371 km.

The coefficients A, B and C are again determined by minimizing the variance of equation (10) with the data and smoothing M adjacent points

$$\delta_i = \sum_{j=K_1}^{K_2} (N_j - (A_i z_j^2 + B_i z_j + C_i))^2. \tag{11}$$

Minimizing Equation (11) and solving directly for A_i, B_i and C_i we obtain

$$A_i = \frac{(M(\overline{Nz}) - (\bar{N})(\bar{z}))(M(\overline{z^3}) - (\bar{z})(\overline{z^2})) - (M(\overline{Nz^2}) - (\bar{N})(\overline{z^2}))(M(\overline{z^2}) - (\bar{z})(\bar{z}))}{(M(\overline{z^3}) - (\overline{z^2})(\bar{z}))(M(\overline{z^3}) - (\bar{z})(\overline{z^2})) - (M(\overline{z^4}) - (\overline{z^2})(\overline{z^2}))(M(\overline{z^2}) - (\bar{z})(\bar{z}))}$$

$$B_i = \frac{(M(\overline{Nz}) - (\bar{z})(\bar{N})) - (M(\overline{z^3}) - (\overline{z^2})(\bar{z}))A_i}{(M(\overline{z^2}) - (\bar{z})(\bar{z}))} \tag{12}$$

$$C_i = \frac{(\bar{N}) - (\overline{z^2})A_i - (\bar{z})B_i}{M}$$

where

$$(\bar{\ }) = \sum_{j=K_1}^{K_2} (\ \ )_j.$$

As in the previous section, by differentiating Equation (10) and replacing the main integral of equation (5) with a finite sum and then integrating between data points, we obtain

$$n(r_i) = -\frac{1}{\pi}\sum_{i=l}^{\infty}\left[2A_i((r_{i+1}^2 - r_l^2)^{1/2} - (r_i^2 - r_l^2)^{1/2}) + (B_i - 2A_i r_s)\log_e \frac{(r_{i+1} + (r_{i+1}^2 - r_l^2)^{1/2})}{(r_i + (r_i^2 - r_l^2)^{1/2})}\right]. \tag{13}$$

Thus, the number density of the absorbing species as radius r_l is determined from equation (13) using the coefficients A_i and B_i calculated for each data point.

4. ATMOSPHERIC MODEL

The molecular oxygen number density profile in the lower thermosphere, obtained from the mean CIRA 1965 model atmosphere, is shown in Fig. 2. For mathematical simplicity, we approximate this profile by an atmosphere with a constant scale height gradient (Nicolet, 1960),

$$H = H_s + \beta(r - r_s) \tag{14}$$

where H_s is the scale height of the atmosphere at radius r_s, and β is the vertical gradient of the scale height. The molecular oxygen number density is then represented as

$$n(r) = n_s\left[\frac{H_s}{H_s + \beta(r - r_s)}\right]^{(1+\beta)/\beta} \tag{15}$$

where $n_s = 2 \times 10^{12}\,\mathrm{cm}^{-3}$, $r_s = 6471$ km, $H_s = 5$ km, and $\beta = 0{\cdot}23$ to give the approximation to the CIRA 1965 molecular oxygen distribution shown in Fig. 2. The tangential column number density of molecular oxygen along the ray path is determined by inserting Equation (15) into Equation (3), expanding the denominator, and integrating to obtain

$$N(r_0) = \left(\frac{2}{r_0}\right)^{1/2} n_s\left[\frac{H_s}{H_s + \beta(r_0 - r_s)}\right]^{1/\delta}\left\{\left[\frac{\beta}{H_s + \beta(r_0 - r_s)}\right]^{-3/2} B\left(\frac{3}{2}, \left(\frac{1}{\delta} - \frac{3}{2}\right)\right) + r_0\left[\frac{\beta}{H_s + \beta(r_0 - r_s)}\right]^{-1/2} B\left(\frac{1}{2}, \left(\frac{1}{\delta} - \frac{1}{2}\right)\right)\right\} \tag{16}$$

where $\delta = \beta/(1 + \beta)$ and $B(x, y)$ is the Beta function, $B(x, y) = \gamma(x)\gamma(y)/\gamma(x + y)$ and $\gamma(x)$ is the Gamma function. The normalized intensity as a function of tangent ray height is calculated from Equation (2) and is shown in Fig. 3 for absorption at a single wavelength

1450 Å in the Schumann–Runge continuum where the molecular oxygen absorption coefficient is approximately 2×10^{-17} cm^2.

Hays *et al.* (1972) presented a typical night-time ozone distribution determined from occultation measurements made by the Orbiting Astronomical Observatory (OAO-2). The

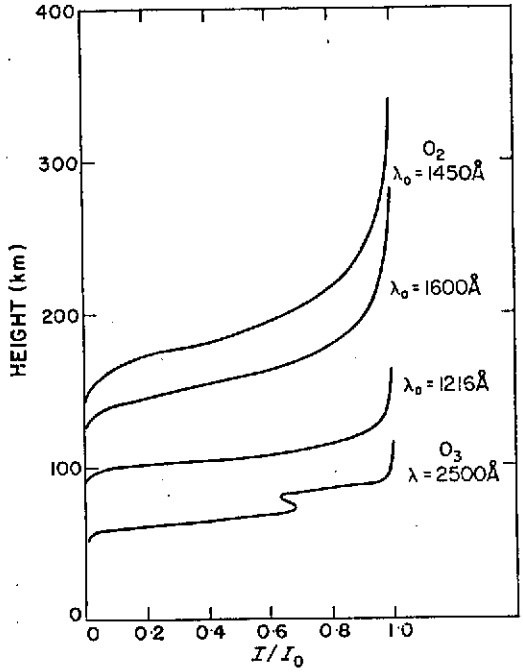

FIG. 3. THE NORMALIZED TANGENTIAL TRANSMISSION OF THE EARTH'S ATMOSPHERE AT VARIOUS WAVELENGTHS AS A FUNCTION OF HEIGHT.

ozone number density profile given in their paper can be reasonably represented as a sum of exponential and Gaussian functions

$$n(r) = n_b \exp(-(r - r_b)/H_b) + n_c \exp(-((r - r_c)/H_c)^2) \tag{17}$$

where $n_b = 5 \times 10^{10}$ cm^{-3}, $r_b = 50$ km, $H_b = 4{\cdot}34$ km, $n_c = 8 \times 10^8$ cm^{-3}, $r_c = 83$ km, and $H_c = 5$ km. The ozone number density distribution obtained from equation (17) is shown in Fig. 2.

The coefficients used in this study give an ozone number density slightly higher than those for a typical night-time ozone distribution determined by Hays *et al.* (1972). This difference, however, is not important because the profiles are similar and the main features of the ozone analysis are preserved in either case.

The total columnar number density along a ray path is obtained by inserting equation (17) into equation (3), expanding the denominator, and integrating to give

$$\begin{aligned} N(r_0) = {} & 2n_b \exp(r_b/H_b) r_0 K_1(r_0/H_b) + 2n_c \exp(-((r_0 - r_c)/H_c)^2) \\ & \times (2r_0)^{-1/2} \left\{ \left(\frac{2}{H_c^2}\right)^{-3/4} \gamma(\tfrac{3}{2}) \exp((r_0 - r_c)^2/(2H_c^2)) \right. \\ & \times D_{-3/2}((2)^{1/2} H_c^{-1}(r_0 - r_c)) + r_0 \left(\frac{2}{H_c^2}\right)^{-1/4} \gamma(\tfrac{1}{2}) \\ & \left. \times \exp((r_0 - r_c)^2/(2H_c^2)) D_{-1/2}((2)^{1/2} H_c^{-1}(r_0 - r_c)) \right\} \end{aligned} \tag{18}$$

where $K_1(x)$ is the modified Bessel function of the first kind, $\gamma(x)$ is the Gamma function, and $D_{-\nu}(x)$ is the parabolic cylinder function. The normalized intensity as a function of tangent ray height is obtained from Equation (18) and Equation (2), and is shown in Fig. 3 for absorption at a single wavelength in the Hartley continuum of ozone at 2500 Å. At this wavelength, ozone has an absorption cross-section of about 10^{-17} cm^{-2}.

5. SAMPLING ERROR

The accuracy in retrieving the number density profile with the data-reduction scheme depends upon (a) the data-acquisition rate or number of data points per scan, (b) the statistical noise inherent in a signal of low intensity, (c) the smoothing parameter M used in the inversion process, (d) knowledge of the satellite position during occultation, and (e) departures from spherical symmetry. The first three items are examined in this paper. Item (d) depends on the satellite tracking network and the degree of accuracy of the orbital

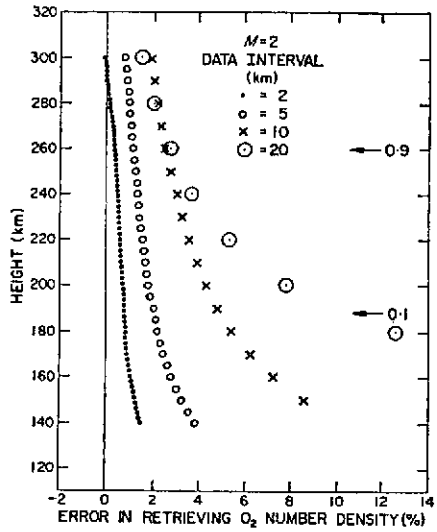

FIG. 4. THE ERROR IN RETRIEVING THE ANALYTIC MOLECULAR OXYGEN NUMBER DENSITY AS A FUNCTION OF HEIGHT FOR VARIOUS DATA-ACQUISITION INTERVALS.

elements. The intensity of the star is measured as a function of time, but by knowing the star's position and the satellite orbital elements, we can relate the intensity to the tangent ray height of the occulting star. Thus, errors in satellite time and position appear as errors in the tangent ray height and will not be discussed in this paper. The last item may be important for certain atmospheric species which change rapidly with time, as perhaps during sunrise or sunset; however, in this analysis, spherical symmetry is assumed.

The error in retrieving the molecular oxygen number density profile using the exponential data-reduction scheme is plotted as a function of height in Fig. 4 for various data-acquisition rates. The tangential column number density for the analytic molecular oxygen distribution is calculated at the various altitudes using Equation (16). These data are inverted using the exponential data-inversion scheme, and the retrieved molecular oxygen number density is compared to the number density given by the analytic model. The errors in retrieving the number density are then plotted in Fig. 4. The results show that the errors are smallest when a large number of data points per occultation scan are used in the

inversion process. The smoothing parameter M is also a factor in the retrieval accuracy. The smoothing parameter is primarily used to smooth the analytic representation of the tangential column number density through noisy data points and its importance will be evident in the next section. But for noise-free data, an increase in the smoothing parameter decreases the retrieval accuracy for a number density profile having a slight curvature.

At high altitudes, the retrieval accuracy would decrease due to the practical requirement of truncating the inversion integral at an upper boundary. It is difficult to convert the normalized intensity to tangential column number density for the upper part of the scan where the normalized intensity approaches 1·0, especially in the presence of statistical noise.

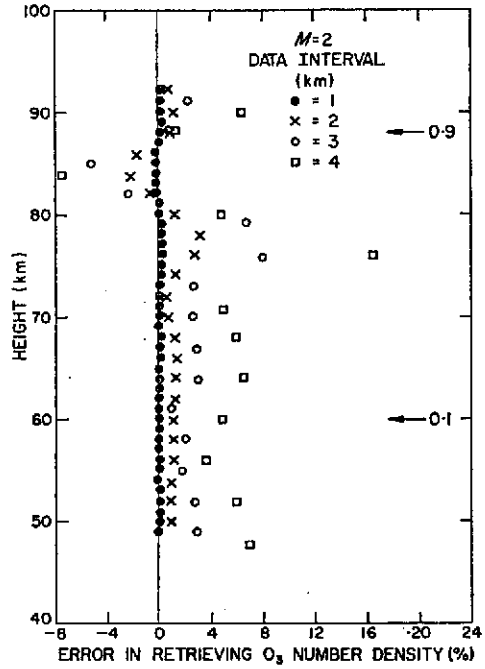

FIG. 5. THE ERROR IN RETRIEVING THE ANALYTIC OZONE NUMBER DENSITY AS A FUNCTION OF HEIGHT FOR VARIOUS DATA-ACQUISITION INTERVALS.

To reduce this error and extend the upper limit of the occultation scan, it is convenient to utilize a model atmosphere and calculate the tangential column number beyond the uppermost data point for use in the inversion integral.

The error in retrieving the model ozone number density profile using the analytic expression for the tangential column number density given by Equation (18) and also using the quadratic data-reduction scheme is shown in Fig. 5. The retrieval is good for a high data-acquisition rate, but as the data-acquisition rate decreases, the accuracy in defining the vertical structure and in particular the ozone bulge near 83 km also decreases. The lowest data-acquisition rate considered in Fig. 5 shows considerable error in retrieving the ozone bulge. These results were obtained using a smoothing parameter of $M = 2$. As the smoothing parameter is increased, the accuracy of retrieving the vertical structure depends critically on the data-acquisition rate. For a particular application, there is a tradeoff between the data-acquisition rate and the smoothing parameter.

For simplicity, the results presented here assume absorption at a single wavelength.

However, the technique which has been developed is general and can be applied to any broadband filter by including a wavelength integration.

6. THEORETICAL ANALYSIS OF STATISTICAL ERRORS

For occultation scans of very low intensity, the statistical noise which is superimposed upon the basic signal intensity becomes an appreciable part of the signal. The errors in retrieving the number density profile of the absorbing species from occultation data having random statistical noise are considered in this section.

(a) *Molecular oxygen.* The solid curve in Fig. 6 shows the calculated normalized intensity variation of a star during occultation using Equations (16) and (2). The peak signal

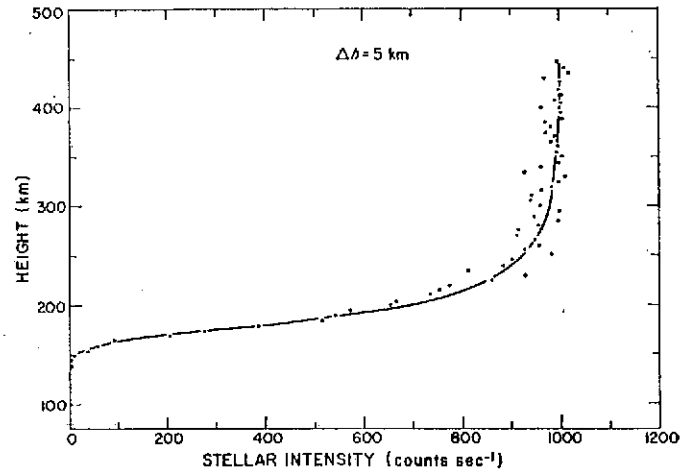

FIG. 6. AN OCCULTATION SCAN IN THE SCHUMANN–RUNGE CONTINUUM OF MOLECULAR OXYGEN AT 1450 Å WITH RANDOMLY SCATTERED STATISTICAL NOISE SUPERIMPOSED. THE STANDARD DEVIATION OF THE NOISE IS PROPORTIONAL TO THE SQUARE ROOT OF THE BASIC SIGNAL LEVEL.

level in this example is approximately 1000 counts sec^{-1} and the calculations are made at a single wavelength of 1450 Å. Also shown in Fig. 6 is the basic scan with a superimposed Poisson noise distribution having a standard deviation proportional to the square root of the signal level. The molecular oxygen number density profiles shown in Fig. 7 for the two scans given in Fig. 6 have been retrieved using the data-reduction scheme described in the previous sections. Other statistical noise distributions yield an ensemble of retrieved molecular oxygen number density profiles which can be statistically analyzed.

If we assume that the tangential column number density is $N = N_0 + \Delta N$ where N_0 is the basic tangential column number density without statistical noise and ΔN is the tangential column number density error due to the statistical noise, then in the approximation given by Equation (6) we expand α and β as

$$\alpha = \alpha_0 + \Delta\alpha$$
$$\beta = \beta_0 + \Delta\beta. \tag{19}$$

Inserting these relationships into Equation (7), expanding the exponential, and subtracting the basic unscattered state, we obtain

$$\delta_i^* = \sum_{j=K_1}^{K_2} [\Delta N_j - \Delta\alpha_i \exp(-\beta_{0i}(z_j - z_i)) + \alpha_{0i}\Delta\beta_i(z_j - z_i)\exp(-\beta_{0i}(z_j - z_i))]^2. \tag{20}$$

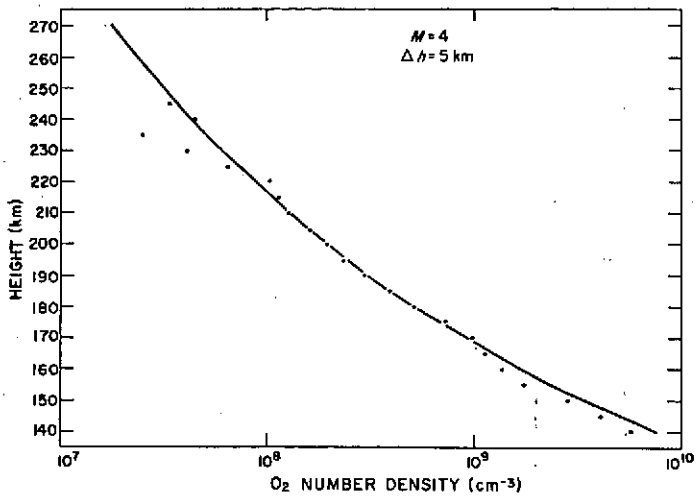

FIG. 7. THE RETRIEVED MOLECULAR OXYGEN NUMBER DENSITY PROFILE FOR THE OCCULTATION SCAN WITH RANDOMLY SCATTERED NOISE SHOWN IN FIG. 6. THE SOLID CURVE GIVES THE ANALYTIC MOLECULAR OXYGEN NUMBER DENSITY DISTRIBUTION.

The coefficient errors $\Delta\alpha_i$ and $\Delta\beta_i$ are calculated in the least squares sense from the relationships

$$\frac{\partial\delta_i^*}{\partial\Delta\alpha_i} = \frac{\partial\delta_i^*}{\partial\Delta\beta_i} = 0 \tag{21}$$

and are given in the Appendix.

The intensity of the star, considering single wavelength absorption, is calculated from Beer's law

$$F_0 = F(\lambda, r_0) = F_\infty(\lambda) \exp\left(-\sigma(\lambda)N(r_0)\right) \tag{22}$$

where $F_\infty(\lambda)$ is the signal measured above the atmosphere in counts $\sec^{-1}$. The linear variation in tangential column number density due to a signal with statistical noise $F = F_0 + \Delta F$ is obtained by introducing the value of N into Equation (22) and expanding the exponential to obtain

$$\Delta N = -\frac{1}{\sigma(\lambda)} \frac{\Delta F}{F(\lambda, r_0)}. \tag{23}$$

If a Poisson random noise with a standard deviation for ΔF proportional to the square root of the basic signal $(F_0)^{1/2}$ is introduced into the expressions for the coefficients $\Delta\alpha_i$ and $\Delta\beta_i$, the mean square errors for the coefficients $\langle\overline{\Delta\alpha_i}\rangle$ and $\langle\overline{\Delta\beta_i}\rangle$ are determined using the propagation of statistical errors theorem and they are presented in the Appendix.

The errors in the number density of the absorbing species at the tangent ray point are determined from the integral

$$\Delta n(r_i) = -\frac{1}{\pi} \int_{r_i}^{\infty} \frac{[\mathrm{d}\,\Delta N/\mathrm{d}r]\,\mathrm{d}r}{\sqrt{r^2 - r_i^2}}. \tag{24}$$

The tangential column number density of the absorbing species is determined by inserting Equation (19) into Equation (6). The noise in the number density of the absorbing

species at the tangent ray point is obtained by expanding the exponential, subtracting the basic state, and differentiating the tangential column number density error ΔN to give

$$\Delta n(r_l) = \frac{1}{\pi} \sum_{i=l}^{\infty} (\beta_{0i} \Delta\alpha_i + \alpha_{0i} \Delta\beta_i) \int_{r_i}^{r_{i+1}} \frac{\exp(-\beta_{0i}(r - r_i))}{\sqrt{r^2 - r_l^2}} \, dr$$
$$- \frac{1}{\pi} \sum_{i=l}^{\infty} \alpha_{0i} \beta_{0i} \Delta\beta_i \int_{r_i}^{r_{i+1}} \frac{(r - r_i) \exp(-\beta_{0i}(r - r_i))}{\sqrt{r^2 - r^2}} \, dr. \quad (25)$$

Integrating, we obtain

$$\Delta n(r_l) = \frac{1}{\pi} \sum_{i=l}^{\infty} (R_i \Delta\alpha_i + S_i \Delta\beta_i) \quad (26)$$

where R_i and S_i are coefficients given in the Appendix. The standard deviation of the number density error at the tangent ray point due to statistical noise is calculated using the propagation of statistical errors theorem

$$\langle \Delta n(r_l) \rangle = T_l F_\infty^{-1/2} \quad (27)$$

where

$$T_l = \frac{1}{\pi} \left[\sum_{i=l}^{\infty} (R_i X_i + S_i Y_i)^2 \right]^{1/2}$$

and X_i and Y_i are given in the Appendix.

(b) *Ozone.* The errors in the ozone number density caused by statistical noise superimposed upon the basic signal are determined from the quadratic data-reduction scheme. The signal intensity variations are related to the tangential column number density variations through Equation (23) and the number density error of ozone at the tangent ray point is obtained from Equation (24). The tangential column number density with superimposed variations caused by statistical noise is $N = N_0 + \Delta N$. The coefficients in Equation (10) are assumed to have a variation $A_i = A_{0i} + \Delta A_i$, $B_i = B_{0i} + \Delta B_i$, and $C_i = C_{0i} + \Delta C_i$. Introducing these variations into Equation (11) and subtracting the basic state, we have

$$\delta_i^* = \sum_{j=K_1}^{K_2} (\Delta N_j - \Delta A_i z_j^2 - \Delta B_i z_j - \Delta C_i)^2. \quad (28)$$

Solving for the coefficients ΔA_i, ΔB_i and ΔC_i, we obtain relationships similar to Equation (12) with the exception that N_j is replaced by ΔN_j

$$\Delta A_i = \sum_{j=K_1}^{K_2} Q_j \Delta N_j$$
$$\Delta B_i = \sum_{j=K_1}^{K_2} Q_j^* \Delta N_j \quad (29)$$

where Q_j and Q_j^* are given in the Appendix. The number density error at the tangent ray point is obtained by inserting Equation (29) into Equation (24) and integrating to give

$$\Delta n(r_l) = -\frac{1}{\pi} \sum_{i=l}^{\infty} \left[\sum_{j=K_1}^{K_2} ((2W_{1i} - 2r_e W_{2i}) Q_j + W_{2i} Q_j^*) \cdot \frac{\Delta F_j}{\sigma F_{0j}} \right] \quad (30)$$

where

$$W_{1i} = (r_{i+1}^2 - r_l^2)^{1/2} - (r_i^2 - r_l^2)^{1/2}$$
$$W_{2i} = \log_e \left(\frac{r_{i+1} + (r_{i+1}^2 - r_l^2)^{1/2}}{r_i + (r_i^2 - r_l^2)^{1/2}} \right).$$

The standard deviation of the number density error at the tangent ray point is calculated using the propagation of statistical errors theorem and assuming that the standard deviation of the noise is proportional to the square root of the basic signal

$$\langle \Delta n(r_i) \rangle = E_i \cdot F_\infty^{-1/2} \tag{31}$$

where

$$E_i = \frac{1}{\pi}\left\{\sum_{i=i}^{\infty}\sum_{j=K_1}^{K_2}\left[[(2W_{1i} - 2r_e W_{2i})Q_j + W_{2i}Q_j^*]\frac{1}{\sigma}\left(\frac{F_\infty}{F_{0j}}\right)^{1/2}\right]^2\right\}^{1/2}.$$

7. ANALYSIS OF STATISTICAL ERRORS

The error in retrieving the molecular oxygen number density from occultation scans having a random statistical noise superimposed upon the basic signal is defined as

$$e(r_i) = \frac{\langle \Delta n(r_i) \rangle}{n(r_i)}. \tag{32}$$

The numerator is the standard deviation of the retrieved number density, given by equation (27) for molecular oxygen and equation (31) for ozone, and $n(r_i)$ is the number density at radius r_i. The standard deviation of the retrieved number density is inversely proportional to the square root of the unattenuated signal level for both molecular oxygen and ozone. Therefore, in Fig. 8 $T_i(n(r_i))^{-1}$ is plotted as a function of altitude for various smoothing parameters M. The error in retrieving the molecular oxygen number density for

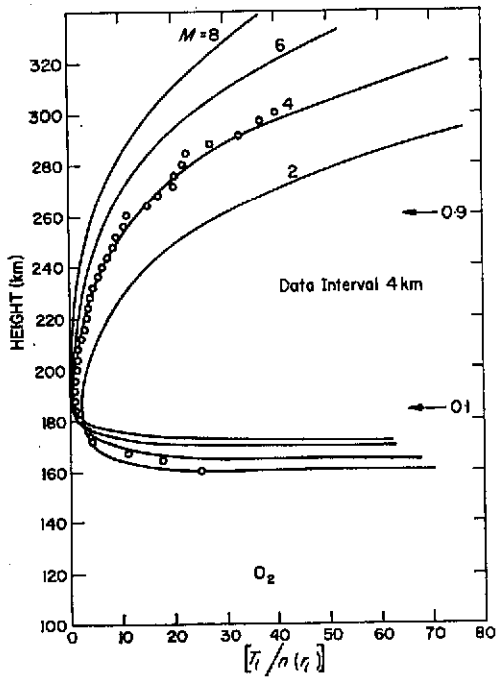

FIG. 8. THEORETICAL ANALYSIS OF ERRORS IN RETRIEVING THE MOLECULAR OXYGEN NUMBER DENSITY FROM OCCULTATION SCANS WITH RANDOM STATISTICAL NOISE SUPERIMPOSED. THE RETRIEVAL ERROR IS OBTAINED BY DIVIDING THE PARAMETER $T_i(n(r_i))^{-1}$ BY $F_\infty^{1/2}$, THE SQUARE ROOT OF THE UNATTENUATED BASIC SIGNAL LEVEL. THE CIRCLES REPRESENT THE RESULTS OF A NUMERICAL ANALYSIS OF ERRORS FOR $M = 4$.

any signal level is obtained by dividing the parameter $T_t(n(r_t))^{-1}$ by $F_\infty^{1/2}$. An increase in the smoothing parameter M decreases the error in retrieving the molecular oxygen number density. However, as discussed earlier, the accuracy of retrieving the basic molecular oxygen number density profile from unscattered occultation scans decreases as the smoothing parameter M increases. Therefore, there exists a value of M which gives a minimum in the overall error in retrieving the molecular oxygen number density profile at a given data-acquisition interval. The results of a numerical analysis of errors are shown in Fig. 8 for 100 occultation scans with different randomly scattered noise distributions. There is general

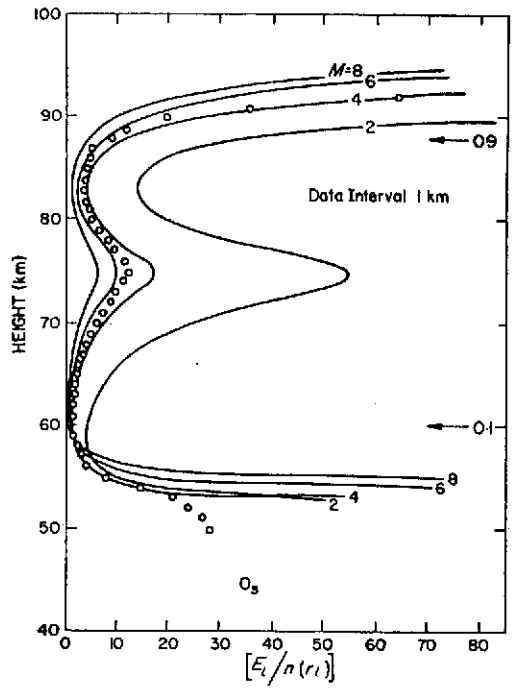

FIG. 9. THEORETICAL ANALYSIS OF ERRORS IN RETRIEVING THE OZONE NUMBER DENSITY FROM OCCULTATION SCANS WITH RANDOM STATISTICAL NOISE SUPERIMPOSED. THE RETRIEVAL ERROR IS OBTAINED BY DIVIDING THE PARAMETER $E_t(n(r_t))^{-1}$ BY $F_\infty^{1/2}$, THE SQUARE ROOT OF THE UNATTENUATED BASIC SIGNAL LEVEL. THE CIRCLES REPRESENT THE RESULTS OF A NUMERICAL ANALYSIS OF ERRORS FOR $M = 4$.

agreement between the results of the theoretical and numerical analysis of errors. Also shown in the figure are arrows indicating the altitudes of the 0·1 and 0·9 normalized intensity points. The retrieval of the molecular oxygen number density is best for data lying between these normalized intensity ratios.

The standard deviation of the retrieved ozone number density is also inversely proportional to the square root of the unattenuated signal level. Therefore, in Fig. 9 the parameter $E_t(n(r_t))^{-1}$ is plotted as a function of height for various smoothing parameters. In general, the error in retrieving the ozone bulge and the number density below about 70 km is low. However, in the region of the ozone minimum near 75 km the retrieval error increases. The data-acquisition interval in this case is 1 km and an increase in the smoothing parameter M decreases the error in retrieving the ozone number density. As the data-acquisition interval increases, the error in retrieving the ozone number density increases.

For a given data-acquisition interval, there also is a value of the smoothing parameter M which gives a minimum in the overall error in retrieving the ozone number density. The circles in Fig. 9 again are the results of a numerical analysis of the errors for 100 ozone occultation scans with different randomly scattered noise distributions. The general agreement between the theoretical and numerical analysis of errors enables us to theoretically calculate the error coefficients and thus determine accuracy of an occultation scan for any signal intensity.

8. DISCUSSION

We have presented a numerical technique for retrieving the number density profile of absorbing atmospheric gases from planetary occultation data having random statistical noise superimposed upon the basic signal. Because of the sensitivity of the Abel integral equation to random noise, some smoothing is required before evaluating the inversion integral. An exponential technique was developed for atmospheric species whose number density profile decreases exponentially with height, whereas the quadratic scheme works better for atmospheric species having a more complex vertical profile. These techniques have been used to reduce the OAO-2 stellar occultation data and obtain the night-time molecular oxygen and ozone distribution in the upper atmosphere (Hays *et al.*, 1972). With a modification to account for the finite size of the solar disk, these techniques have also been used to reduce the SOLRAD-8 solar occultation data (Roble and Norton, 1972). The retrieval errors are determined by knowing the approximate signal level and acquisition rate of the occultation data. For each specific case, there is a minimum in the retrieval error determined by the degree of smoothing for the appropriate data-acquisition rate and basic signal level. Generally, the best accuracy is achieved between the normalized intensity limits of 0·1–0·9 where the derivative in the numerator of the Abel integral equation changes rapidly. Figure 2 shows that by selecting the appropriate spectrally isolated wavelength interval, the number density distribution at practically any altitude may be obtained in the region where the tangential column number density is approximately equal to the inverse of the effective cross-section.

The analysis was performed for single wavelength absorption, whereas measurements are made for some finite passband determined by the characteristics of the monitoring spectrometer or photometer. In this case, an additional integration over wavelength is required in the analysis, but it does not fundamentally alter the results as long as the absorption process is spectrally isolated. Actually, a wavelength interval selected to cover a continuum region where the absorption cross-section is smoothly increasing or decreasing allows deepest penetration into the atmosphere. The altitude range of the occultation data is greater in this case than for the case of a constant cross-section over the selected wavelength interval.

Acknowledgments—We are grateful for the assistance of Messrs. K. Hansen, J. Hastings and M. Graves who provided the numerical calculations and plotting. A. Lundberg typed the manuscript.

REFERENCES

BARR, W. L. (1962). Method for computing the radial distribution of emitters in a cylindrical source. *J. opt. Soc. Amer.* **52**, 885.

BRANNON, P. J. and HOFFMAN, J. M. (1971). Molecular oxygen density measurements from 80 to 140 kilometers. *J. geophys. Res.* **76**, 4630.

BRYAM, E. T., CHUBB, T. A. and FRIEDMAN, H. (1957). The dissociation of molecular oxygen at high altitudes, in *Threshold of Space*, 211 pp. Pergamon Press, London.

CARVER, J. H., MITCHELL, P. and MURRAY, E. L. (1964). Molecular oxygen density and Lyman-α absorption in the upper atmosphere. *J. geophys. Res.* **69**, 3755.
CARVER, J. H., HORTON, B. H. and BURGER, F. G. (1966). Nocturnal ozone distribution in the upper atmosphere. *J. geophys. Res.* **74**, 6873.
CIRA (1965). *COSPAR International Reference Atmosphere*, 312 pp. North-Holland, Amsterdam.
FESENKOV, V. G. (1967). A satellite technique for sounding the optical properties of the atmosphere. *Soviet Astronomy-AJ*, **11**, 1.
HAYS, P. B. and ROBLE, R. G. (1968a). Atmospheric properties from the inversion of planetary occultation data. *Planet. Space Sci.* **16**, 1197.
HAYS, P. B. and ROBLE, R. G. (1968b). Stellar spectra and atmospheric composition. *J. atmos. Sci.* **25**, 1141.
HAYS, P. B., ROBLE, R. G. and SHAH, A. N. (1972). Terrestrial atmospheric composition from stellar occultations. *Science* **176**, 793.
HINTEREGGER, H. E. (1962). Absorption spectrometric analysis of the upper atmosphere in the EUV region. *J. atmos. Sci.* **19**, 351.
HINTEREGGER, H. E. and HALL, L. A. (1969). Thermospheric densities and temperatures from EUV absorption measurements by OSO-III. *Space Res.* **IX**, 519. North-Holland.
JOHNSON, F. S., PURCELL, J. D. and TOUSEY, R. (1951). Measurements of the vertical distribution of atmospheric ozone from rockets. *J. geophys. Res.* **56**, 583.
JURSA, A. S., NAKAMURA, M. and TANAKA, Y. (1963). Molecular oxygen distribution in the upper atmosphere. *J. geophys. Res.* **68**, 6145.
JURSA, A. S., NAKAMURA, M. and TANAKA, Y. (1965). Molecular oxygen distribution in the upper atmosphere—II. *J. geophys. Res.* **70**, 2699.
KUPPERIAN, J. E., BRYAM, E. T. and FRIEDMAN, H. (1969). Molecular oxygen densities in the mesosphere at Fort Churchill. *J. atmos terr. Phys.* **16**, 174.
LINK, F. (1969). *Eclipse Phenomena in Astronomy*, 268 pp. Springer-Verlag, New York.
LOCKEY, G. W. A., HORTON, B. H. and ROFE, B. (1969). Satellite measurement of upper atmospheric molecular oxygen density. *Nature Lond.* **223**, 387.
MAY, B. R. (1971). A method of determining the density of thermospheric gases from measurements of solar ultra-violet light absorption at grazing-ray and near-vertical incidence. *Planet. Space Sci.* **19**, 27.
MILLER, D. E. and STEWART, K. H. (1965). Observations of atmospheric ozone from an artificial earth satellite. *Proc. R. Soc.* **A288**, 540.
NICOLET, M. (1960). The properties and constitution of the upper atmosphere, in *Physics of the Upper Atmosphere* (Ed. J. A. Ratcliffe), pp. 577. Academic Press, New York.
NORTON, R. B. and WARNOCK, J. M. (1968). Seasonal variation of molecular oxygen near 100 kilometers. *J. geophys. Res.* **73**, 5798.
OPAL, C. B. and MOOS, H. W. (1969). Night-time molecular oxygen densities in the 100–130 km region from Schumann-Runge absorption. *J. geophys. Res.* **74**, 2398.
QUESSETTE, J. A. (1970). On the measurement of molecular oxygen concentration by absorption spectroscopy. *J. geophys. Res.* **75**, 839.
RAWCLIFFE, R. D., MELOY, G. E., FRIEDMAN, R. M. and ROGERS, E. H. (1963). Measurement of vertical distribution of ozone from a polar orbiting satellite. *J. geophys. Res.* **68**, 6425.
REID, R. H. G. (1971). Number densities of atomic oxygen and molecular nitrogen in the thermosphere. *Planet. Space Sci.* **19**, 801.
REID, R. H. G. and WITHBROE, G. L. (1970). The density and vibrational distribution of molecular oxygen in the lower thermosphere. *Planet. Space Sci.* **18**, 1255.
ROBLE, R. G. and NORTON, R. B. (1972). Thermospheric molecular oxygen from solar u-v occultation data. Submitted to *J. geophys. Res.* **77**.
STEWART, K. H. and WILDMAN, P. J. L. (1967). Preliminary results of molecular oxygen observations from the Ariel III satellite. *Proc. R. Soc.* **A311**, 591.
THOMAS, L. and NORTON, R. B. (1967). Absorption of solar x rays and density changes between 140 and 160 kilometers. *J. geophys. Res.* **72**, 5552.
THOMAS, L., VENABLES, F. H. and WILLIAMS, K. M. (1965). Measurements of solar x-ray fluxes by the U.S. Naval Research Laboratory satellite 1964-01-D. *Planet. Space Sci.* **13**, 807.
VENKATESWARAN, S. V., MOORE, J. G. and KRUEGER, A. J. (1961). Determination of the vertical distribution of ozone by satellite photometry. *J. geophys. Res.* **66**, 1751.
WATANABE, K. (1958). UV absorption processes in the upper atmosphere. *Advan. Geophys.* **5**, 153.
WEEKS, L. H. and SMITH, L. G. (1968). Molecular oxygen concentrations in the upper atmosphere by absorption spectroscopy. *J. geophys. Res.* **73**, 4835.
WILDMAN, P. J. L., KERBY, M. K. and SHAW, M. S. (1969). Molecular oxygen measurements from 100 to 150 km at Woomera, Australia. *J. atmos. terr. Phys.* **31**, 951.

APPENDIX

Several of the coefficients discussed in the text are presented in this Appendix.

$$\Delta\alpha_i = \frac{\sum_{j=K_1}^{K_2}\left[\frac{\exp(-\beta_{0i}(z_j - z_i))}{\{\bar{z}_i^1\}} - \frac{(z_j - z_i)\exp(-\beta_{0i}(z_j - z_i))}{\{\bar{z}_i^2\}}\right]\Delta N_j}{\frac{\{\bar{z}_i^0\}}{\{\bar{z}_i^1\}} - \frac{\{\bar{z}_i^1\}}{\{\bar{z}_i^2\}}}$$

$$\Delta\beta_i = \frac{1}{\alpha_{0i}}\left\{\frac{\sum_{j=K_1}^{K_2}\left[\frac{\exp(-\beta_{0i}(z_j - z_i))}{\{\bar{z}_i^0\}} - \frac{(z_j - z_i)\exp(-\beta_{0i}(z_j - z_i))}{\{\bar{z}_i^1\}}\right]\Delta N_j}{\frac{\{\bar{z}_i^2\}}{\{\bar{z}_i^1\}} - \frac{\{\bar{z}_i^1\}}{\{\bar{z}_i^0\}}}\right\}$$

where

$$\{\bar{z}_i^0\} = \sum_{j=K_1}^{K_2}\exp(-2\beta_{0i}(z_j - z_i))$$

$$\{\bar{z}_i^1\} = \sum_{j=K_1}^{K_2}(z_j - z_i)\exp(-2\beta_{0i}(z_j - z_i))$$

$$\{\bar{z}_i^2\} = \sum_{j=K_1}^{K_2}(z_j - z_i)^2\exp(-2\beta_{0i}(z_j - z_i))$$

$$\overline{\langle\Delta\alpha_i\rangle} = \frac{X_i}{F_\infty^{1/2}}$$

where

$$X_i = \left[\sum_{j=K_1}^{K_2}\left\{\frac{\left[\frac{\exp(-\beta_{0i}(z_j - z_i))}{\{\bar{z}_i^1\}} - \frac{(z_j - z_i)\exp(-\beta_{0i}(z_j - z_i))}{\{\bar{z}_i^2\}}\right]\frac{1}{\sigma}\left(\frac{F_\infty}{F_{0j}}\right)^{1/2}}{\frac{\{\bar{z}_i^0\}}{\{\bar{z}_i^1\}} - \frac{\{\bar{z}_i^1\}}{\{\bar{z}_i^2\}}}\right\}^2\right]^{1/2}$$

and

$$\overline{\langle\Delta\beta_i\rangle} = \frac{Y_i}{F_\infty^{1/2}}$$

where

$$Y_i = \left[\frac{1}{\alpha_{0i}}\sum_{j=K_1}^{K_2}\left\{\frac{\left[\frac{\exp(-\beta_{0i}(z_j - z_i))}{\{\bar{z}_i^0\}} - \frac{(z_j - z_i)\exp(-\beta_{0i}(z_j - z_i))}{\{\bar{z}_i^1\}}\right]\frac{1}{\sigma}\left(\frac{F_\infty}{F_{0j}}\right)^{1/2}}{\frac{\{\bar{z}_i^2\}}{\{\bar{z}_i^1\}} - \frac{\{\bar{z}_i^1\}}{\{\bar{z}_i^0\}}}\right\}^2\right]^{1/2}$$

$$R_i = \beta_{0i}\varepsilon^{-1/2}\left\{\left(1 + \frac{1}{2}\frac{\Delta}{\varepsilon} - \frac{1}{4\beta_{0i}\varepsilon}\right)\left(\frac{\pi}{\beta_{0i}}\right)^{1/2}[\operatorname{erf}((\beta_{0i}\gamma)^{1/2}) - \operatorname{erf}((\beta_{0i}\Delta)^{1/2})]\exp(\beta_0\Delta) + \frac{1}{2\beta_{0i}\varepsilon}[\gamma^{1/2}\exp(-\beta_{0i}\eta) - \Delta^{1/2}]\right\}$$

where $\Delta = r_i - r_i$

$\gamma = r_{i+1} - r_i$

$\varepsilon = r_i + r_i$

$\eta = r_{i+1} - r_i$

$$S_i = \left(\frac{\pi}{\beta_{0i}}\right)^{1/2}[\mathrm{erf}((\beta_{0i}\gamma)^{1/2}) - \mathrm{erf}((\beta_{0i}\Delta)^{1/2})][\alpha_{0i}\varepsilon^{-1/2}(1 + \tfrac{1}{2}\Delta\varepsilon^{-1} - (4\beta_{0i}\varepsilon)^{-1})$$
$$- \alpha_{0i}\beta_{0i}\varepsilon^{-1/2}((4\beta_{0i})^{-1}(2 + \Delta\varepsilon^{-1}) - \tfrac{1}{2}(2\Delta + \Delta^2\varepsilon^{-1}) - \tfrac{3}{8}\beta_{0i}^{-2}\varepsilon^{-1})]$$
$$. \exp(\beta_{0i}\Delta) + (2\beta_{0i})^{-1}[\gamma^{1/2}\exp(-\beta_{0i}\eta) - \Delta^{1/2}]$$
$$. [\alpha_{0i}\varepsilon^{-3/2} + \alpha_{0i}\beta_{0i}\varepsilon^{-1/2}(2 + 2\Delta\varepsilon^{-1})]$$
$$- \alpha_{0i}\beta_{0i}(4\beta_{0i}^2\varepsilon^{3/2})^{-1}[\gamma^{1/2}(2\beta_{0i}\gamma + 3)\exp(-\beta_{0i}\eta) - \Delta^{1/2}(2\beta_{0i}\Delta + 3)]$$

$$Q_j = \left[\left(\frac{P}{K}(\overline{z^2}) - \frac{L(\bar{z})}{K}\right) + \frac{LM}{K}z_j - \frac{PM}{K}z_j^2\right]$$

$$Q_j^* = \left[\left(\frac{L^2}{PK}(\bar{z}) - \frac{(\bar{z})}{P} - \frac{L}{K}(\overline{z^2})\right) + \left(\frac{M}{P} - \frac{L^2M}{PK}\right)z_j + \frac{LM}{K}z_j^2\right]$$

$$L = (M(\overline{z^3}) - (\bar{z})(\overline{z^2}))$$

$$P = (M(\overline{z^2}) - (\bar{z})(\bar{z}))$$

$$K = [(M(\overline{z^3}) - (\overline{z^2})(\bar{z}))(M(\overline{z^3}) - (\bar{z})(\overline{z^2})) - (M(\overline{z^4}) - (\overline{z^2})(\overline{z^2}))(M(\overline{z^2}) - (\bar{z})(\bar{z}))].$$

Appendix III.a.

This Appendix gives some details of data processing which is employed to obtain molecular oxygen profiles and ozone profiles from occultation data. The details are divided into three parts, or processes, dealing with (1) the computation of tangential column number density for molecular oxygen, $N(O_2, r_o)$; (2) the computation of tangential column number density for ozone, $N(O_3, r_o)$; and (3) the retrieval of number density of either gas. Computer programs with accompanying notes are included.

Process 1

To obtain $N(O_2, r_o)$, the raw modulus 256 occultation data on the strip chart or digital printout are converted to normalized signal intensity by a program filed in "PLOT". The input to this program is the sequence of counts taken at an interval of $\frac{1}{2}$ sec spacecraft time. The measure of intensity which is used is the difference between successive counts. The output consists of a graph of normalized signal intensity v. time and the corresponding punched cards.

Following the conversion of the data to normalized intensity, a program filed in "OAOPR" is activated to complete the process. First, the ray tangent point location is computed. Then an interpolation table is formed consisting of normalized signal intensity v. tangential column number density. The table is then used to find $N(O_2, r_o)$ corresponding to the normalized, measured signal intensity.

Process 2

To obtain $N(O_3, r_o)$, the raw occultation data on the strip chart or digital printout are converted to normalized signal intensity by the "PLOT" program, and the "OAOPR" program is activated as for O_2. However, in this case corrections to $N(O_3, r_o)$ are made for the effects of the O_2 Herzberg bands and Rayleigh scattering upon ozone.

Process 3

Once the tangential column number density, N, is computed for all m data levels, a parabolic fit is forced upon N(h) and the smoothed values are then inverted by the finite differencing scheme,

$$n(r_j) = -\frac{2}{\pi}\frac{d}{dr}\int_r^\infty \frac{r}{r_o}\left(r_o^2 - r^2\right)^{-\frac{1}{2}} N(r_o)\, dr_o$$

$$= -\frac{2}{\pi}\int_r^\infty \left(r_o^2 - r^2\right)^{-\frac{1}{2}} \frac{dN(r_o)}{dr_o}\, dr_o$$

Details of the smoothing technique and inversion for various species is given in the attached paper on inversion techniques.

```
$SIG SAFF C=510 'MAURICE GRAVES'
**LAST SIGNON WAS: 09:36.59   12-29-71
 USER "SAFF" SIGNED ON AT  21:18.13 ON 12-29-71
$LIST PLOT
     1            DIMENSION AY(150),Y(150)
     2            DIMENSION BY(150)
     2.05         DIMENSION YINT(150)
     2.1          READ(5,861)  (BY(K),K=1,80)
     2.15         PRINT 861, (BY(K),K=1,80)
     3            READ(5,894)  N,MAX
     3.5          PRINT 894, N,MAX
     4            READ 893,(AY(I),I=1,N)
     4.1          LMT=5
     4.2          PRINT 893, (AY(I),I=1,N)
     5            DO 882 K=1,LMT
     6       882  Y(K)=AY(K)
     6.1          JA=LMT-1
     6.2          DO 1 K=1,JA
     6.3       1  YINT(K)=Y(K)-Y(K+1)
     7            J=N-LMT
     7.1          WRITE(6,861)  (BY(K),K=1,80)
     8            WRITE(6,899)
     9       899  FORMAT(20X,8HEXPECTED,9X,6HACTUAL,14X,10HDIFFERENCE,10X,
    10           18HRECORDED,12X,9HINTENSITY,/,22X,5HVALUE,9X,5HVALUE,35X,
    11           25HVALUE//)
    11.1          PZ=0.15*MAX
    12            DO 883 K=1,J
    12.1          Y(K)=AY(K)
    12.2          DO 2 MP=1,JA
    12.3       2  Y(K+MP)=Y(K+MP-1)-YINT(K+MP-1)
    12.41         YB=(Y(K)+ Y(K+1)+ Y(K+2)+ Y(K+3)+ Y(K+4))*0.2
    12.42         AI=(Y(K)-2.*Y(K+1)+2.*Y(K+3)-Y(K+4))/(-12.)
    12.43         BI=(4.*Y(K)+Y(K+1)+ Y(K+3)+4.*Y(K+4) -10.*YB)/14.
    12.44         CI=(Y(K)-8.*Y(K+1)+8.*Y(K+3)-Y(K+4))/12.
    12.45         B=(-9.*AI)+BI
    12.46         C=(27.*AI)-(6.*BI)+CI
    12.47         D=-(27.*AI)+9.*BI-3.*CI-2.*BI+YB
    12.5          P1=216*AI+36*B+6*C+D
    12.52         L=K+2
    13            A=(Y(L)-2.*Y(L+1)+Y(L+2))/2.
    14            B=(-5.*Y(L)+8.*Y(L+1)-3.*Y(L+2))/2.
    15            C=3.*Y(L)-3.*Y(L+1)+Y(L+2)
    20            P=16.*A+4.*B+C
    20.2          P=(P+P1)/2.
    21            X=AY(K+LMT)
    22            L=0
    22.1          PRINT 3,K,J,X,P,P1
    22.2     3     FORMAT(T2,2I5,3F20.6)
    23       886  IF (ABS(X-P)-160.) 884,885,885
    24       884  IF ((P-X) .GT. 100.) X=X+MAX
    24.2          PW=0.08*YINT(K+LMT-2)
    24.4          IF (PW .LT. PZ) PW=PZ
    24.42         IF (PW .GT.160.) PW=160.
    24.5          IF ((Y(K+LMT-2)-Y(K+LMT-1)).GT.(Y(K+LMT-1)-X+PW)) X=X-MAX
    24.8          Y(K+LMT)=X
    25            B=X-P
    26            C=Y(K+LMT-1)-Y(K+LMT)
    26.1          YINT(K+LMT-1)=C
    27            WRITE(6,895) K,P,X,B,AY(K+LMT),C
    28        895  FORMAT(I5,5F20.0)
```

```
      883  CONTINUE
           J=N-1
           WRITE(7,861)  (BY(K),K=1,80)
           WRITE(7,865)  (YINT(K),K=1,J)
           WRITE(6,898)
      898  FORMAT('1       GRAPH OF INTENSITY VS. TIME'//)
           READ(5,860)  DY,CY,EY
      860  FORMAT(3A1)
           PRINT 861,  (BY(K),K=1,80)
           DO 692 K=1,12
      692  BY(K)=10*K
           WRITE(6,681)  (BY(K),K=1,12)
      681  FORMAT(/3X,12F10.0)
           DO 690 K=1,150
      690  BY(K)=CY
           DO 691 K=1,25
      691  BY(5*(K-1)+1)=EY
           WRITE(6,861)  (BY(K),K=1,120)
           BY(1)=DY
           DO 870 K=2,150
      870  BY(K)=BY(K-1)
           N=N-1
           JB=1
           DO 741 J=1,N
           IF(YINT(J) .GT. YINT(JB)) JB=J
      741  CONTINUE
           DO 888 K=1,N
           BY(1)=CY
           JA=K/5
           JA=JA*5
           IF (JA .EQ. K) BY(1)=EY
            L=YINT(K)*100./YINT(JB)
           BY(L)=EY
           PRINT 861,(BY(J),J=1,120),L
      861  FORMAT(120A1,I5)
           BY(L)=BY(L+1)
      888  CONTINUE
      865  FORMAT(12F6.0)
      893  FORMAT(14F5.0)
      894  FORMAT(2I5)
      887  CALL EXIT
           RETURN
      885  L=L+1
           X=AY(K+LMT)-MAX*L
           PRINT 4,K,L,MAX,X
      4     FORMAT(T2,3I5,F20.6)
           IF(L-400) 886,887,887
           END
END OF FILE
```

Part 1: Line numbers 1-6

In this part, an informative comment card is read (line 2.1), the number of data values (N) and the maximum counts on calibration (MAX) are read (line 3), the raw data (AY) are read (line 4), and the first 5 values are set in Y (line 6). These five values must be monotonic estimates of values on the curve of actual (not normalized) intensity.

Part 2: Line numbers 6.1-12.5)

In this part, an allowable departure of a predicted value of intensity from the actual value is established. This departure is ±0.15 (line 11.1). Then the coefficients (AI, B, C, D) for cubic curve-fitting with five points are calculated (lines 12-12.47), and a sixth point is predicted (line 12.5).

Part 3: Line numbers 12.52-20.2

In this part, a parabolic curve-fitting is carried out for the third, fourth, and fifth points, yielding a new prediction of the sixth point (line 20). An average of the two predictions becomes the final estimate (line 20.2) of the sixth point. This procedure continues within loop 883 until the entire set of data points is exhausted.

Part 4: Line numbers 21-29

In this part, the modulo conversion is accomplished, based upon some intuitive conditions regarding signal intensity. The resulting signal intensities (C) are written out (line 27).

Part 5: Line numbers 30-71

In this part, the signal intensities are punched (line 32.1) for the data input to the final processing program. The intensity values are also plotted (line 57) after normalization (line 54.1).

```
1ST OAOPR
    1       C      THIS IS THE PARABOLIC LEAST SQUARE INVERSION FOR OCCULTATION DATA
    2       C   THIS PROGRAM FOR SETTING STAR ONLY.****
    3             IMPLICIT REAL*8(A-H,O-T,X-Z)
    4             DIMENSION PHI(150),ALAMC(150)
    5             COMMON Z(200),XN(200),A(200),B(200),C(200),ALT,WLL(100),FILT(100)
    6            1FIO(100),SG(100),SGO2(100),SGM(100),CCM(200),NP,MPX
    7             DIMENSION DA(200),FOF(200),TNO(200)
    8             DIMENSION CF(200),CO2(200),R&R(200)
    9             DIMENSION X(200),FN(200),TN(200),FNO(200),ZP(200)
   10             DIMENSION DEN(200),ZN(200)
   11             DIMENSION Q(20),T(150)
   12             DIMENSION RO(200)
   13             DIMENSION UD(200),UZ(200)
   14             DIMENSION UT(200)
   15       C*****************************************************************
   16       C*                    PART-1
   17       C*
   18       C*  THIS PART CALCULATES TANGENT RAY HEIGHT POINT. INPUT IS 5 VALUES
   19       C*  OF SPACECRAFT LONG. LAT. AND ALT. IN 10 SEC. GMT INTERVAL, 5 VALUES
   20       C*  OF GHA OF ARIES IN 10MIN. GMT INTERVAL, DEC. AND R.A. OF OCCULT- *
   21       C*  ING STAR, THE STARTING TIME IN HR., MIN., AND SEC., AND NUMBER OF
   22       C*  DATA POINTS NEEDED
   23
   24       C*****************************************************************
   25
   26             C1=1./57.2957795131
   27             WRITE(6,109)
   28         109  FORMAT(//10X,' S/C POSITION, LONG. LAT., AND ALT. IN 10 SEC.'
   29            1 'STEPS AND',/,10X,' GHA. OF ARIES IN TEN MINUTE STEPS')
   30             READ 11,Y1,Y2,Y3,Y4,Y5
   31             PRINT 11, Y1,Y2,Y3,Y4,Y5
   32             CALL SET(Y1,Y2,Y3,Y4,Y5,A4,B4,C4,D4)
   33             READ 11,Y1,Y2,Y3,Y4,Y5
   34             PRINT 11, Y1,Y2,Y3,Y4,Y5
   35             CALL SET(Y1,Y2,Y3,Y4,Y5,A2,B2,C2,D2)
   36             READ 11,Y1,Y2,Y3,Y4,Y5
   37             PRINT 11, Y1,Y2,Y3,Y4,Y5
   38             CALL SET(Y1,Y2,Y3,Y4,Y5,A3,B3,C3,D3)
   39             READ 11,Y1,Y2,Y3,Y4,Y5
   40             PRINT 11, Y1,Y2,Y3,Y4,Y5
   41             CALL SET(Y1,Y2,Y3,Y4,Y5,A5,B5,C5,D5)
   42             READ 11,Y1,Y2,Y3,Y4,Y5
   43             PRINT 71, Y1,Y2,Y3
   44         71  FORMAT(///5X,'STAR DECLINATION',F5.1,' DEGREES',F5.1,' MINUTES',
   45            1F7.2,'SECONDS')
   46             DEC=Y1+(Y2/60.)+(Y3/3600.)
   47             READ 11,Y1,Y2,Y3,Y4,Y5
   48             PRINT 72, Y1,Y2,Y3
   49         72  FORMAT(5X,'STAR RIGHT ASCENTION',F5.1,' HOURS',F5.1,' MINUTES',
   50            1F7.2,'SECONDS')
   51              RA=(Y1+(Y2/60.)+(Y3/3600.))*15.00
   52             DEC=DEC/57.29578
   53             RA=RA/57.29578
   54       C   TRIGONOMETRIC COMPUTATIONS START HERE.
   55              DCL=DCOS(DEC)*DCOS(RA)
   56              DCM=DCOS(DEC)*DSIN(RA)
   57              DCN=DSIN(DEC)
   58             READ 612,T1,T2,T3,NP
```

```
      612  FORMAT(3F10.5,I5)
           PRINT 641, T1,T2,T3
      641  FORMAT(5X,'STARTING TIME ',F5.1,'HR',F5.1,'MIN.',F7.4,'SEC.'
          1 ' AND TIME IS INCREASING')
           T1=T1+(T2+(T3/60.))/60.
           NPP=NP
           I=0
       73  IF (T2 .LT. 10.) GO TO 74
           T2=T2-10.
           GO TO 73
       74  L=T3/10.
           TX=T2+(L*10./60.)
       75  IF (T3 .LT. 10.) GO TO 7
           T3=T3-10.
           GO TO 75
        7    S=1.+(T3/10.)
C*  SPACECRAFT POSITIONS AND GHA OF ARIES ARE CALCULATED AT DIFFERENT
C*  GMT TIME BY USING THE FUNCTION CAL WHICH USES THE CURVE
C*  Y=A*T*T + B*T + C
           PHIS=CAL(S,A2,B2,C2,D2)*C1
           ALT=CAL(S,A3,B3,C3,D3)
           ALAMS=CAL(S,A4,B4,C4,D4)*C1
           IF (ALAMS .LT. 0.) ALAMS=6.28318+ALAMS
           X=3.+((TX+(T3/60.))/10.)
           ALAMG=CAL(X,A5,B5,C5,D5)*C1
           I=I+1
           M=NP-I+1
           PA=DCOS(ALAMS)
           PB=DCOS(PHIS)
           PC=DCOS(ALAMG)
            D=DSIN(ALAMS)
            E=DSIN(ALAMG)
           DCA=PA*PB*PC-D*PB*E
           DCB=D*PB*PC+PA*PB*E
            DCC=DSIN(PHIS)
           CALL HEIGHT(PHIS,RSAT,RR)
       13  XS=RSAT*DCA
           YS=RSAT*DCB
           ZS=RSAT*DCC
           RS=DSQRT(XS*XS+YS*YS+ZS*ZS)
           ARG=DCA*DCL+DCB*DCM+DCC*DCN
           BETA=3.1415926536-DARCOS(ARG)
           W=DCOS(BETA)
           XO=XS+RSAT*W*DCL
           YO=YS+RSAT*W*DCM
           IF(YO.LT.0..AND.ARG.GE.0.)BETA=6.283186-BETA
           IF(YO.LT.0..AND.ARG.LT.0.)BETA=3.141593+BETA
           ZO=ZS+RSAT*W*DCN
           ROO=DSQRT(XO*XO+YO*YO+ZO*ZO)
           PHIO(M)=DATAN(ZO/DSQRT(XO*XO+YO*YO))
           ALAMO(M)=DARCOS(XO/DSQRT(XO*XO+YO*YO))-ALAMG
           QF=DSIN(BETA)
           DCLS=XO/(RSAT*QF)
           DCMS=YO/(RSAT*QF)
           DCNS=ZO/(RSAT*QF)
           CPER=DCL*DCLS+DCM*DCMS+DCN*DCNS
           CALL HEIGHT(PHIO(M),RP,RR)
           HO=ROO-RR
           ZP(M)=HO*100000.
           R(M)=ROO*100000.
```

```
119           RO(M)=RR*100000.
120            PHIO(M)=PHIO(M)*57.295
121           ALAMO(M)=ALAMO(M)*57.295
122           PSI=(1.5707963268-BETA)/C1
123            T3=T3+(62.915/116.34)
124           IF(I .LT. NP) GO TO 7
125        11   FORMAT(5F10.5)
126      C*****************************************************************
127      C*                    PART-2
128      C*
129      C*  THIS PART TAKES AS INPUT THE FILTER TRANSMISSION, CROSS SECTION
130      C*  AND STAR SPECTRUM. THEN A TABLE OF TOTAL INTEGRATED NUMBER DENSITY
131      C*  TN VS. NORMALISED SIGNAL FNO, IS COMPUTED
132      C*****************************************************************
133           TX=ALAMO(NP)/15.0
134           T1=T1+TX
135           IF (T1 .LE. 0.) T1=T1+24.0
136           IF (T1 .GT. 24.0) T1=T1-24.0
137           L1=T1
138           T1=(T1-L1)*60.
139           L2=T1
140           T1=(T1-L2)*60.
141           NTAB=106
142      C                        INPUT DATA
143      C       FILTR DATA IN STEPS OF 20A.
144           READ 351,FX,FY,IO2
145        351  FORMAT(2F5.0,I5)
146           MPX=1.001+(FY-FX)/20.
147           DO 302 I=1,MPX
148        302  WLL(I)=FX+(I-1)*20.
149           IF (IO2 .NE. 2) GO TO 1260
150           MPX=MPX+13
151           READ 1201,(WLL(I),I=25,MPX)
152        1201 FORMAT(8F10.3)
153        1260 READ 300,(FILT(I),I=1,MPX)
154      C       CROSS-SECTION DATA
155           READ 600,(SG(I),I=1,MPX)
156      C       STAR SPECTRUM IN STEPS OF 20A.
157           READ 303,(FIO(I),I=1,MPX)
158         300 FORMAT(11F5.3)
159         303 FORMAT(11F5.0)
160         600 FORMAT(6E10.2)
161           SUN=0.
162           DO 101 J=2,MPX
163        101  SUN=SUN+((FILT(J)*FIO(J)+FILT(J-1)*FIO(J-1))/2.*(WLL(J)-WLL(J-1)
164      C  THIS SECTION MAKES A TABLE OF TOTAL INTEGRATED NUMBER
165      C  DENSITY VS. NORMALISED SIGNAL.
166           DO 800 INO=1,NTAB
167           READ(3,1216) TT
168        1216 FORMAT(5E16.6)
169           IF (IO2 .NE. 2) GO TO 1261
170           READ(2,1216) (SG(I),I=25,MPX)
171        1261 CONTINUE
172           TN(INO)=TT
173           SUM=0.
174           DO 1000 J=2,MPX
175        1000  SUM=SUM+((FILT(J)*FIO(J)*DEXP(-SG(J)*TT)+FILT(J-1)*FIO(J-1)*
176           1DEXP(-SG(J-1)*TT))/2.)*(WLL(J)-WLL(J-1))
177           FNR=SUM/SUN
178           IF (FNR .LT. 1.D-20) FNR=1.D-20
```

```
179           FNO(IBO)=FNP
180       800 CONTINUE
181       C*****************************************************************
182       C*                    PART-3
183       C*
184       C*  INPUT TO THIS PART IS THE MEASURED SIGNAL. THEN NORMALISED SIGNAL
185       C*  FOF IS USED TO DETERMINE TOTAL INTEGRATED NUMBER DENSITY TNO
186       C*  BY INTERPOLATION IN THE TABLE COMPUTED IN PART-2
187       C*****************************************************************
188             READ 1001, (Q(I),I=1,10)
189             PRINT 1001, (Q(I),I=1,10)
190        1001 FORMAT(10A8)
191        1002 FORMAT(I3)
192       C  OCCULTATION DATA
193             READ 760,(DA(I),I=1,NPP)
194        760  FORMAT(12F6.0)
195             DMIA=DA(1)
196             DO 857 I=1,NPP
197             IF(DA(I).LT.DMIA) DMIA=DA(I)
198         857 CONTINUE
199             DO 861 I=1,NPP
200         861 DA(I)=DA(I)-DMIA
201             NMXY=NPP-4
202             SUC=0.
203             DO 761 I=NMXY,NPP
204         761 SUC=SUC+DA(I)
205             DAO=SUC/5.
206             DO 762 I=1,NPP
207         762 FOF(I)=DA(I)/DAO
208              WRITE(6,1004)
209        1004  FORMAT(//'MODIFIED INPUT DATA'/)
210              PRINT 1005,(DA(I),I=1,NPP)
211        1005  FORMAT(10F8.0)
212       C  THIS SECTION CALCULATES TOTAL INTEGRATED NUMBER DENSITY;
213       C  USING MEASURED SIGNAL AND PREVIOUSLY COMPUTED TABLE.
214             DO 611 J=1,NTAB
215             Z(J)=DLOG(FNO(J))
216             XN(J)=DLOG(TN(J))
217         611 CONTINUE
218       609   FORMAT(T5,2D15.6)
219             M=4
220             NP=NTAB
221             CALL PARAB(M)
222             DO 630 L=1,NPP
223             IF (FOF(L) .LE. 0.) FOF(L)=1.D-5
224             DO 792 I=1,NTAB
225             IF(FOF(L).GE.FNO(I).AND.FOF(L).LT.FNO(I+1))GO TO 613
226         792 CONTINUE
227       613   J=I
228             X=DLOG(FOF(L))
229             TNO(L)=A(J)*X*X+B(J)*X+C(J)
230             TNO(L)=DEXP(TNO(L))
231       614   FORMAT(T5,2D15.6)
232       630   CONTINUE
232.1           IF(IO2.NE.0) GO TO 2501
233       C*****************************************************************
234       C*                    PART-3A                                    *
235       C*  IN THIS PART, THE OZONE COLUMN DENSITY IS CORRECTED FOR
236       C*  HERZBERG AND RAYLEIGH SCATTERING                             *
237       C*****************************************************************
```

```
      READ 2006,(SGC2(I),I=1,MPX)
 2006  FORMAT(7E10.2)
       DO 2005 I=1,MPX
       SGM(I)=3.9813D-23*((1890.+(I-1)*20.)*1.D-4)  **(-4.05)
 2005  CONTINUE
  814  FORMAT(1X,6E15.4)
       WRITE(6,815)
  815  FORMAT(//3X,'WAVE L',7X,'FILTER',10X,'STAR INT.',5X,
     1'O3 X-SECTION',3X,'O2 X-SECTION',3X,'RAYLEIGH X-SECTION'//)
       DO 877 I=1,MPX
       WRITE(6,814) WLL(I),FILT(I),FIO(I),SG(I),SGO2(I),SGM(I)
  877  CONTINUE
       READ 2000, ITEST, EPSC
       READ 2000, MZZ, ZZO, DZZ
 2000  FORMAT(I5,2E12.4)
       WRITE(6,3001) ITEST,EPSC,MZZ,ZZO,DZZ
 3001  FORMAT(/T4,'ITEST = ',I4,' EPSC = ',F7.4,' MZZ = ',I5,
     1' ZZO = ',D10.3,' DZZ = ',D10.3/)
       READ 2009,(CCM(I),I=1,MZZ)
 2009  FORMAT(T2,7E9.2)
       DO 2500 II=1,NPP
       I=NPP+1-II
       ITT=0
       KK=(ZP(I)-ZZO)/DZZ+1
       IF(KK.LE.1) KK=1
       CO2(I)=CCM(KK)*DEXP((ZP(I)-(ZZO+DZZ*(KK-1)))*DLOG(CCM(KK+1)
     1/CCM(KK))/DZZ)
       CM(I)=CC2(I)/0.2095
       SUN=FAT(0.0,CO2(NPP),CM(NPP))
       FATO=DLOG(FOF(I))+SUN
       IF(FATO.LE.1.0E-5) FATO=1.0E-5
       C1=TNO(I)
       F1=FAT(C1,CO2(I),CM(I))
       C2=C1*0.75
       IF(C2.LE.1.0D10) C2=1.0D10
 2002  F2=FAT(C2,CO2(I),CM(I))
       IF(DABS(F2-F1).LE.1.0E-10) GO TO 2004
       C3=C1+(FATO-F1)*(C2-C1)/(F2-F1)
       IF(DABS(C3).GE.1.0E35) GO TO 2004
       ITT=ITT+1
       IF(DABS((C3-C2)/C2).LE.EPSC) GO TO 2004
       IF((ITT-ITEST).GT.1) GO TO 2004
       IF(DABS((F1-FATO)/(F2-FATO)).LE.1.0) GO TO 2003
       F1=F2
       C1=C2
 2003  C2=C3
       GO TO 2002
 2004  CONTINUE
       TNO(I)=C3
       IF(C3.LT.0.0) TNO(I)=0.0
 2500  CONTINUE
C*****************************************************************
C*                    PART-4
C*
C*  THIS PART FITS A PARABOLA THROUGH TANGENT RAY HEIGHT ZP COMPUTED
C*  IN PART-1 VS. TOTAL INTEGRATED NUMBER DENSITY TNO COMPUTED IN PART
C*  -3. THEN USING LEAST SQUARE COEFFICIENTS, INVERSION IS CARRIED ON
C*  TO COMPUTE THE NUMBER DENSITY. THIS NUMBER DENSITY IS, THEN, USED
C*  IN THE CALCULATION OF MOLECULAR OXYGEN TEMPERATURE.
C*****************************************************************
```

```
      2501   NP=NPP
             DO 1211 I=1,NPP
             Z(I)=ZP(I)
      1211   XN(I)=TNC(I)
             PI=3.1415926536
      C      THIS SECTION OBTAINS THE COEFFICIENTS FOR LEAST SQUARE PARABOLA
             M=8
             WRITE(6,21) M
        21   FORMAT('1','     SMOOTHING WITH M=',I3//)
             WRITE(6,123)
             CALL PARAB(M)
       123    FORMAT('     IGNORE TEMP. IN OZONE RESULTS'//)
        12   FORMAT(5X,6E12.4)
             N1=NP-1
             DO 4 J=1,N1
             DEN(J)=0.0
             DO 5 I=J,N1
              D=2.*A(I)
         5   DEN(J)=DEN(J)+D*(DSQRT(R(I+1)**2-R(J)**2)-DSQRT(R(I)**2-R(J)**2)
            1+(B(I)-2.*A(I)*RO(I))* DLOG((R(I+1)+DSQRT(R(I+1)**2-R(J)**2))/
            2(R(I)+DSQRT(R(I)**2-R(J)**2)))
             DEN(J)=-DEN(J)/PI
         4   CONTINUE
             WRITE(6,601) L1,L2,T1
       601    FORMAT(5X,'LOCAL STARTING TIME',I6,'HOUR,',I6,'MINUTE,'
            1F7.3,'SECONDS.')
             WRITE(6,23)
        23    FORMAT(//10X,'HEIGHT',9X,'NUMBER',9X,'TEMP.',10X,'LAT.',11X,
            1'LONG.',10X,'COLUMN',10X,'NORMALIZED',10X,'O2 COLUMN DENSITY',
            2/11X,'IN CM.',8X,'DENSITY',8X,'IN DEG. K.',5X,'IN DEG.',8X,
            3'IN DEG.',8X,'DENSITY',9X,'INTENSITY',11X,'DENSITY',/)
             N1=N1-1
             DO 977 J=1,N1
             T(J)=0.0
             DO 150 I=J,N1
             A2=DEN(I+1)/(R(I+1)**2)
             A1=DEN(I)/(R(I)**2)
             A1=DABS(A1)
             A2=DABS(A2)
        150   T(J)=T(J)+(A2-A1)/DLOG(A2/A1)*(Z(I+1)-Z(I))
             T(J)=(3.8038D-4)*T(J)/DEN(J)
             T(J)=T(J)*RO(I)*RO(I)
        977   WRITE(6,22) Z(J),DEN(J),T(J),PHIO(J),ALAMO(J),XN(J),FOF(J),CO2
        22    FORMAT(4X,6E15.6,E18.6,E19.6)
             STOP
       978   DO 911 J=1,N1
             UD(J)=DEN(J)
             UZ(J)=Z(J)
             UT(J)=T(J)
        911  IF (UD(J) .LE. 0.0) UD(J)=1.0E 01
             UYMIN=7.0
             UYEX=0.5
             UXMIN=40.0E 05
             UDX=20.0E 05
             IF (IO2 .EQ. 0) GO TO 1531
             CALL PLTOFS(100.0,100.0,UXMIN,UDX,1.5,1.0)
             UPX=100.
             UPDX=100.
             CALL PAXIS(1.5,1.,16HTEMP. IN DEG. K.,-16,10.,0.,UPX,UPDX,-1.)
             CALL PAXIS(1.5,1.,15HALTITUDE IN CM.,15,8.,90.,UXMIN,UDX,-0.5)
```

```
      CALL PLOT1D(1.5,1.0,0.5,0.5,20,15)
      CALL PLINE(UT(1),UZ(1),N1,1,1,1,2,1)
      CALL PSYMB(1.5,9.5,-0.1,Q(1),0.0,80)
      IF (M .EQ. 4) GO TO 1530
      CALL PSYMB(1.5,9.25,-0.1,3HM=8,0.0,3)
      GO TO 1532
 1530 CALL PSYMB(1.5,9.25,-0.1,3HM=4,0.0,3)
 1532 CALL PLTEND
 1531  CONTINUE
      CALL PLTOFS(UYMIN,UYEX,UXMIN,UDX, 1.5, 1.0)
      CALL PLGAXS(1.5,1.0,14HNUMBER DENSITY,-14,10.0,0.0,UYMIN,-UYEX)
      CALL PAXIS(1.5,1.0,15HALTITUDE IN CM.,15,8.0,90.0,UXMIN,UDX,-0.5
      CALL PLGGRD(1.5,1.0,1.0/UYEX,10.0,8.0,0.0)
      CALL PGRID(1.5,1.0,10.0,0.5,1,15)
      CALL PLTLOG(2)
      CALL PLINE(UD(1),UZ(1),N1,1,1,1,2,1)
      CALL PLTREC
      CALL PSYMB(1.5,9.5,-0.1,Q(1),0.0,80)
      IF ( M .EQ. 4) GO TO 912
      CALL PSYMB(1.5,9.25,-0.1,3HM=8,0.0,3)
      GO TO 913
  912 CALL PSYMB(1.5,9.25,-0.1,3HM=4,0.0,3)
  913 CALL PLTEND
    6  CONTINUE
      CALL EXIT
      END
C*************************************************************************
C*                    PART-5
C*
C*  SUBROUTINE SET TAKES 5 EQUIDISTANT VALUES AND FITS A LEAST SQUARE
C*  PARABOLA Y=P*X*X + Q*X + R . COEFFICIENTS P,Q AND R ARE RETURNED
C*************************************************************************
      SUBROUTINE SET(Y1,Y2,Y3,Y4,Y5,P,Q,R,S)
      IMPLICIT REAL*8(A-H,O-Z)
      COMMON Z(200),XN(200),A(200),B(200),C(200),ALT,WLL(100),FILT(10(
     1FIO(100),SG(100),SGO2(100),SGM(100),CCM(200),NP,MPX

      P=((2.*Y1)-Y2-(2.*Y3)-Y4+(2.*Y5))/14.
      Q=((-146.*Y1)+(46.*Y2)+(120.*Y3)+(74.*Y4)-(92.*Y5))/140.
      R=((126.*Y1)-(56.*Y3)-(42.*Y4)+(42.*Y5))/70.
      RETURN
      END
C*************************************************************************
C*                    PART-6
C*
C*  SUBROUTINE HEIGHT CALCULATES THE RADIUS OF EARTH RR, AND DISTANT
C*  RP OF A POINT FROM CENTER OF EARTH; WHEN LATTITUDE PHI, AND ALTIT
C*  ALT, OF THE POINT ARE KNOWN.
C*************************************************************************
      SUBROUTINE HEIGHT(PHI,RP,RR)
      IMPLICIT REAL*8(A-H,O-Z)
      COMMON Z(200),XN(200),A(200),B(200),C(200),ALT,WLL(100),FILT(10(
     1FIO(100),SG(100),SGO2(100),SGM(100),CCM(200),NP,MPX
      REAL*8 KAPPA



      EC=.0818202
      R=6378.387
      DENOM=DSQRT(1.-(EC*EC*DSIN(PHI)*DSIN(PHI)))
```

```
      RCOS=DCOS(PHI)*R/DENOM
      RSIN=R*(1.-EC*EC)*DSIN(PHI)/DENOM
      RR=DSQRT(RCOS*RCOS+RSIN*RSIN)
      PHIP=DARSIN(RSIN/RR)
      KAPPA=3.1415926536
      RP=DSQRT(RR*RR+ALT*ALT-2.*RR*ALT*DCOS(KAPPA))
      RETURN
      END
C*****************************************************************
C*                    PART-7
C*
C*  SUBROUTINE PARAB FITS THE LEAST SQUARE PARABOLA THROUGH M POINTS
C*  AT A TIME IN THE CURVE OF Z VS. XN. THE PROCESS IS CONTINUED FOR
C*  NP POINTS AND COEFFICIENTS A,B AND C ARE RETURNED TO MAIN PROGRAM
C*  NOTE THAT XN=A*Z*Z + B*Z + C
C*****************************************************************
      SUBROUTINE PARAB(M)
      IMPLICIT REAL*8(A-H,O-Z)
      COMMON Z(200),XN(200),A(200),B(200),C(200),ALT,WLL(100),FILT(100)
     1FIO(100),SG(100),SGO2(100),SGM(100),CCM(200),NP,MPX
      L=M/2
      DO 2 I=1,NP
      IZ=NP+1-L
      K=1
      IF(I.GT.L.AND.I.LT.IZ) K=I-L
      IF(I.GE.IZ) K=NP-M
      ZB=0.
      Z2B=0.
      Z3B=0.
      Z4B=0.
      XNB=0.
      ZNB=0.
      Z2NB=0.
      K2=K+M
      DO 3 J=K,K2
      ZB=ZB+Z(J)
      Z2B=Z2B+Z(J)**2
      Z3B=Z3B+Z(J)**3
      Z4B=Z4B+Z(J)**4
      ZNB=ZNB+Z(J)*XN(J)
      Z2NB=Z2NB+XN(J)*(Z(J)**2)
3     XNB=XNB+XN(J)
      J=I
      M1=M
      M=M+1
      A(J)=((M*ZNB-XNB*ZB)*(M*Z3B-ZB*Z2B)-(M*Z2NB-XNB*Z2B)*(M*Z2B-ZB**
     1)/((M*Z3B-Z2B*ZB)*(M*Z3B-ZB*Z2B)-(M*Z4B-Z2B**2)*(M*Z2B-ZB**2))
      D=A(J)
      B(J)=((M*ZNB-ZB*XNB)-(M*Z3B-ZB*Z2B)*D)/(M*Z2B-ZB*ZB)
      E=B(J)
      C(J)=(XNB-D*Z2B-E*ZB)/M
      M=M1
2     CONTINUE
      RETURN
      END
      FUNCTION CAL(X,A,B,C,D)
      IMPLICIT REAL*8(A-H,O-Z)
      CAL=(A*X**2)+(B*X)+C
       RETURN
      END
```

```
      FUNCTION FAT(CO3,CO2,CM)
      IMPLICIT REAL*8(A-H,O-T,V-Z)
C
C     THIS FUNCTION GENERATES THE SIGNAL OF A STAR AS SEEN THROUGH AN
C     ATMOSPHERE WITH COLUMN DENSITIES CO3,CO2,CM AND VIEWED THROUGH
C     FILTER WITH TRANSMISSION FILT(I) AT WAVELENGTH WLL(I)
C
      COMMON Z(200),XN(200),A(200),B(200),C(200),ALT,WLL(100),FILT(10
     1FIO(100),SG(100),SGO2(100),SGM(100),CCM(200),NP,MPX
      X=SG(1)*CO3+SGO2(1)*CO2+SGM(1)*CM
      IF(DABS(X).GT.50.) X=50.
      X1=FILT(1)*FIO(1)*DEXP(-X)
      FAT=0.0
      DO 10 I=2,MPX
      X=SG(1)*CO3+SGO2(I)*CO2+SGM(I)*CM
      IF(DABS(X).GT.50.) X=50.
      X2=FILT(1)*FIO(I)*DEXP(-X)
      FAT=FAT+0.5*(X1+X2)*(WLL(I)-WLL(I-1))
10    X1=X2
      FAT=DLOG(FAT)
      RETURN
      END
 160.12    160.69    161.26    161.84    162.42
-26.32    -27.06    -27.30    -27.53    -27.76
 778.6     778.7     778.9     779.0     779.1
 298.4833  300.9916  303.4983  306.005   308.5116
 28.0      55.0      26.01582
 0.0       6.0       53.1338
 13.0      29.0      32.0        065
1800.3000.    00
 .020 .021 .022 .024 .026 .030 .035 .040 .048 .055 .060
 .070 .080 .090 .100 .130 .160 .200 .260 .360 .420 .520
 .620 .740 .840 .940 .9901.000 .980 .940 .880 .840 .800
 .780 .740 .680 .640 .600 .500 .400 .360 .300 .240 .200
 .170 .140 .120 .100 .080 .060 .050 .042 .040 .037 .035
 .033 .030 .028 .025 .023 .020
  7.80E-19  7.50E-19  7.00E-19  6.50E-19  5.80E-19  5.20E-19
  4.70E-19  4.30E-19  3.80E-19  3.40E-19  3.20E-19  3.20E-19
  3.30E-19  3.60E-19  4.30E-19  5.20E-19  6.60E-19  8.80E-19
  1.10E-18  1.40E-18  1.80E-18  2.20E-18  2.70E-18  3.20E-18
  3.90E-18  4.50E-18  5.20E-18  5.80E-18  6.60E-18  7.40E-18
  8.00E-18  9.00E-18  1.00E-17  1.01E-17  1.10E-17  1.20E-17
  1.20E-17  1.15E-17  1.10E-17  1.08E-17  1.05E-17  1.00E-17
  9.80E-18  9.00E-18  8.20E-18  7.60E-18  6.80E-18  6.00E-18
  5.00E-18  4.50E-18  4.00E-18  3.40E-18  2.70E-18  2.30E-18
  1.90E-18  1.50E-18  1.20E-18  9.00E-19  7.00E-19  5.40E-19
  3.95E-19
    18  20    20  18    20  20    22  22    22  22    24
   24  26    26  26    28  30    32  32    34  36    36
   40  38    38  38    40  36    34  34    32  30    32
   30  32    30  34    34  30    32  32    32  32    34
   38  34    34  34    36  34    36  36    36  36    36
   36  36    38  38    38  40
  1.00E-19  9.00E-20  5.00E-20  3.00E-20  1.30E-20  3.00E-22  1.35E-
  7.40E-23  4.80E-23  3.30E-23  2.55E-23  2.10E-23  1.75E-23  1.50E-
  1.30E-23  1.17E-23  1.05E-23  9.55E-24  8.00E-24  7.40E-24  6.65E-
  6.20E-24  5.65E-24  5.15E-24  4.60E-24  4.15E-24  3.55E-24  2.20E-
  2.70E-24  2.30E-24  1.95E-24  1.70E-24  1.45E-24  1.28E-24  1.12E-
  0.        0.        0.        0.        0.        0.        0.
  0.        0.        0.        0.        0.        0.        0.
```

```
538         0.          0.          0.          0.          0.          0.          0.
539         0.          0.          0.          0.          0.
540         100         .0100
541         116         23.D5       1.D5
OF FILE
```

Part 1: Line numbers 1-125

In this part, the spacecraft position values are entered for use in interpolation. There are five such values for longitude, latitude, and altitude furnished by GSFC several weeks after the occultation. The first of these five values corresponds to the time (given at a 10-second interval) which is less than but nearest to the starting time. The Greenwich hour angle of Aries is then read in for five times spaced ten minutes apart and centered upon the time less than but nearest to the starting time. Star position information is also entered, followed by the starting time and the number of data points. The position of the data point is computed from the above inputs, using subroutines HEIGHT and SET and function CAL. Program comments for Part I give additional details.

Notation

DEC = declination of star, in radians
RA = right ascension of star, in radians
NP, NPP = number of data points in scan
PHIS = latitude of subsatellite point in radians
ALT = altitude of spacecraft, in cm
ALAMS = longitude of subsatellite point, in radians
ALAMG = Greenwich hour angle of Aries, in radians
RSAT, RP = distance of subsatellite point from Earth's center, in cm
ROO, R = distance of data point from Earth's center, in cm
HO, ZP = height of data point, in cm
RO, RR = radius of Earth along a line to the data point, in cm
PHIO = latitude of data poins, in degrees
ALAMO = longitude of data point, in degrees
T1, T2, T3, TX, X, S = temporal variables

Part 2: Line numbers 126-180

In this part, the filter transmission values, the appropriate absorption cross section, and the star spectrum are entered for the pertinent wave band at a 20 Å interval. A normalization factor for the signal intensity is computed and a table of normalized signal intensity v. tangential column density (integrated number density) is formed. The latter values are already stored in file CROSSDAT.

Notation

NTAB	=	number of tabular points
FX	=	beginning wavelength of band, in Å
FY	=	final wavelength of band, in Å
IO2	=	switch for gaseous species and absorption cross section (1:ozone, 2:O_2, 3:O_2 with Hudson's cross section)
MPX	=	number of wavelength intervals in band
WLL	=	wavelength
FILT	=	normalized value of filter transmission
SG	=	absorption cross section, in cm^2
FIO	=	spectral star intensity, in digital voltmeter counts/time interval
SUN	=	normalizing factor, in counts/time interval
TT, TN	=	tabular tangential column density, in cm^{-2}
SUM	=	filtered signal intensity integrated over wavelength, in counts/time interval
FNR, FNO	=	tabular, normalized signal intensity corresponding to TT

Part 3: Line numbers 181-233

In this part, a comment card is read which identifies the occultation data. The data are then entered, the background noise (minimum signal) is removed, and the data are normalized. Using (m+1) smoothing points, a logarithmic interpolation is performed in subroutine PARAB to get the least squares coefficients for the column densities corresponding to the "modified input data."

Notation

DA	=	star intensity observed during occultation, in counts/time interval
DMIA	=	minimum value of DA
FOF	=	normalized, measured signal intensity
TNO	=	column density along stellar ray path in cm^{-2}
A, B, C	=	least squares coefficients for a parabolic fit
M	=	one less than the number of smoothing points taken for a least squares fit

Part 3A: Line numbers 234-288 (for ozone only)

In this part, a correction to the ozone column density is made for the removal of Herzberg and Rayleigh scattering. To accomplish this, a functional inversion of F(r) is necessary, where

$$F(r) = \frac{\int_0^\infty T(\lambda)I_o(\lambda)\exp\left[-\sigma_{O_2}(\lambda)N_{O_2}(r)-\sigma_M(\lambda)N_M(r)-\sigma_{O_3}(\lambda)N_{O_3}(r)\right]d\lambda}{\int_0^\infty T(\lambda)I_o(\lambda)d\lambda}$$

F	=	normalized signal intensity
T	=	filter transmission
I_o	=	spectral stellar intensity
σ_i	=	cross-sectional value of i^{th} species or of molecular scattering (M), in cm^2
N_i	=	tangential column density of i^{th} species (N_M = total for all species), in cm^{-2}

The desired quantity is $N_{O_3}(r)$. To carry out this operation, $\sigma_{O_2}(\lambda)$ is read in for the ozone band being considered e. g., 1800-3000 Å, with the Herzberg continuum being included. $\sigma_n(\lambda)$ is then computed for the same wavelength region from Rayleigh's formula,

$$\sigma_R(\lambda) = 3.981 \times 10^{-28}(10^{-4}\lambda)^{-4.05} cm^2 \quad (\lambda \text{ in Å})$$

Some representative values of O_2 tangential column density are read in at a 5-km interval from 10 km to 310 km, and exponential interpolation is employed to find this quantity at each data point height. It is then converted to total tangential column density for all species and the final value of N_{o_3} is reached through Newton's inerative method. In this method, an initial guess of N_M is made for the value of $N_{o_3}^{(o)}$ and function "FAT" produces a signal F_1 which is depleted by passage through an atmosphere with tangential column densities N_{o_3}, N_{o_2} and N_M and through the filter. The second guess $N_{o_3}^{(1)}$ reduces $N_{o_3}^{(0)}$ by one quarter, and if the resulting signal F_2 is close enough to F_1 we have the N_{o_3} which is sought. Otherwise, a new $N_{o_3}^{(j)}$ is computed by the formula

$$N_{o_3}^{j} = N_{o_3}^{j-2} + (F_o - F_{j-1})(N_{o_3}^{j-1} - N_{o_3}^{j-2})/(F_j - F_{j-1})$$

where F_o is the sum of the "FAT" functional evaluation for the case where $N_{o_3} = 0$ (actually a new normalizing factor) and the log of the signal corresponding to N_M. A second tolerance test is provided by $\left|(N_{o_3}^{j} - N_{o_3}^{j-1})/N_{o_3}^{j-1}\right| \leq \epsilon$ and a limit is placed on the number of iterations. The data points are taken from top to bottom and certain safeguards are included for computational instability encountered at the lowest levels.

Notation		
SGO2	=	O_2 cross section (σ_{o_2}), in cm^2
SGM	=	Rayleigh scattering cross section (σ_M), in cm^2
ITEST	=	maximum number of iterations
ITT	=	iteration counter
EPSC	=	tolerance
MZZ	=	number of values in interpolation table for O_2 column density
ZZO	=	base height of interpolation table, in cm
DZZ	=	vertical interval in table, in cm

Notation (cont'd)

CCM = tabular O_2 column density, in cm^{-2}

CO_2 = interpolated O_2 column density (NO_2), in cm^{-2}

CM = total column density (N_M), in cm^{-2}

SUN = new normalizing factor

FATO(F_o), C1($N_{O_3}^{j-2}$), C2($N_{O_3}^{j-1}$), C3($N_{O_3}^{j}$), F1(F_{j-1}), F2(F_j)
= parameters in Newton's method

Part 4: Line numbers 289-383

Using subroutine PARAB, the coefficients are obtained for fitting a curve of total tangential column density against tangent ray height, and the mathematical inversion is performed to get number density. Please refer to the notes on the O_2 error analysis for details on this procedure as well as the computation of temperature.

A STOP statement (line 342) negates CALCOMP plotting. When STOP is removed, the plotter produces number density graphs for two smoothing values. When molecular oxygen is being investigated, it draws two additional graphs for temperature.

Notation

Z = height, in cm

XN = tangential column density, in cm^{-2}

DEN = number density, in cm^{-3}

T = molecular temperature, in ^{o}K

Parts 5-7: Line numbers 384-499

Subroutine SET returns the coefficients after fitting a least squares parabola through five equidistant points, whereas subroutine PARAB fits any number of points which need not be equidistant. Additional information is available in the program comments and in notes by Mr. A. Shah.

Part 8: Line numbers 500-541

Sample data are listed for an ozone run. They are:

Line	
500	Longitude of spacecraft at a 10-sec interval, beginning with the value nearest to, but less than, the starting time of the scan, in deg
501	Latitude of spacecraft, ditto, in deg
502	Altitude of spacecraft, ditto, in km
503	Greenwich hour angle of Aries at a 10-min interval, centered around the value which is nearest to, but less than, the starting time of the scan, in deg
504	Declination of star in deg, min, sec
505	Right ascension of star in hr, min, sec
506	Starting time in hr, min, sec and number of data points
507	Beginning and ending wavelengths, in $\mathring{A}$, and species identifier
508-513	S2F5 filter
514-524	Ozone cross section, in cm^2
525-530	Stellar spectral values of intensity over the same wavelength intervals
531-539	Molecular oxygen cross section over the same wavelength intervals
540-541	Control values for corrections in Part 3A

Appendix III b.

This Appendix explains the procedure of finding a random number from a Poisson distribution as an additive scattering term. The procedure is made necessary by the fact that a Gaussian error distribution with a variance equal to the signal intensity causes negative values to occur at times when the scattered signal is superposed upon a basic signal as low as 5 counts/Δt.

The Poisson distribution gives the probability of the number of occurences of an event within a given time interval, e.g., 1 sec, and it is quite pertinent to the present case. A Poisson distribution, as described by the expression

$$p(n) = \exp\left[-t\right] \frac{t}{n!}$$

has the values shown in figure when t = 10, 1, and 0.1. n must be an integer, but t, the mean signal intensity, is a real number. Since we seek a random number from a Poisson distribution to be added to the signal as random noise, an inversion of the formula is desired. In lieu of this difficult inversion, we can search for a random number, y, $0 \leq y \leq 1$, which will permit an n to be generated such that $p(n) \leq y \leq p(n+1)$. When the inequality succeeds, n is accepted as the simulated signal intensity.

The procedure is employed successfully when the signal is between 10^{-1} and 10 counts/Δt. At lower values of the basic signal, the computer search for Poisson random variables becomes too time-consuming so the signal is then left intact.

Appendix IIIc.

This Appendix uses a simple flow chart and copies of error analysis programs with notes to give the details of the numerical error analysis for each of the species studied. Both single wavelength and broad waveband cases are considered.

The first flow chart applies to molecular oxygen, which is assumed to have a monotonically decreasing number density with increasing height. Following this figure is a program, "THREE", which handles the braodband filter case. Explanatory notes may be found at the end of the program.

The second flow chart applies to ozone, which is assumed to have a Gaussian-peaked feature superimposed upon a monotonically decreasing number density with increasing height. Following this figure is a program "OZNUM", which applies to the broadband filter. Explanatory notes for this program terminate the Appendix.

O_2

1. NUMERICAL SIMULATION

a. SINGLE WAVELENGTH

$N_0 = 2m^* e^{-\frac{h}{H}} r_0 K_1\left(\frac{r_0}{H}\right)$

$\frac{\partial T}{\partial z} = 0$

$100 \le h \le 180\,\text{KM}$

$m_0' = -\frac{1}{\pi}\frac{d}{dr}\int_r^\infty \frac{r}{r_0} N(r_0)(r_0^2 - r^2)^{-\frac{1}{2}} dr_0$

$m_0 = m_z^* e^{-\frac{h}{H}}$

$100 \le h \le 180\,\text{KM}$

$\frac{m_0' - m_0}{m_0}(h)$

b. BROADBAND

$(I_s)_{1280\text{-}1920\,\text{Å}}$

$N_0 = 2m^* e^{-\frac{h}{H}} r_0 K_1\left(\frac{r_0}{H}\right)$

$\frac{\partial T}{\partial z} = 0$

$80 \le h \le 260\,\text{KM}$

$F_0 = \phi I_s e^{-\sigma N_0}$

$80 \le h \le 260\,\text{KM}$

$N_0 = A(\ln F_0)^2 + B(\ln F_0) + C$

$F_0 + \Delta F_0$

(α)

(α)

$m_0' = -\frac{2}{\pi}\frac{d}{dr}\int_r^\infty \frac{r}{r_0} N(r_0)(r_0^2 - r^2)^{-\frac{1}{2}} dr_0$

$m_0 = m^* e^{-\frac{h}{H}}$

$80 \le h \le 260\,\text{KM}$

$\frac{m_0' - m_0}{m_0}(h)$

MEAN, STD. DEV. 30 CASES ΔF_0

T = TEMPERATURE

SUBSCRIPT 0 → DATA POINT HEIGHT

N = COLUMN DENSITY

m^* = NUMBER DENSITY AT A REFERENCE LEVEL

h = HEIGHT ABOVE A REFERENCE LEVEL

H = SCALE HEIGHT OF AN ISOTHERMAL ATMOSPHERE

r = DISTANCE FROM EARTH'S CENTER

I_s = STELLAR RADIATION INTENSITY

F = SIGNAL INTENSITY

ϕ = FILTER FACTOR

σ = ABSORPTION CROSS-SECTION

A B C = COEFFICIENTS FOR LEAST SQUARES FITTING

```
IC SAFF                'MAURICE GRAVES'
LAST SIGNON WAS: 09:59.31   01-22-71
SER "SAFF" SIGNED ON AT  18:32.09 ON 01-23-71
IST THESE(1,5C)
      C      MOLECULAR OXYGEN NUMERICAL ERROR ANALYSIS, BROADBAND FILTER
      C
            IMPLICIT REAL*8(A-H,O-Z)
            DIMENSION SG(100),WL(100),FIC(100),FILT(100),GNUMB(400),XHL(400)
           1DEN(400),DERR(400),ZKM(400),DERRA(400),DERRSQ(400),EMEAN(400),
           2SIGMA(400),F(16)
            COMMON FSUB(400)
            COMMON Z(400),XN(400),A(400),B(400),C(400),XP(4),FNC(400),
           1FCP(400),TWW(400),TNC(400),FC,XNC,RE,NP
            DATA DERRA,DERRSQ/800*0./
            SF=10.05
            VM=1.0
            WLO=5000.0-8
            TF=21000.
            FCO=1.785D15
            PI=3.1415927
            RE=6371.05
            FC=61.05
            FP=80.05
            XNC=8.72D13
            NP=211
            NPP=181
            NFF=NPP
            FCP=.505
            NN=2
            NH=1
            JIYMAX=6
            JIZMAX=6
            JIX=0
            JIY=0
            JIZ=0
      C
      C     WHEN NN=MMM, THE PROGRAM COMPUTES MEAN AND STANDARD DEVIATION
      C     OF PERCENTAGE ERROR AT 2KM SPACING FOR MM CASES.  WHEN
      C     NN .NE. MMM, THE PROGRAM COMPUTES PERCENTAGE ERROR AND TEMP.
      C     AT VARIOUS SPACINGS WITH RANDOM ERROR(NN=2) OR WITHOUT
      C     RANDOM ERROR(NN=1).
      C
            MM=5
            MMM=30
            IF(NN.EQ.MMM)WRITE(6,20)MM
     20      FORMAT(//21H   STATISTICS FOR MM=,I3/)
            IF(NN.EQ.MMM)NH=2
      C
      C     INPUT O2 CROSS SECTION(SG),WAVELENGTH INTERVAL(WL(J)),
      C     S4F1 FILTER TRANSMISSION(FILT)
      C
            READ 600,(SG(I),I=1,32)
     600     FORMAT(6E11C.2)
            DO 300 I=1,32
     300    WL(I)=1280.+(I-1)*20.
            READ 601,(FILT(I),I=1,32)
     601     FORMAT(11D5.3)
      C
      C     COMPUTE BLACKBODY STAR SPECTRUM AND ADJUST TO GET DESIRED
      C     MAXIMUM COUNT RATE
```

```
      C
            DO 301 I=1,52
            FIO(I)=DEXP(-(.921*WL(I)+19.3875))*(WL(I)**5)/((WL(I)*1.D-8)**5)*(DEX
           1P(1.438/(WL(I)*1.D-8*TF))-1.)/(DEXP(1.438/(WL(I)*1.D-8*TF))-1.)*(1.D-7)
            FIO(I)=FIO(I)*FOO
      301   CONTINUE
      C
      C     COMPUTE NORMALIZATION FACTOR
      C
            SUN=0.
            DO 302 J=2,52
      302   SUN=SUN+((FILT(J)*FIO(J)+FILT(J-1)*FIO(J-1))/2.*(WL(J)-WL(J-1)))
            WRITE(6,303) SUN
       303   FORMAT(F10.4)
            RO=210.05/(NP-1)
      C
      C     FORM A TABLE OF COLUMN DENSITY(TT) VERSUS SIGNAL INTENSITY
      C     (SUM) BASED UPON AN INTEGRATION OF THE FORMULA FOR TT WHICH
      C     ASSUMES SPHERICAL STRATIFICATION AND AN ISOTHERMAL ATMOSPHERE
      C
            DO 800 IHO=1,NP
            SUM=0.
            RO=RE+HO+(IHO-1)*HD
            ZO=RO-RE
            IF(IHO.EQ.182) XNO=5.D13
            IF(IHO.EQ.183) XNO=3.D13
            IF(IHO.EQ.184) XNO=1.D13
            DO 701 I=185,210
            XK=(I-184)/2.
       701   IF(IHO.EQ.I) XNO=1.D13/1.01**XK
            TT=XNO*DEXP(-(ZO-80.05)/SH)*DSQRT(1.57079*SH*RO)
           1*(1.+3.*SH/(8.*RO)-15./32.*(SH/RO)**2+315./216.*(SH/RO)**3)
            IF(IHO.EQ.211) TT=1.D-10
            TT(IHO)=TT
            DO 1000 J=2,52
      1000  SUM=SUM+((FILT(J)*FIO(J)*DEXP(-SG(J)*TT)+FILT(J-1)*FIO(J-1)*
           1DEXP(-SG(J-1)*TT))/2.)*(WL(J)-WL(J-1))
            FNO(IHO)=SUM/SUN
            FSUB(IHO)=SUM
       800   CONTINUE
            IF(NN.EQ.2)GO TO 802
      C
      C     LOOP FOR NO RANDOM ERRORS IN SIGNAL INTENSITY AND VARIOUS
      C     DATA POINT SPACINGS
      C
            DO 7 JIZ=1,JI/MAX
            DO 602 IH=1,NPP,NH
            FOF(IH)=FNO(IH)
            WRITE(6,501)IH,IWW(IH),FNO(IH),FOF(IH)
       501   FORMAT(T2,I5,3015.6)
       602   CONTINUE
            GO TO 806
       802   CONTINUE
            IF(MM.NE.MMM)GO TO 803
      C
      C     LOOP FOR ACCRUING ERRORS IN O2 DENSITY RESULTING FROM
      C     RANDOMLY SCATTERED SIGNAL INTENSITY, FOR MANY CASES,
      C     WITH A SINGLE DATA POINT SPACING
      C
            DO 18 JIX=1,MM
```

```
  803   CONTINUE
C
C     SET UP FOR GAUSS SSP AND RANDU SSP
C
      IX=203+100*(JIX-1)
      IF(MM.NE.MMM)IX=201
      JX=IX
      AM=0.
      P(1)=0.
      IF(MM.EQ.MMM)GO TO 804
C
C     LOOP FOR RANDOM ERRORS IN SIGNAL INTENSITY AND VARIOUS
C     DATA POINT SPACINGS
C
      DO 28 JIY=1,JIYMAX
  804  DO 810 IH=1,NPP,NH
      SUM=FSUB(IH)
      IF(SUM.LT.10.)GO TO 9
      SD=DSQRT(SUM)
      CALL GAUSS(IX,SD,AM,V)
      FOF(IH)=(SUM+V)/SUN
  503  IF(FOF(IH).GE.1.)FOF(IH)=1.-1.D-5
      IF(FOF(IH).LT.FNO(1))FOF(IH)=FNO(1)+1.D-12
      N=100
      GO TO 809
   9   IF(SUM.LT..1)FOF(IH)=FNO(IH)
      IF(SUM.LT..1)N=0
      IF(SUM.LT..1)GO TO 809
C
C     DETERMINE A RANDOM NUMBER FROM A POISSON DISTRIBUTION
C     WHEN .1<SIGNAL INTENSITY<10.
C
      NMAX=SUM+5.
      F=DEXP(-SUM)
      P(2)=SUM*F
   2   GSUM=P(2)
      CALL RANDU(JX,JY,YFL)
      DO 1 N=2,NMAX
      IF(N.EQ.2)GO TO 10
      U=SUM**(N-1)*F
      D=1.
      II=N-2
      DO 3 J=1,II
   3   D=(N-J)*D
      GSUM=GSUM+U/D
      P(N)=GSUM
  10     IF(P(N).GE.YFL.AND.P(N-1).LE.YFL)GO TO 12
      IF(MM.NE.MMM)WRITE(6,91)N,P(N-1),P(N),YFL
  91   FORMAT(I5,3F12.5)
   1   CONTINUE
  13   JX=JY
      GO TO 2
  12   JX=JY
      FOF(IH)=(N-2)/SUN
      IF(FOF(IH).LT.1.D-10)FOF(IH)=1.D-10
  809   IF(MM.NE.MMM)WRITE(6,805)IH,FOF(IH),FNO(IH),N,YFL
  805  FORMAT(I5,2D15.6,I5,F10.5)
  810  CONTINUE
  806  HDP=HDP*2.
      IF(MM.EQ.MMM)HDP=2.D5
```

```
      NPH=(NPH-1)/2+1
      IF(JIY.EQ.1)NPH=181
      IF(JIZ.EQ.1)NPH=181
      IF(MM.EQ.MMM)NPH=91
C
C     COMPUTE O2 NUMBER DENSITY FROM AN EXPONENTIAL MODEL
C     ATMOSPHERE FOR LATER COMPARISON WITH RETRIEVED VALUES
C
      DO 801 IHO=1,NPH
      RO=RE+HO+(IHO-1)*HDP
      CALL ATMOD(RO)
      ONUMD(IHO)=XP(2)
      RHTO(IHO)=RO
      ZKM(IHO)=RHTO(IHO)-RE
  801  CONTINUE
C
C     INTERPOLATE IN THE TABLE TO FIND COLUMN DENSITY(TNO) FROM
C     A SIGNAL INTENSITY(FOF) WHICH IS A SIMULATION OF THE
C     MEASURED SIGNAL
C
      DO 502 J=1,NP
      Z(J)=DLOG(FNO(J))
      XN(J)=DLOG(TWW(J))
  502  CONTINUE
      M=8
      IF(NN.EQ.1)M=2
      CALL PARAB(M)
      DO 630 L=1,NPP,NH
      DO 612 I=1,NP
      IF(FOF(L).GE.FNO(I).AND.FOF(L).LT.FNO(I+1))GO TO 613
  612 CONTINUE
  613 J=I
      X=DLOG(FOF(L))
      TNO(L)=A(J)*X*X+B(J)*X+C(J)
      TNO(L)=DEXP(TNO(L))
  630  CONTINUE
C
C     INVERT COLUMN DENSITY(TNO) TO GET O2 NUMBER DENSITY(DEN)
C
      DO 700 J=1,NPH
      Z(J)=ZKM(J)
      K=J*NH-(NH-1)
  700  XN(J)=TNO(K)
      M=8
      IF(NN.EQ.1)M=2
      CALL PARAB(M)
      N1=NPH-1
      DO 4 J=1,N1
      DEN(J)=0.
      DO 5 I=J,N1
      D=2.*A(I)
    5 DEN(J)=DEN(J)+D*(DSQRT(RHTO(I+1)**2-RHTO(J)**2)-DSQRT(RHTO(I)**
     1RHTO(J)**2))+(B(I)-2.*A(I)*RE )*DLOG((RHTO(I+1)+DSQRT(RHTO(I+1)
     2-RHTO(J)**2))/(RHTO(I)+DSQRT(RHTO(I)**2-RHTO(J)**2)))
      DEN(J)=-DEN(J)/PI*2.
C
C     COMPUTE ERROR AND ACCRUE ERROR SUMS
C
      DERR(J)=(DEN(J)-ONUMD(J))/ONUMD(J)
      DERRSQ(J)=DERRSQ(J)+DERR(J)*DERR(J)
```

```
      DERRA(J)=DERRA(J)+DERR(J)
    4 CONTINUE
      WRITE(6,85)JIZ,JIY,JIX
   85  FORMAT(/3I5)
      IF(MM.EQ.MMM)GO TO 18
      WRITE(6,24)NPH
   24  FORMAT(//26H   NUMBER OF DATA POINTS =,I3/)
      WRITE(6,25)NP
   25  FORMAT(/29H   NUMBER OF TABULAR POINTS =,I3//)
   26  WRITE(6,23)
   23 FORMAT(//15X,1HZ,14X,1HT,14X,3HNO2,12X,4HCNO2,14X,4HDERR//)
      C
      C     COMPUTE TEMPERATURE FROM A FORM OF THE HYDROSTATIC LAW
      C
      N1=N1-1
      DO 6 J=1,N1
      T=0.
      DO 7 I=J,N1
      A2=DEN(I+1)/(RHTO(I+1)**2)
      A1=DEN(I)/(RHTO(I)**2)
      A1=DABS(A1)
      A2=DABS(A2)
    7  T=T+(A2-A1)/DLOG(A2/A1)*(ZKM(I+1)-ZKM(I))
      T=(3.8038E-4)*T/DEN(J)
      T=T*RHTO(I)*RHTO(I)
      IF(MM.NE.MMM)WRITE(6,22)ZKM(J),T,DEN(J),ONUMD(J),DERR(J)
   22 FORMAT(10X,5D15.6)
    6  CONTINUE
      NH=NH*2
      IF(MM.EQ.MMM)NH=2
      IF(NN.EQ.1)GO TO 8
      IF(MM.EQ.MMM)GO TO 18
   28  CONTINUE
      IF(NN.EQ.2.AND.MM.NE.MMM)GO TO 83
   18  CONTINUE
      IF(MM.EQ.MMM)GO TO 79
    8  CONTINUE
      IF(MM.NE.MMM)GO TO 80
   79  WRITE(6,82)
   82  FORMAT(//8X,1HZ,10X,10HMEAN ERROR,7X,5HSIGMA,10X,5HSUMSQ,
     111X,3HSUM/)
      C
      C     COMPUTE STATISTICS FROM ACCRUED SUMS
      C
      DO 80 J=1,N1
      DMEAN(J)=DERRA(J)/(MM*1.)
      SIGMA(J)=DSQRT(DERRSQ(J)/(MM*1.)-DMEAN(J)*DMEAN(J))
      WRITE(6,81)ZKM(J),DMEAN(J),SIGMA(J),DERRSQ(J),DERRA(J)
   81  FORMAT(5D15.6)
   80  CONTINUE
   83  CALL EXIT
      END
      SUBROUTINE PARAB(M)
      C
      C     PARAB FINDS THE SECOND ORDER LEAST SQUARES COEFFICIENTS
      C     A,B, AND C FOR INPUT VECTORS Z AND XN, USING M+1 SMOOTHING
      C     POINTS
      C
      IMPLICIT REAL*8(A-H,O-Z)
      COMMON FSUB(400)
```

```
      COMMON Z(400),XN(400),A(400),B(400),C(400),XP(4),FNO(400),
     1FOF(400),TWW(400),TNO(400),HO,XNO,RE,NP
      L=M/2
      DO 2 I=1,NP
      IZ=NP+1-L
      K=1
      IF(I.GT.L.AND.I.LT.IZ)K=I-L
      IF(I.GE.IZ)K=NP-M
      ZB=0.
      Z2B=0.
      Z3B=0.
      Z4B=0.
      XNB=0.
      ZNB=0.
      Z2NB=0.
      K2=K+M
      DO 3 J=K,K2
      ZB=ZB+Z(J)
      Z2B=Z2B+Z(J)**2
      Z3B=Z3B+Z(J)**3
      Z4B=Z4B+Z(J)**4
      ZNB=ZNB+Z(J)*XN(J)
      Z2NB=Z2NB+XN(J)*(Z(J)**2)
3     XNB=XNB+XN(J)
      J=I
      M1=M
      M=M+1
      Y=(M*Z3B-Z2B*ZB)*(M*Z3B-ZB*Z2B)-(M*Z4B-Z2B**2)*(M*Z2B-ZB**2)
      IF(DABS(Y).LT.1.D-40) A(J)=0.
      IF(DABS(Y).LT.1.D-40) GO TO 1
      A(J)=((M*ZNB-XNB*ZB)*(M*Z3B-ZB*Z2B)-(M*Z2NB-XNB*Z2B)*(M*Z2B-ZB*
     1)/((M*Z3B-Z2B*ZB)*(M*Z3B-ZB*Z2B)-(M*Z4B-Z2B**2)*(M*Z2B-ZB**2))
1      D=A(J)
      YY=M*Z2B-ZB**2
      IF(DABS(YY).LT.1.D-40) B(J)=0.
      IF(DABS(YY).LT.1.D-40) GO TO 11
      B(J)=((M*ZNB-ZB*XNB)-(M*Z3B-ZB*Z2B)*D)/(M*Z2B-ZB*ZB)
11     E=B(J)
      C(J)=(XNB-D*Z2B-E*ZB)/M
      M=M1
2     CONTINUE
      RETURN
      END
      SUBROUTINE ATMOD(RW)
C
C     ATMOD FINDS THE O2 NUMBER DENSITY AT ALTITUDE ZW
C
      IMPLICIT REAL*8(A-H,O-Z)
      COMMON FSUB(400)
      COMMON Z(400),XN(400),A(400),B(400),C(400),XP(4),FNO(400),
     1FOF(400),TWW(400),TNO(400),HO,XNO,RE,NP
      RE=6371.D5
      ZW=RW-RE
      XP(2)=8.72013*DEXP(-(ZW-80.D5)/10.D5)
      RETURN
      END
   2.50E-19  5.00E-19  1.50E-18  2.30E-18  8.00E-18  1.30E-17
   1.40E-17  1.41E-17  1.42E-17  1.30E-17  1.26E-17  1.10E-17
   1.00E-17  8.20E-18  7.00E-18  6.00E-18  4.50E-18  3.50E-18
   2.50E-18  1.80E-18  1.20E-18  8.00E-19  5.50E-19  3.50E-19
```

```
367       2.00E-19  1.60E-19  1.00E-19  8.00E-20  5.00E-20  3.00E-20
368       1.30E-20  7.00E-21
369     .040 .080 .120 .160 .230 .320 .440 .600 .700 .920 .980
370     .9901.000 .990 .980 .970 .960 .880 .780 .640 .500 .400
371     .320 .260 .200 .170 .110 .080 .060 .040 .030 .020
ND OF FILE
```

Part I: Line numbers 1-62

In this part, the initial parameter values are set and the input data are read.

Notation

SH = O_2 scale height for an isothermal atmosphere, in cm

VM = visual magnitude of star

WLO = reference wavelength for stellar spectrum, in cm

TF = Effective blackbody stellar temperature, in ^oK

FOO = adjusting factor for obtaining a desired fictitious count rate at the top of the scan

RE = average radius of the earth, in cm

HO, HP = base height of the O_2 profile, in cm

XNO = O_2 number density at the base height, in molecules/cm^3

NP = number of points in a formulated table of normalized signal v. column density. Note: column density = mass of species in a 1 cm^2 channel centered on the stellar ray, also called the total integrated number density.

NPP, NPH = number of data points in the profile

HDP = halfstepsize for computing O_2 densities in an exponential atmosphere, in cm

NN = switch for introducing random error into the signal intensity

NH = stepsize for computing O_2 number densities, in number of tabular data points

JIYMAX = limiting value of the number of data point spacings used, with random error in signal

JIZMAX = limiting value of the number of data point spacings used, without random error in signal

JIX, JIY, JIZ =counters

MM, MMM = switch for selecting one of three paths (see program comments)

SG = O_2 absorption cross sectional values in cm^2; the values are listed at the end of the program

WL = wavelength in cm

FILT = normalized values of S4F1 filter transmission; the values are listed after the SG values at the end of the program

FIO = stellar spectral intensity, in digital voltmeter counts/sec

Part II: Line numbers 63-96

In this part, a normalization factor for the signal intensity is computed and a table of normalized signal intensity v. column density (see NP under Notation, Part I) is formed. In making the table, arbitrary values of O_2 number density are selected which cover the expected range of values of the species profile. Then the expression for the column density, $N = 2\int_{r_0}^{\infty} n(r)\, r\,(r^2 - r_0^2)^{-\frac{1}{2}}\, dr$ is integrated numerically by an expansion of the modified Bessel function of the first kind, assuming an isothermal atmosphere:

$$N_0 = 2 n_0^* e^{-\frac{r_0 - r_0^*}{H}} r_0 K_1\left(\frac{r}{H}\right) = 2 n_0^* e^{-\frac{r_0 - r_0^*}{H}} \left(\frac{\pi H r_0}{2}\right)^{1/2} \left(1 + \frac{3}{8}\frac{H}{r_0} + \cdots\right)$$

n_o = number density

r_o = distance to the earth's center

H = scale height

K_1 = modified Bessel function of the first kind

Superscript * refers to the reference height, which is 80 Km in this case. Then the signal intensity corresponding to N is computed from the expression,

$$I = \int_0^{\infty} T(\lambda)\, I_{\infty}(\lambda)\, e^{-\sigma(\lambda) N}\, d\lambda \left[\int_0^{\infty} T(\lambda)\, I_{\infty}(\lambda)\, d\lambda\right]^{-1}$$

T = filter transmission

λ = wavelength

σ = species cross section

I_{∞} = integrated stellar spectral intensity without atmospheric attenuation

Complete notes on the derivation of the formula for N_c are included on the pages preceeding Part III. There are some minor differences in notation.

Notation

SUN = integration factor, or the integrated stellar spectral intensity, in counts/sec

HD = stepsize for altitude of the ray's tangent point used in the calculation of the column densities, in cm

IHO = counter and altitude setter; in lines 81-89 it is used to arbitraririly reduce the column density to near zero at the upper end of the scan

SUM = filtered signal intensity integrated over wavelength, in counts/sec

RO = distance from the center of the earth to the ray's tangent point, in cm

ZQ = altitude of the ray's tangent point, in cm

TT, TWW = column density for the table, computed at altitude ZQ, in cm^{-2}

FNO = integrated, normalized signal intensity corresponding to TT

FSUB = storage vector for the integrated, unnormalized signal intensity corresponding to TT, in counts/sec

Part III: Line numbers 97-174

In this part, the simulated signal intensity is obtained. If no random error is to be admitted, lines 98-108 select certain tabular values of the integrated, normalized signal intensity as the simulated signal intensity. If random error is to be introduced, there are two possibilities: (1) scatter the signal values with a set of random numbers from a Gaussian distribution with its mean = 0 and its variance = the signal intensity; (2) find positive integral values of the signal from a Poisson distribution having its parameter = signal intensity.

A Poisson distribution is characterized by the probability function,

$P(n) = 0$, n not an integer

$$P(n) = \frac{I^n e^{-I}}{n!}, \quad n = 0, 1, 2, \ldots$$

I = mean signal intensity, the Poisson parameter in this case

To find an n which belongs to a Poisson distribution, the procedure employed (lines 123, 125, and 145-171) is this:

1. Seek a random number (YFL) between 0 and 1 which permits a random variable, n, to be found such that $P(n) < YFL < P(n+1)$.
   a. The search begins with n = 0 and proceeds with increasing integral values. This permits the probabilities to be cumulated, i.e.,
   $$P(3) = \frac{I^3 e^{-I}}{2!} + P(2) + P(1).$$
   b. An upper limit on n of I + 5 is imposed for computing economy.
   c. If n = 0 is the outcome, substitute a small positive value for 0 ($n = 10^{-10}$) to allow subsequent computation to continue.

2.* Assign n as the value of the signal

In practice, the Poisson random variables were sought when $0.1 < I < 10$. At the lower limit, $P(n \geq 1) = 0.12$, and the search procedure is quite time-consuming at lesser values of I. Below 0.1, the tabular number is accepted as the simulated signal, but a different smoothing procedure in the interpolation subroutine produces a number density unlike that for the no-scatter case. At the upper limit and beyond, the Gaussian distribution yields a real number which is added to the signal in a rapid computer operation.

Notation

JIZ = loop counter for no-scattering case

FOF = simulated (measured) signal intensity, in counts/sec

JIX = loop counter for any quantity of scattering cases with a single data-point spacing

IX = GAUSS subroutine argument; it must be changed manually at the start of a run if new random numbers are desired; it is an odd, positive integer

JX = RANDU subroutine argument; it must be changed manually before each entry to avoid repetition

AM = GAUSS subroutine argument: the mean of the distribution

P = probability of a Poisson random variable equalling the integral value of the subscript minus 1

JIY = loop counter for one scattering case with variable data-point spacing

SD = GAUSS subroutine argument: the standard deviation of the distribution

* n-2 in the program corresponds to the n discussed here.

V = GAUSS subroutine argument: the value returned

N = indicator of the program path taken and the Poisson integer

NMAX = upper limit on the Poisson integer

U = numerator in the Poisson formula

D = denominator in the Poisson formula

Part IV: Line numbers 175-238

In this part, O_2 number densities from an exponential atmosphere pinned at 80 Km are computed (lines 175-191) for later comparison with retrieved number densities. The former values are furnished by subroutine ATMOD.

In order to carry out a mathematical inversion leading to retrieved number density, the column density must first be obtained. This is achieved through a logarithmic interpolation scheme as follows:

1. The table (Part III) is converted to the natural logarithms of signal intensity (FNO) and column density (TNO).
2. Using subroutine PARAB, a least squares parabola is fitted to M + 1 values of ln(FNO). This is done at each tabular value of ln(FNO) to obtain the coefficients (A, B, C).
3. The simulated signal (FOF) is located between tabular values of FNO, its logarithm is found, and the column density (N) is computed by

$$N_i = \exp\left[A_i (\ln I)^2 + B_i \ln I = C_i\right] .$$

Tests with various numbers of smoothing points indicate that 3(M = 2) is the optimum number for unscattered signal intensities and 9 (M = 8) is optimum for randomly scattered data.

The mathematical inversion is represented by

$$m_c' = -\frac{2}{\pi}\frac{d}{dr}\int_r^\infty \frac{r}{r_c} N(r_c)(r_c^2 - r^2)^{-\frac{1}{2}} dr_c ,$$

and the error analysis may be expected to invert $N(r_o)$ according to an expression such as

$$m(r_j) = -\frac{2}{\pi}\sum_{i=j}^{m-1}\left\{\frac{N_{i+1}-N_i}{r_{i+1}-r_i}\ln\left[\frac{r_{i+1}+(r_{i+1}^2-r_j^2)^{1/2}}{r_i+(r_i^2-r_j^2)^{1/2}}\right]\right\}$$

However, as may be seen in the ensuing notes, the random noise being superposed is

$$\Delta m(r_c) = -\frac{2}{\pi}\int_{r_c}^\infty \frac{d\Delta N}{dr}(r^2 - r_c^2)^{-\frac{1}{2}} dr ,$$

and smoothing of ΔN is necessary, i.e., $\Delta N = A(r-r_o)^2 + B(r-r_o) + C$.

The resulting formula is

$$\Delta m(r_j) = -\frac{2}{\pi} \sum_{i=j}^{\infty} \left\{ A_i \left(r_{i+1}^2 - r_j^2\right)^{1/2} - \left(r_i^2 - r_j^2\right)^{1/2} + \left(B_i - 2A_i r_o\right) \ln \left[\frac{r_{i+1} + \left(r_{i+1}^2 - r_j^2\right)^{1/2}}{r_i + \left(r_i^2 - r_j^2\right)^{1/2}} \right] \right.$$

The coefficients A_i and B_i are again supplied by subroutine PARAB, the arguments of the table becoming altitude (ZKM) and column density (TNO).

The error, $(n_o' - n_o) / n_o$ is finally computed at each altitude level and its sums and squares of sums are accrued for multiple cases (lines 232-238).

Notation

ONUMD, XP(2) = O_2 number density from the exponential model atmosphere, in cm^{-3}

RHTO, RO = distance of the ray tangent point from the earth's center, in cm

ZKM = altitude of the ray tangent point, in cm

Z = abscissa of the table

XN = ordinate of the table

M = one less than the number of smoothing points taken for a least squares fit in subroutine PARAB

X = entry value for a logarithmic interpolation

DEN = retrieved number density, in cm^{-3}

DERR = error in number density

DERRSQ = sum of squares of DERRs

DERRA = sum of DERRs

A, B, C, = least squares coefficients for a parabolic fit

Part V: Line numbers 239-288

In this part, the molecular temperature (T) is computed from the expression

$$\bar{T}_{O_2} = \frac{m\bar{g}}{k\, n_{O_2}(z)} \int_z^\infty n_{O_2}(\rho)\, d\rho$$

which is derived from the hydrostatic approximation (see the following notes).

If multiple cases are being handled, the mean and standard deviation are then computed for the errors at each altitude level.

Notation

T = molecular temperature, in ^{o}K

MM, MMM = number of cases for error statistics

DMEAN = mean error in number density

SIGMA = one standard deviation of number density error

Part VI: Line numbers 353-361

In this part, the O_2 scattering cross sectional values are listed at an interval of 20 Å (lines 353-358).

The S4F1 filter transmission values, adjusted to a maximum value of 1.0, are also listed at the same wavelength interval (lines 359-361).

ERROR ANALYSIS STRATEGIES

O_3

1. NUMERICAL SIMULATION

a. SINGLE WAVELENGTH

$N_0 = 2m_1^* e^{\frac{h}{H_1}} r_0 K_1\left(\frac{r_0}{H_1}\right) + 2m_2^* e^{\frac{h'}{H_2}} r_0 \cdot$ (terms in $D_{-\nu}, \gamma$)

$\frac{\partial T}{\partial z} = 0$

$50 \le h \le 100$ KM

$50 \le h' \le 100$ KM

$\rightarrow m_0' = -\frac{1}{\pi}\frac{d}{dr}\int_r^\infty \frac{r}{r_0} N(r_0)(r_0^2 - r^2)^{-\frac{1}{2}} dr_0 \rightarrow \frac{m_0' - m_0}{m_0}$

$m_0 = m_1^* e^{-\frac{h}{H_1}} + m_2^* e^{-\left(\frac{h'}{H_2}\right)^2}$

$50 \le h \le 100$ KM

b. BROADBAND

$(I_s)_{1800-3000\text{Å}}$

$N_0 = 2m^* e^{-h/H_1} r_0 K_1\left(r_0/H_1\right) +$ + TERMS IN $D_{-\nu}, \gamma$

$\frac{\partial T}{\partial z} = 0$

$30 \le h \le 100$ KM

$\rightarrow F_0 = \phi I_s e^{-\tau N_0}$

$40 \le h \le 210$ KM

$\rightarrow N_0 = A(LN\,F_0)^2 + B(LN\,F_0) + C \rightarrow (\alpha)$

$\rightarrow F_0 + \Delta F_0$

$(\alpha) \rightarrow m_0' = -\frac{2}{\pi}\frac{d}{dr}\int_r^\infty \frac{r}{r_0} N(r_0)(r_0^2 - r^2)^{-\frac{1}{2}} dr_0$

$m_0 = m_1^* e^{-\frac{h}{H}} + m_2^* e^{-\left(\frac{h'}{H'}\right)^2}$

$30 \le h \le 100$ KM

$\rightarrow \frac{m_0' - m_0}{m_0}(h) \rightarrow$ MEAN, STD. DEV., 30 CASES ΔF_0

h' = HEIGHT ABOVE "GAUSSIAN" REFERENCE LEVEL

H_1 = O_3 SCALE HEIGHT

H_2 = O_3 " " AROUND THE "GAUSSIAN" ALT.

m_1^* = NUMBER DENSITY AT A REFERENCE LEVEL

m_2^* = NUMBER DENSITY AT THE "GAUSSIAN" ALT

$D_{-\nu}$ = WEBER PARABOLIC CYLINDER FUNCTION

γ = GAMMA FUNCTION

REST OF NOTATION SAME AS FOR O_2

```
SIG SAFF T=10 P=10      'MAURICE GRAVES'
*LAST SIGNON WAS: 16:25.53   07-06-71
USER "SAFF" SIGNED ON AT  15:32.47 ON 07-12-71
LIST CZNUM
     1      C      OZONE NUMERICAL ERROR ANALYSIS
     2      C
     3             IMPLICIT REAL*8(A-H,O-Z)
     4             DIMENSION SG(100),WL(100),FIC(100),FILT(100),CNUMD(400),RHTO(40
     5            1DEN(400),DERR(400),ZKM(400),TNOX(400),P(16),ERRA(400),
   5.1            2ERRSQ(400),EMEAN(400),SIGMA(400)
     6             COMMON Z(400),XN(400),A(400),B(400),C(400),XP(4),FNO(400),
     7            1FOF(400),TWW(400),TNO(400),HC,XNO,RE,NP
   7.1             DATA ERRA,ERRSQ/800*0./
     8             SH=4.34D5
     9             XNOO3=8.D8
    10             ZWOO=83.D5
    11             SEOO=5.D9
    12             WM=1.
    13             WLO=5000.D-8
    14             TF=19000.
    15             FCO=.981D16
    16             PI=3.1415926535897 93
    18             FE=6371.D5
    19             HC=30.D5
    20             RE=HC
    21             XNO=5.D10
    22             NP=171
    23             NPP=141
    24             NEW=NPP
    25             HLP=5.D4
    26             MM=2
    27             NN=1
 I  27.1           JIY=0
    27.2           JIZ=0
    28      C
    29      C      WHEN MM=MMM, THE PROGRAM COMPUTES MEAN AND STANDARD DEVIATION
    30      C      OF PERCENTAGE ERROR AT RDF SPACING FOR MM CASES.  WHEN
    31      C      MM .NE. MMM, THE PROGRAM COMPUTES PERCENTAGE ERROR AND TEMP.
    32      C      AT VARIOUS SPACINGS WITH RANDOM ERROR(NN=2) OR WITHOUT
    33      C      RANDOM ERROR(NN=1).
    34      C
    35             MM=10
    36             MMM=10
    37             IF(MM.EQ.MMM)WRITE(6,20)MM
    38       20     FORMAT(//21H   STATISTICS FOR MM=,I3/)
    40      C
    41      C      INPUT O3 CROSS SECTION (SG), WAVELENGTH INTERVAL(WL), FILTER
    42      C      TRANSMISSION(FILT)
    43      C
    44             READ(5,600)  (SG(I),I=1,61)
    45      600    FORMAT(6D10.2)
    46             DO 300 I=1,61
    47      300    WL(I)=1800.+(I-1)*20.
    48      C
    49      C      FILTER SIZE TRANSMISSION
    50      C
    51             READ(5,601)  (FILT(I),I=1,61)
    52      601    FORMAT(11F5.3)
    53      C
    54      C      COMPUTE BLACKBODY STAR SPECTRUM AND ADJUST TO GET DESIRED
```

```
      C       MAXIMUM COUNT RATE
      C
            DO 301 I=1,61
            FIO(I)=DEXP(-(.921*VM+19.3875))*(WLO**5)/((WL(I)*1.D-8)**5)*(DEX
           11.438/(WLO*TF))-1.)/(DEXP(1.438/(WL(I)*1.D-8*TF))-1.)*(1.D-7)
            FIO(I)=FIO(I)*FOO
      301   CONTINUE
      C
      C       COMPUTE NORMALIZATION FACTOR
      C
            SUN=0.
            DO 302 J=2,61
      302   SUN=SUN+((FILT(J)*FIO(J)+FILT(J-1)*FIO(J-1))/2.*(WL(J)-WL(J-1)))
            WRITE(6,303)SUN
       303   FORMAT(/D15.6/)
            HD=170.D5/(NP-1)
      C
      C       FORM A TABLE OF COLUMN DENSITY(TT) VERSUS SIGNAL INTENSITY
      C       (SUM) BASED UPON AN INTEGRATION OF THE FORMULA FOR TT WHICH
      C       ASSUMES SPHERICAL STRATIFICATION AND AN ISOTHERMAL ATMOSPHERE
      C
            DO 800 IHO=1,NP
            SUM=0.
            RO=RP+HO+(IHO-1)*HD
            ZO=RO-RP
            TT=XNO*DEXP(-(ZO-50.D5)/SH)*DSQRT(1.57079*SH*RO)
           1*(1.+3.*SH/(8.*RO)-15./32.*(SH/RO)**2+315./216.*(SH/RO)**3)
            C1=2./(SHOO*SHOO)
            VA=ZO-ZWOO
            VB=VA*1.4142/SHOO
            IF(DABS(VB).GT.12.8)TTG=0.
            IF(DABS(VB).GT.12.8)GO TO 14
            CYL1=ECFN(-.5,VB)
            CYL2=ECFN(-1.5,VB)
            TTG=(XNOO3*DEXP(-(VA/SHOO)**2)/DSQRT(2.*RO))*(.8862269/(C1
           1**.75)*DEXP(VA*VA/(2.*SHOO*SHOO))*CYL2+RO/(C1**.25)*1.7724538*
           2DEXP(VA*VA/(2.*SHOO*SHOO))*CYL1)
       14     TNOX(IHO)=TT+TTG
            IF(IHO.GT.162)TT=10.**((NP-IHO)/5.)
            IF(IHO.EQ.171)TT=1.D-10
            TWW(IHO)=TT
            DO 1000 J=2,61
       1000   SUM=SUM+((FILT(J)*FIO(J)*DEXP(-SG(J)*TWW(IHO))+FILT(J-1)*
           1FIO(J-1)*DEXP(-SG(J-1)*TWW(IHO)))/2.)*(WL(J)-WL(J-1))
            FNO(IHO)=SUM/SUN
            WRITE(6,504)IHO,TWW(IHO),FNO(IHO),TTG
       504    FORMAT(I2,I5,4D15.6)
      800   CONTINUE
            IF(NN.EQ.2)GO TO 900
      C
      C       LOOP FOR NO RANDOM ERRORS IN SIGNAL INTENSITY AND VARIOUS
      C       DATA POINT SPACINGS
      C
            JIZMAX=5
            DO 8 JI2=1,JIZMAX
       900    DO 801 IHO=1,NPP,NH
            SUM=0.
            DO 1001 J=2,61
       1001   SUM=SUM+((FILT(J)*FIO(J)*DEXP(-SG(J)*TNOX(IHO))+FILT(J-1)*
           1FIO(J-1)*DEXP(-SG(J-1)*TNOX(IHO)))/2.)*(WL(J)-WL(J-1))
```

```
112             FCF(IHO)=SUM/SUN
113             WRITE(6,501)IHC,TNOX(IHC),FCF(IHO)
114      501     FORMAT(I2,I5,2D15.6)
115      801    CONTINUE
116             IF(NN.EQ.1)GO TO 806
117             IF(MM.NE.MMM)GO TO 803
118      C
119      C      LOOP FOR ACCRUING ERRORS IN O3 DENSITY RESULTING FROM
120      C      RANDOMLY SCATTERED SIGNAL INTENSITY, FOR MANY CASES,
121      C      WITH A SINGLE DATA POINT SPACING
122      C
123             DO 18 JIX=1,MM
124      803     CONTINUE
125      C
126      C      SET UP FOR GAUSS SSP AND RANDU SSP
127      C
128             IX=203+100*(JIX-1)
129             IF(MM.NE.MMM)IX=201
130             JX=IX
131             AM=0.
132             P(1)=0.
133             IF(MM.EQ.MMM)GO TO 804
135.1    C
136      C      LOOP FOR RANDOM ERRORS IN SIGNAL INTENSITY AND VARIOUS
137      C      DATA POINT SPACINGS
138      C
139             JIYMAX=1
140             DO 28 JIY=1,JIYMAX
141      804     DO 810 IH=1,NPP,NH
142             SUM=FCF(IH)*SUN
143             IF(SUM.LT.10.)GO TO 9
144             SD=DSQRT(SUM)
145             CALL GAUSS(IX,SD,AM,V)
146             FCF(IH)=(SUM+V)/SUN
147      503    IF(FCF(IH).GE.1.)FCF(IH)=1.-1.D-5
148             IF(FCF(IH).LT.FNO(1))FCF(IH)=FNO(1)+1.D-12
149             N=100
150             GO TO 809
151      9      IF(SUM.LT..1)FCF(IH)=FNO(IH)
152             IF(SUM.LT..1)N=0
153             IF(SUM.LT..1)GO TO 809
154      C
155      C      DETERMINE A RANDOM NUMBER FROM A POISSON DISTRIBUTION
156      C      WHEN .1<SIGNAL INTENSITY<10.
157      C
158             NMAX=SUM+5.
159             F=DEXP(-SUM)
160             P(2)=SUM*F
161      2      GSUM=P(2)
162             CALL RANDU(JX,JY,YFL)
163             DO 1 N=2,NMAX
164             IF(N.EQ.2)GO TO 10
165             U=SUM**(N-1)*F
166             D=1.
167             II=N-2
168             DO 3 J=1,II
169      3       D=(N-J)*D
170             GSUM=GSUM+U/D
171             P(N)=GSUM
172      10     IF(P(N).GE.YFL.AND.P(N-1).LE.YFL)GO TO 12
```

```
      1     CONTINUE
     13     JX=JY
            GO TO 2
     12     JX=JY
            FOF(IH)=(N-2)/SUN
            IF(FOF(IH).LT.1.D-10)FOF(IH)=1.D-10
  809        IF(MM.NE.MMM)WRITE(6,805)IH,FOF(IH),FNO(IH),N,YFL
  805       FORMAT(I5,2D15.6,I5,F10.5)
  810    CONTINUE
  806    HDE=HDE*2.
         IF(MM.EQ.MMM)HDE=.5D5
         NPH=(NPH-1)/2+1
         IF(JIY.EQ.1)NPH=141
         IF(JI2.EQ.1)NPH=141
         IF(MM.EQ.MMM)NPH=281
C
C        COMPUTE O2 NUMBER DENSITY FROM AN EXPONENTIAL MODEL
C        ATMOSPHERE WITH A SUPERPOSED GAUSSIAN CURVE FOR LATER
C        COMPARISON WITH RETRIEVED VALUES
C
         DO 807 IHC=1,NPH
         RC=RE+HC+(IHC-1)*HDE
         CALL ATMOD(RO)
         ONUMD(IHC)=XP(2)
         RHTO(IHC)=RO
         ZKM(IHC)=RHTO(IHO)-RE
  807    CONTINUE
C
C        INTERPOLATE IN THE TABLE TO FIND COLUMN DENSITY(TNO) FROM
C        A SIGNAL INTENSITY(FOF) WHICH IS A SIMULATION OF THE
C        MEASURED SIGNAL
C
         DO 502 J=1,NP
         Z(J)=DLOG(FNO(J))
         XN(J)=DLOG(TWK(J))
  502    CONTINUE
         M=8
         IF(NN.EQ.1)M=2
         CALL PARAB(M)
         DO 630 I=1,NPP,NH
         IF(FOF(I).LT.FNO(1))FOF(L)=FNO(1)+1.D-12
         DO 612 I=1,NP
         IF(FOF(L).GE.FNO(I).AND.FOF(I).LT.FNO(I+1)) GO TO 613
  612    CONTINUE
  613     J=I
         X=DLOG(FOF(L))
         TNO(L)=A(J)*X*X+B(J)*X+C(J)
         TNO(I)=DEXP(TNO(L))
  630    CONTINUE
C
C        INVERT COLUMN DENSITY(TNO) TO GET O2 NUMBER DENSITY(DEN)
C
         DO 700 J=1,NPH
         Z(J)=ZKM(J)
         K=J*NH-(NH-1)
  700    XN(J)=TNO(K)
         M=8
         IF(NN.EQ.1)M=2
         CALL PARAB(M)
         N1=NPH-1
```

```
231             DO 4 J=1,N1
232             DEN(J)=0.
233             DO 5 I=J,N1
234             B=2.*A(I)
235             DT=DABS(RHTO(I)**2-RHTO(J)**2)
236       5      DEN(J)=DEN(J)+B*(DSQRT(RHTO(I+1)**2-RHTO(J)**2)-DSQRT(DT))
237            1+(B(I)-2.*A(I)*RE)*DLOG((RETO(I+1)+DSQRT(RHTO(I+1)**2
238            2-RHTO(J)**2))/(RHTO(I)+DSQRT(DT)))
239             DEN(J)=-DEN(J)/PI*2.
240       C
241       C     COMPUTE ERROR AND ACCRUE ERROR SUMS
242       C
243             DERR(J)=(DEN(J)-ONUMD(J))/CNUMD(J)
243.1           DERRSQ(J)=DERRSQ(J)+DERR(J)*DERR(J)
244             DERRA(J)=DERRA(J)+DERR(J)
245       4     CONTINUE
246             WRITE(6,85)JIZ,JIY,JIX
247        85    FORMAT(/3I5)
248             IF(MM.EQ.MMM)GO TO 18
249             WRITE(6,24)NPE
250       24    FORMAT(//26H   NUMBER OF DATA POINTS =,I3/)
251             WRITE(6,25)NP
252       25    FORMAT(/29H   NUMBER OF TABULAR POINTS =,I3//)
253             WRITE(6,23)
254       23    FORMAT(//18X,1HZ,13X,3HNO3,12X,4HCNO3,12X,4HDERR//)
255             N1=N1-1
256             DO 6 J=1,N1
257             IF(MM.NE.MMM)WRITE(6,22)ZKM(J),DEN(J),CNUMD(J),DERR(J)
258       22    FORMAT(10X,4D15.6)
259       6     CONTINUE
260        29    NH=NH*2
261             IF(MM.EQ.MMM)NH=1
262             IF(NN.EQ.1)GO TO 8
263             IF(MM.EQ.MMM)GO TO 18
264       28    CONTINUE
265             IF(NN.EQ.2.AND.MM.NE.MMM)GO TO 83
266        18    CONTINUE
267             IF(MM.EQ.MMM)GO TO 79
268       8     CONTINUE
269             IF(MM.NE.MMM)GO TO 80
270        79    WRITE(6,82)
271        82    FORMAT(//8X,1HZ,10X,10HMEAN ERROR,7X,5HSIGMA,10X,5HSUMSQ,
272            111X,3HSUM/)
273       C
274       C     COMPUTE STATISTICS FROM ACCRUED SUMS
275       C
276             DO 80 J=1,N1
277             DMEAN(J)=DERRA(J)/(MM*1.)
278             SIGMA(J)=DSQRT(DERRSQ(J)/(MM*1.)-DMEAN(J)*DMEAN(J))
279             WRITE(6,81)ZKM(J),DMEAN(J),SIGMA(J),DERRSQ(J),DERRA(J)
280        81    FORMAT(5D15.6)
281        80    CONTINUE
282        83    CALL EXIT
283             END
284             SUBROUTINE PARAB(M)
285       C
286       C     PARAB FINDS THE SECOND ORDER LEAST SQUARES COEFFICIENTS
287       C     A,B, AND C FOR INPUT VECTORS Z AND XN, USING M+1 SMOOTHING
288       C     POINTS
289       C
```

```
290             IMPLICIT REAL*8(A-H,O-Z)
291             COMMON Z(400),XN(400),A(400),B(400),C(400),XP(4),FNO(400),
292            1FCF(400),TWW(400),TNC(400),BC,XNO,RE,NP
293             I=M/2
294             DO 2 I=1,NP
295             IZ=NP+1-I
296             K=1
297             IF(I.GT.1.AND.I.LT.IZ)K=I-1
298             IF(I.GE.IZ)K=NP-M
299             ZB=0.
300             Z2B=0.
301             Z3B=0.
302             Z4B=0.
303             XNB=0.
304             ZNB=0.
305             Z2NB=0.
306             K2=K+M
307             DO 3 J=K,K2
308             ZB=ZB+Z(J)
309             Z2B=Z2B+Z(J)**2
310             Z3B=Z3B+Z(J)**3
311             Z4B=Z4B+Z(J)**4
312             ZNB=ZNB+Z(J)*XN(J)
313             Z2NB=Z2NB+XN(J)*(Z(J)**2)
314       3     XNB=XNB+XN(J)
315             J=I
316             M1=M
317             M=M+1
318             Y=(M*Z3B-Z2B*ZB)*(M*Z3B-ZB*Z2B)-(M*Z4B-Z2B**2)*(M*Z2B-ZB**2)
319             IF(DABS(Y).LT.1.D-40) A(J)=0.
320             IF(DABS(Y).LT.1.D-40)GO TO 1
321             A(J)=((M*ZNB-XNB*ZB)*(M*Z3B-ZB*Z2B)-(M*Z2NB-XNB*Z2B)*(M*Z2B-ZB*
322            1)/((M*Z3B-Z2B*ZB)*(M*Z3B-ZB*Z2B)-(M*Z4B-Z2B**2)*(M*Z2B-ZB**2))
323       1     D=A(J)
324             YY=M*Z2B-ZB**2
325             IF(DABS(YY).LT.1.D-40) B(J)=0.
326             IF(DABS(YY).LT.1.D-40) GO TO 11
327             B(J)=((M*ZNB-ZB*XNB)-(M*Z3B-ZB*Z2B)*D)/(M*Z2B-ZB*ZB)
328       11    B=B(J)
329             C(J)=(XNB-D*Z2B-B*ZB)/M
330             M=M1
331       2     CONTINUE
332             RETURN
333             END
334             SUBROUTINE ATMOD(RW)
335       C
336       C       ATMOD FINDS THE O3 NUMBER DENSITY AT ALTITUDE ZW FOR AN
337       C     ISOTHERMAL ATMOSPHERE WITH A SUPERPOSED GAUSSIAN CURVE
338       C
339             IMPLICIT REAL*8(A-H,C-Z)
340             COMMON Z(400),XN(400),A(400),B(400),C(400),XP(4),FNO(400),
341            1FCF(400),TWW(400),TNC(400),BC,XNO,RE,NP
342             RE=6371.D5
343             ZW=RW-RE
344             XP(2)=5.D10*DEXP(-(ZW-50.D5)/4.34D5)+8.D8*DEXP(-((ZW-83.D5)
345            1/5.D5)**2)
346             RETURN
347             END
348             SUBROUTINE GAMMA(XX,GX,IER)
349             IMPLICIT REAL*8(A-H,O-Z)
```

```
      IF(XX-57.) 6,6,4
    4 IER=2
      GX=1.D75
      RETURN
    6 X=XX
      ERR=1.0D-6
      IER=0
      GX=1.0
      IF(X-2.0) 50,50,15
   10  IF(X-2.0) 110,110,15
   15 X=X-1.0
      GX=GX*X
      GO TO 10
   50 IF(X-1.) 60,120,110
   60 IF(X-ERR) 62,62,80
   62  Y=FLOAT(IDINT(X))-X
      IF(DABS(Y)-ERR) 130,130,64
   64 IF(1.-Y-ERR) 130,130,70
   70 IF(X-1.) 80,80,110
   80 GX=GX/X
      X=X+1.
      GO TO 70
  110 Y=X-1.
      GY=1.0+Y*(-0.5771017+Y*(0.9858540+Y*(-0.8764218+Y*(0.8328212+
     1Y*(-0.5684729+Y*(0.2548205+Y*(-0.05149930)))))))
      GX=GX*GY
  120 RETURN
  130 IER=1
      RETURN
      END
      FUNCTION EGFN(V,X)
      IMPLICIT REAL*8(A-H,O-Z)
      SQRTPI=1.772453850905516
      SQRT2=1.41421356237309
      FAC1=2.**(-.5*V-.5)*SQRTPI*DEXP(-.25*X*X)
      CALL GAMMA(.5*V+1.,GAM1,IER)
      CALL GAMMA(.5*V+.5,GAM2,IER)
      FAC2=CFHG(.5*V+.5,.5,.5*X*X)/GAM1-SQRT2*X*CFHG(.5*V+
     11.,1.5,.5*X*X)/GAM2
      EGFN=FAC1*FAC2
      RETURN
      END
      FUNCTION CFHG(A,C,X)
      IMPLICIT REAL*8(A-H,O-Z)
      SUM=1.
      TERM=1.
      S=1.
    1  TERM=TERM*X*(A+S-1.)/(S*(C+S-1.))
      SUM=SUM+TERM
      S=S+1.
      IF(SUM.EQ.0.)GO TO 1
      IF(DABS(TERM/SUM).GE..0000001) GO TO 1
      CFHG=SUM
      RETURN
      END
OF FILE
```

```
$LIST TEMP
      1        7.8CD-19  7.5CD-19  7.00E-19  6.5CD-19  5.80E-19  5.20D-19
      2        4.7CE-19  4.30D-19  3.80D-19  3.4CD-19  3.20D-19  3.20D-19
      3        3.30D-19  3.6CD-19  4.30E-19  5.20D-19  6.60D-19  8.80D-19
      4        1.10E-18  1.4CD-18  1.80E-18  2.2CD-18  2.70D-18  3.20D-18
      5        3.9CD-18  4.5CD-18  5.20E-18  5.80D-18  6.60E-18  7.40D-18
      6        8.00E-18  9.00D-18  1.00D-17  1.01D-17  1.10D-17  1.20D-17
      7        1.20D-17  1.15D-17  1.10E-17  1.08D-17  1.05D-17  1.00D-17
      8        9.80E-18  9.00D-18  8.20E-18  7.60D-18  6.8CD-18  6.00D-18
      9        5.0CD-18  4.5CD-18  4.00E-18  3.40D-18  2.70D-18  2.30D-18
     10        1.90E-18  1.5CD-18  1.20E-18  9.0CD-19  7.00D-19  5.40D-19
     11        3.20E-18
     12      .020 .021 .022 .024 .026 .030 .035 .040 .048 .055 .060
     13      .070 .080 .090 .100 .130 .160 .200 .260 .360 .420 .520
     14      .620 .740 .840 .940 .990 1.00 .980 .940 .880 .840 .800
     15      .780 .740 .680 .640 .600 .500 .400 .360 .300 .240 .200
     16      .170 .140 .120 .100 .080 .060 .050 .042 .040 .037 .035
     17      .033 .030 .028 .025 .023 .020
END OF FILE
```

Part I: Line numbers 1-61

In this part, the initial parameter values are set and the input data are read.

Notation

SH = O_3 scale height for an isothermal atmosphere, in cm

XNOO3 = O_3 number density at Gaussian peak, in molecules/cm^3

ZWOO = altitude of Gaussian peak, in cm

SHOO = half-depth of Gaussian layer, in cm

VM = visual magnitude of star

WLO = reference wavelength for stellar spectrum, in cm

TF = effective blackbody stellar temperature, in ^oK

FOO = adjusting factor for obtaining a desired fictitious count rate at the top of the scan

RE = mean radius of the earth, in cm

HO, HP = base height of the O_3 profile, in cm

XNO = O_3 number density at the base height in molecules/cm^3

NP = number of points in a formulated table of normalized signal intensity v. column density. Note: column density = mass of species in a 1 cm^2 channel centered on the stellar ray, also called the total, or integrated, number density

NPP, NPH = number of data points in the profile

HDP = halfstepsize for computing O_3 densities in an exponential atmosphere, in cm

NN = switch for introducing random error into the signal intensity

NH = stepsize for computing O_3 number density, in number of data point intervals skipped

MM, MMM = test for selecting one of three paths (see program comments)

SG = O_3 absorption cross sectional values, in cm^2; the values are listed at the end of the program

WL = wavelength, in cm

FILT = normalized values of S2F5 filter transmission; the values are listed at the end of the program

FIO = stellar spectral intensity, in digital voltmeter counts/time interval

Part II: Line numbers 61.1 - 99

A table of normalized signal intensity v. column density is formed in the same way as for O_2 (p. 10 of O_2 notes). The reference height is now 50 Km.

In addition, a representation of the mesospheric O_3 peak is obtained by use of the Weber cylinder function. To avoid data roughness at the altitudinal limits of the superposed Gaussian curve, the cylinder function is forced between 40 Km and 130 Km.

Notation

SUN = integration factor, or the integrated stellar spectral intensity; in counts/time interval

HD = stepsize for altitude of the ray's tangent point used in the calculation of column density, in cm

IHO = counter and altitude setter; in lines 90-91 it is used to arbitratily reduce the column density to near zero at the upper end of the scan

RO = distance from the center of the earth to the ray's tangent point, in cm

ZQ = altitude of the ray's tangent point, in cm

TT, TWW = column density for the table, computed at altitude ZQ, in cm^{-2}

VB = parameter for Weber cylinder function

C1, CYL1, CYL2 = parameters for column density in Gaussian superimposed curve

TTG = column density in Gaussian contribution, in molecules/cm^3

TNOX = total column density, in molecules/cm^3

SUM = filtered signal intensity integrated over wavelength, in counts/time interval

FNO = integrated, normalized signal intensity corresponding to TT in the table

Part III: Line numbers 100 - 181

This part is essentially unchanged from the O_2 program.

A signal is computed from

$$I = \int_0^\infty \tau(\lambda)\, I_\infty(\lambda)\, e^{-\tau(\lambda) N}\, d\lambda \left[\int_0^\infty \tau(\lambda)\, I_\infty(\lambda)\, d\lambda \right]^{-1},$$

which has the Gaussian superimposed column densities incorporated in "N". If the signal is scattered, a Poisson distribution is available at the lower end of the scan ($0.1 < I < 10.$) If the signal intensity is less than 0.1, the scattering is bypassed.

Notation

JIZ, JIZMAX = loop counter and its limiting value for no scattering case

FOF = simulated (measured) signal intensity, in counts/time interval

JIX = loop counter for MM scattering cases with a specific data point spacing

IX, JX, AM, P, SD, V, N, NMAX, U, D = GAUSS and RANDU subroutine arguments; Poisson parameters as in O_2 program

JIY, JIYMAX = loop counter and its limiting value for a scattering case with variable data-point spacing

Part IV: Line numbers 182 - 245

The procedure and notation are identical to those used in the O_2 error analysis. However, subroutine ATMOD yields the model O_3 through solution of the expression

$$n(O_3) = n^* \exp\left[-(h-h^*)/H\right] + n' \exp\left[-(h-h')/H'\right]^2$$

where

n = number density, in molecules/cm^3

n* = number density at a reference altitude, in molecules/cm^3

h = altitude, in cm

h* = reference altitude, in cm

H = scale height of O_3, in cm

n' = O_3 number density at Gaussian peak, in molecules/cm^3

h' = altitude of Gaussian peak, in cm

H' = half-depth of Gaussian layer, in cm

Numerical values are inserted into ATMOD for the above parameters.

Part V: Line numbers 246 - 283

Temperature computations are omitted.

If multiple cases are being handled, the mean and standard deviation are computed for the error at each altitude level.

Notation

MM, MMM = number of cases for error statistics

DMEAN = mean error in number density, in percent

SIGMA = one standard deviation of number density error, in percent

Part VI: Line numbers 1 - 17

O_3 cross sectional values are listed row by row at an interval of 20 Å (lines 1 - 11).

S2F5 filter transmission values, adjusted to a maximum value of 1.0, are also listed at the same wavelength interval (lines 12 - 17).

Appendix IV. Orbital Errors

The effects of the uncertainty in satellite position have been traced by imposing small input errors upon the satellite coordinates and mapping the error departures of the ray tangent point. The symbols used are as in Section 3, Section 3, with the addition of star-superscripts to denote reference, or zero-error quantities. A special case is assumed, for convenience, which places the spacecraft and the stellar ray in the equatorial plane, and the source star at the First Point of Aries in the same plane.

Tangent ray errors are shown in Figures 1-4 which have distance scales on the abscissae to supplement degree indicators of longitude and latitude. They disclose that altitude errors in tangent ray point nearly match vertical satellite displacements; they amount to a few meters when a satellite is displaced latitudinally 10 Km; and they reach magnitudes of a few Km when a satellite is displaced longitudinally 10 Km. Thus, as expected the tangent ray heights are quite sensitive to the longitudinal accuracy of spacecraft positioning.

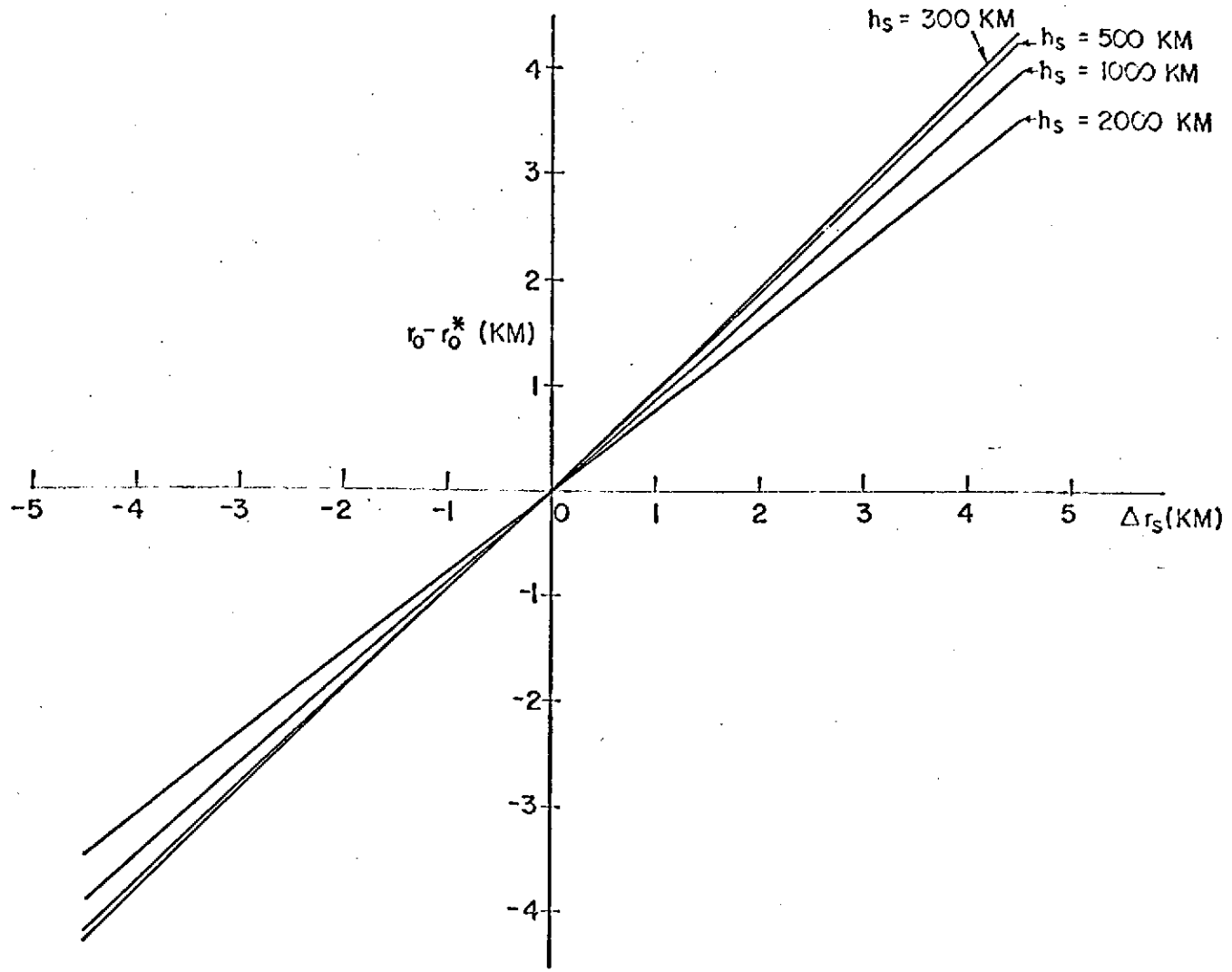

Figure 1. Tangent ray height error as a function of satellite height error and altitude.

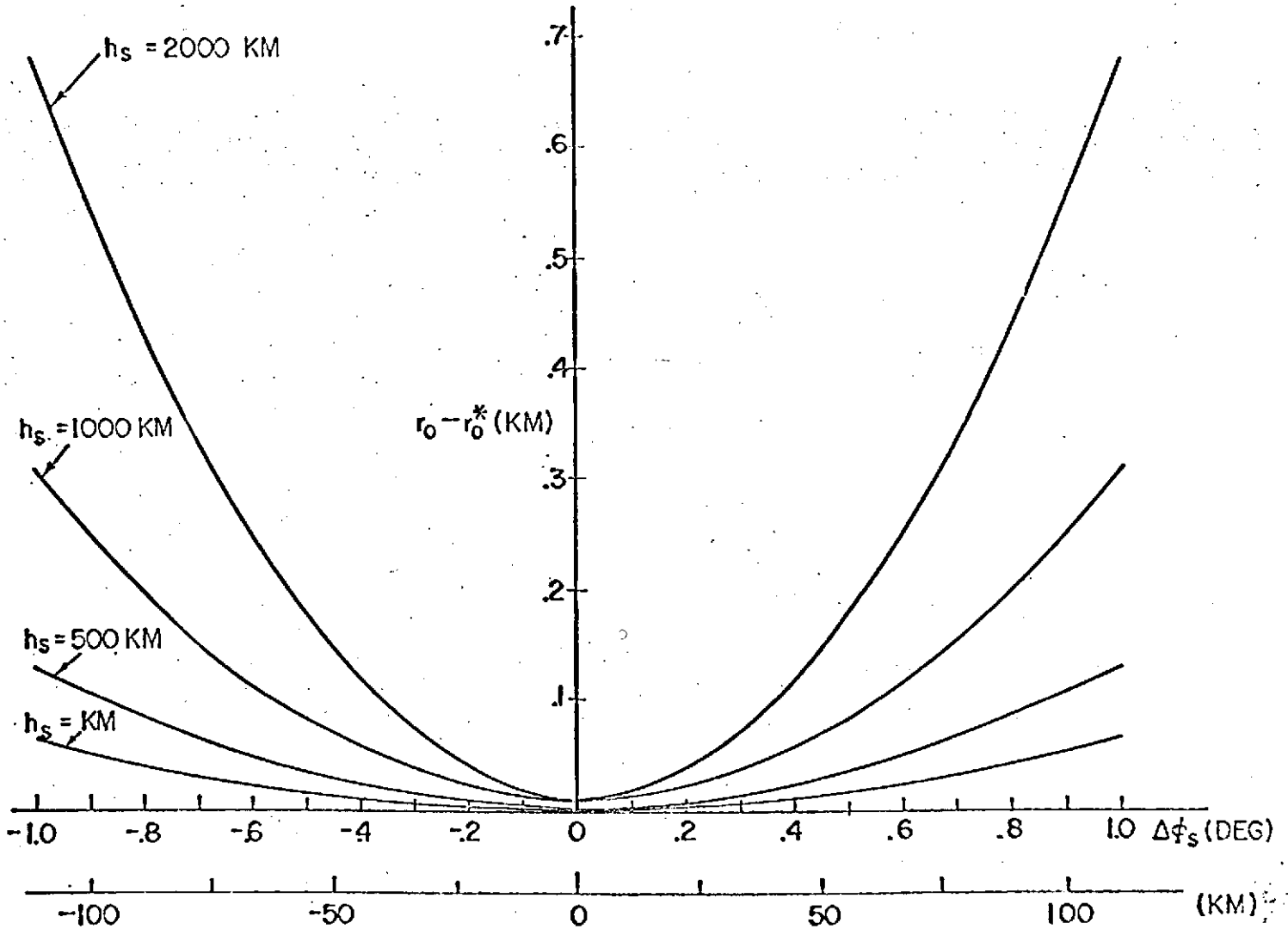

Figure 2. Tangent ray height error as a function of satellite latitude error.

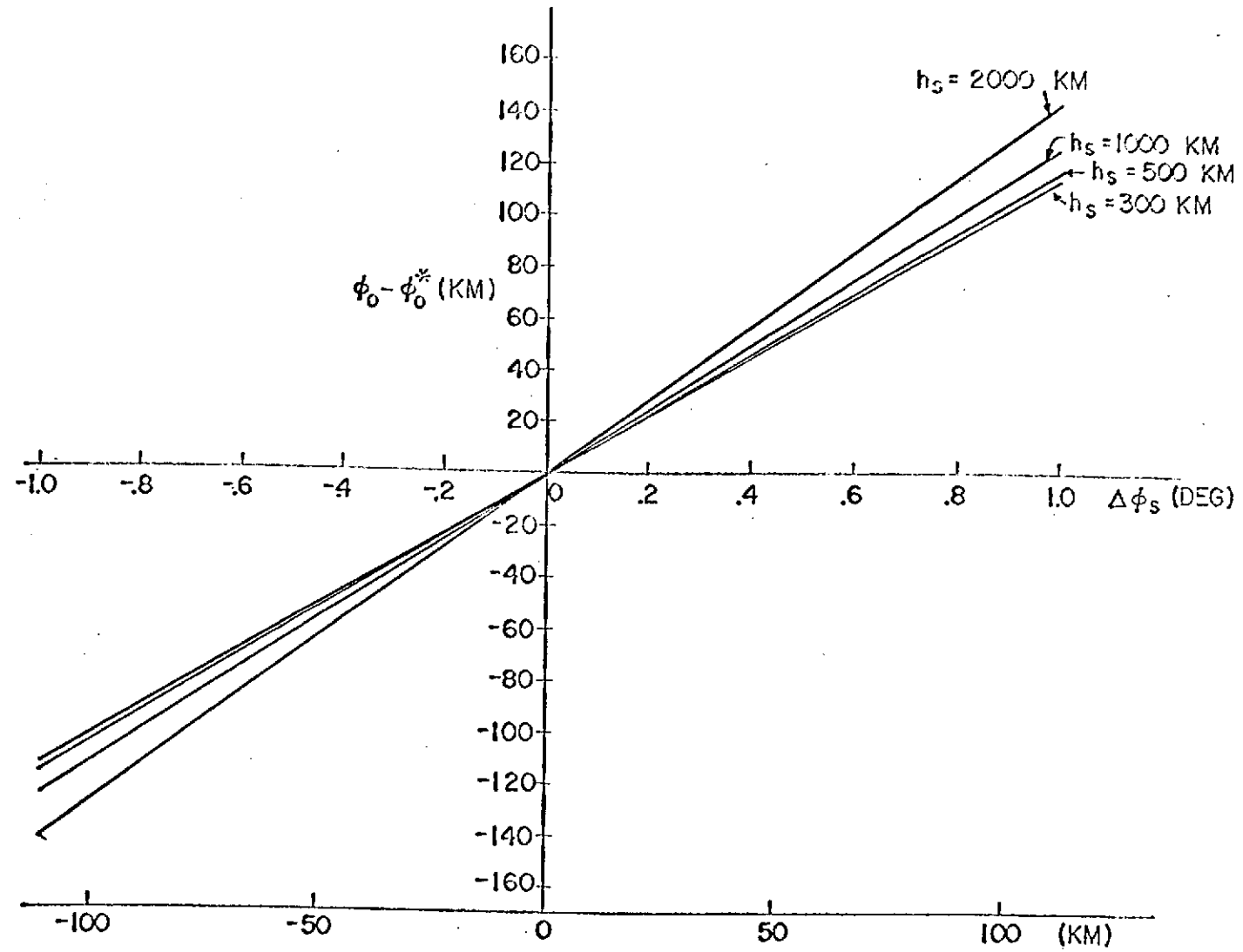

Figure 3. Tangent point longitude error as a function of satellite longitude error.

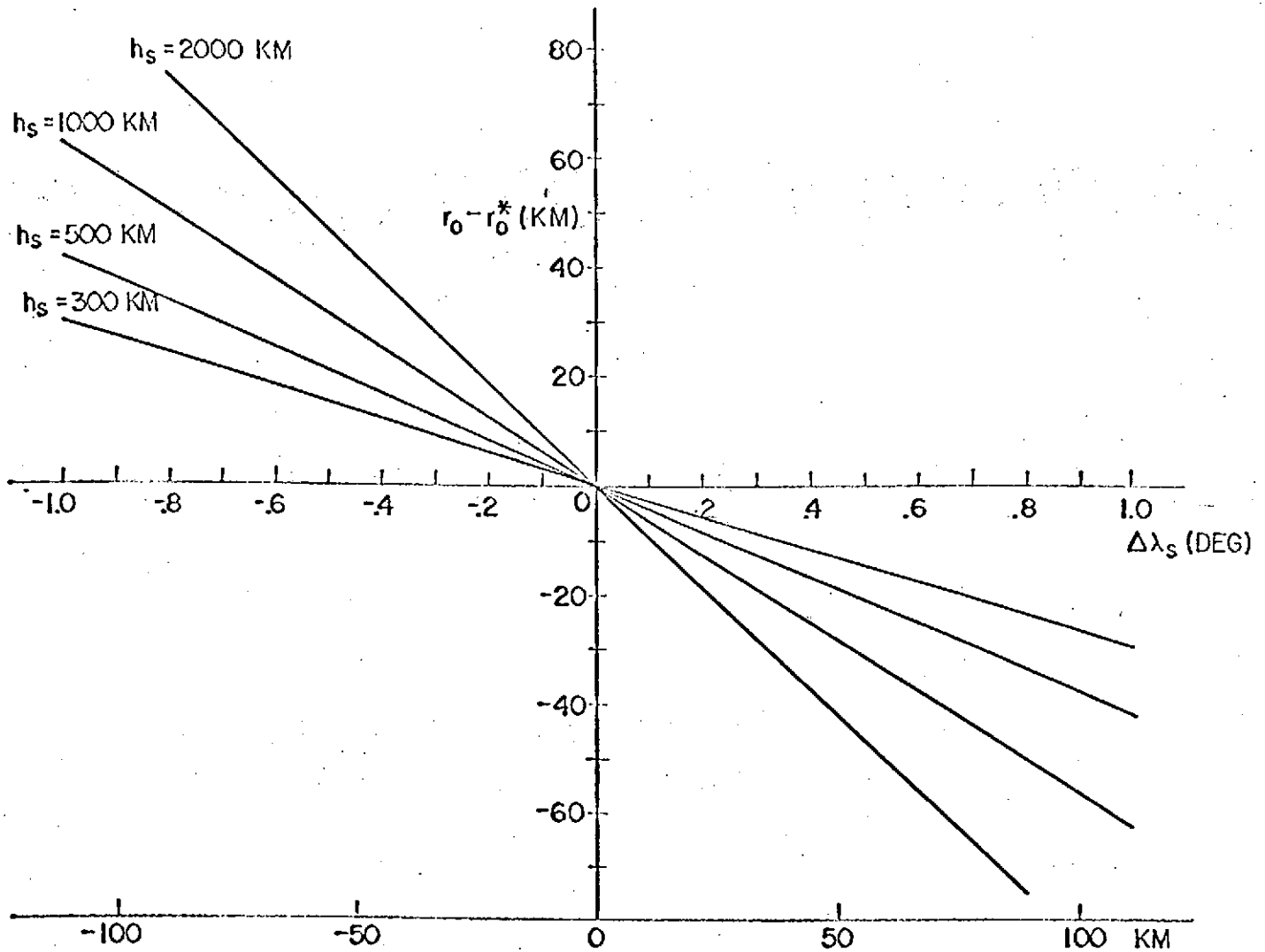

Figure 4. Satellite tangent ray height error as a function of satellite longitude error.

APPENDIX V.

Stellar Occultation Measurements of Molecular Oxygen in the Lower Thermosphere

Planet. Space Sci. 1973, Vol. 21, pp. 339 to 348. Pergamon Press. Printed in Northern Ireland

STELLAR OCCULTATION MEASUREMENTS OF MOLECULAR OXYGEN IN THE LOWER THERMOSPHERE

P. B. HAYS
Departments of Aerospace Engineering, Meteorology and Oceanography, University of Michigan, Ann Arbor, Michigan 48105, U.S.A.

and

R. G. ROBLE
National Center for Atmospheric Research, Boulder, Colorado 80302, U.S.A.

(*Received in final form* 8 *August* 1972)

Abstract—Stellar ultraviolet light near 1500 Å is attenuated in the Earth's upper atmosphere due to strong absorption in the Schumann–Runge continuum of molecular oxygen. The intensity of stars in the Schumann–Runge continuum region has been monitored by the University of Wisconsin stellar photometers aboard the OAO-2 satellite during occultation of the star by the Earth's atmosphere. These data have been used to determine the molecular oxygen number density profile at the occultation tangent point. The results of 14 stellar occultations obtained in low and middle latitudes are presented giving the night-time vertical number density profile of molecular oxygen in the 140–200 km region. In general, the measured molecular oxygen number density is about a factor of 2 lower than the number densities predicted by the *CIRA* 1965 model. Also, the number density at a given height appears to decrease with decreasing solar activity. Measurements taken at low latitudes during the August 1970 geomagnetic storm showed a decrease in the molecular oxygen number density at a given height several days after the peak of the storm followed by a slow recovery to pre-storm densities.

1. INTRODUCTION

The first attempt at determining the molecular oxygen concentration in the upper atmosphere by u.v. absorption spectroscopy was made on a V-2 rocket experiment in 1949 (Friedman *et al.*, 1951). The molecular oxygen concentration was obtained from the solar u.v. absorption measurements made at various altitudes by a spectrometer aboard the rocket. Since then, numerous rocket flights have been made to examine the molecular oxygen distribution and its variations, in addition to determining the u.v. spectra of the Sun (Byram *et al.*, 1955; Kupperian *et al.*, 1959; Jursa *et al.*, 1963; Hall *et al.*, 1963; Hinteregger *et al.*, 1965; Week and Smith, 1968; Opal and Moos, 1969; Quessette, 1970; Brannon and Hoffman, 1971).

The molecular oxygen distribution in the altitude range 100–200 km has also been determined from mass spectroscopic measurements (Schaefer and Nichols, 1964; Nier *et al.*, 1964; Hedin and Nier, 1966; Schaefer, 1968; Krankowsky *et al.*, 1968; von Zahn and Gross, 1969). In addition to molecular oxygen, the other major and minor constituents of the upper atmosphere are likewise determined as a function of altitude during the rocket flight.

More recently, satellites have been used to determine the properties of the upper atmosphere from u.v. absorption measurements. The satellites have monitored the attenuation of solar u.v. radiation in various isolated wavelength intervals during occultation at orbital sunrise and sunset. These data have been used to retrieve the neutral air density (Thomas *et al.*, 1965; Kreplin, 1965; Venables, 1967; Landin *et al.*, 1965; Landin *et al.*, 1967) and the molecular oxygen distribution in the lower thermosphere (Thomas and Norton, 1967; Norton and Warnock, 1968; Link, 1969; Stewart and Wildman, 1969; Lockey

et al., 1969; Reid and Withbroe, 1970; May, 1971; Roble and Norton, 1972). These measurements, however, are limited only to sunrise and sunset.

Hays and Roble (1968a) suggested that u.v. stars may be used as source for occultation measurements to determine the night-time distribution of molecular oxygen and ozone in the lower thermosphere and upper mesosphere. Their calculations showed that in the spectral region near 1500 Å attenuation is primarily due to absorption by molecular oxygen, and that Rayleigh scattering and absorption by other minor constituents can be neglected.

During the past few years, we have used the Orbiting Astronomical Observatory (OAO-2) to obtain u.v. stellar occultation data in various spectral intervals. These data have been used to obtain the night-time molecular oxygen number density and neutral gas temperature in the lower thermosphere from about 140–200 km. The purpose of this paper is to describe the experimental technique and discuss the results which were obtained during quiet and disturbed geomagnetic conditions.

2. EXPERIMENTAL TECHNIQUE

The general details of the stellar occultation technique (Fig. 1) have been described by Hays and Roble (1968a, b), Hays *et al.* (1972) and Roble and Hays (1972). Here we describe the specifics of the occultation measurements made by the OAO-2 satellite.

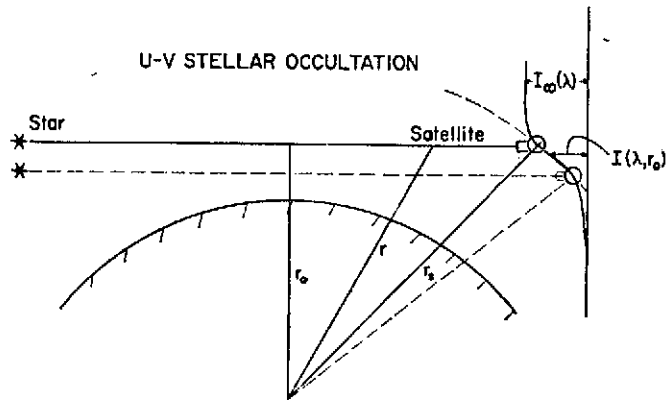

FIG. 1. GEOMETRY OF STELLAR OCCULTATION, $r_o = r_t$.

The OAO-2 satellite has one 16 in. dia u.v. telescope, four 8 in. dia u.v. telescopes, and an u.v. spectrometer having a resolution of approximately 5 Å. The University of Wisconsin optical package, used in conjunction with the telescopes, consists of a series of u.v. filters which are used for stellar photometry. Filter (4–1) shown in Fig. 2 has a broadband transmission function centered near 1450 Å in the Schumann continuum region of molecular oxygen. This filter was used to obtain the molecular oxygen distributions from the stellar occultation measurements. The detection systems of the u.v. telescopes have a variable time integration range. The data shown in Fig. 4, which is typical of the high data rate occultation scans, has approximately a 1·5 km altitude resolution between data points.

Prior to occultation of the star by the Earth, an unattenuated u.v. spectrum of the star is obtained from the spectrometer. As an example, the spectrum for a typical bright u.v. star is shown in Fig. 3 for the wavelength region of the molecular oxygen u.v. filter. Although only a measurement of the relative change of the u.v. stellar intensity is required during occultation (Hays and Roble, 1968a), the spectral distribution of the star's energy

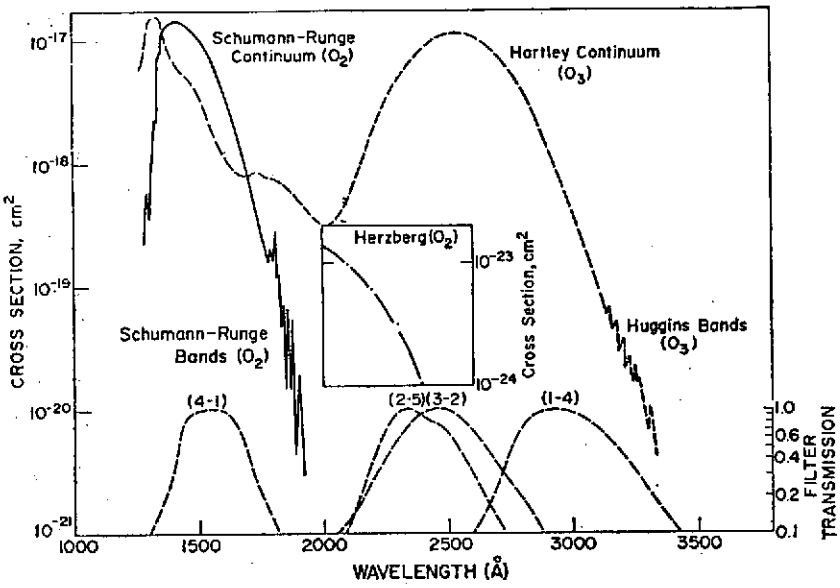

FIG. 2. ABSORPTION CROSS SECTIONS FOR MOLECULAR OXYGEN AND OZONE IN THE SPECTRAL REGION EXTENDING FROM 1000 TO 3500 Å. DASHED CURVES ARE THE O.A.O. STELLAR PHOTOMETER FILTER TRANSMISSION CURVES USED IN THIS STUDY.

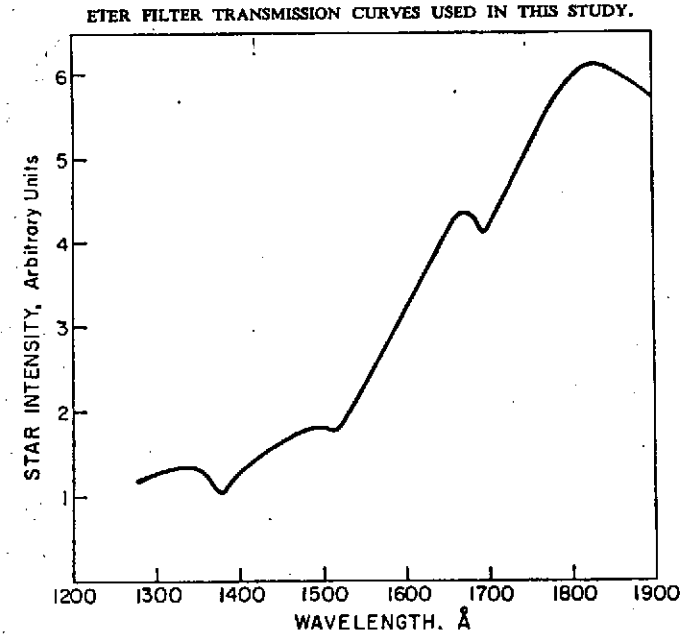

FIG. 3. TYPICAL SPECTRUM OF A STAR USED AS AN OCCULTATION LIGHT SOURCE.

flux is required to determine the transmission through the broadband filter. Thus, a detailed stellar spectrum covering the spectral passband of the filter is necessary for data reduction.

A schematic diagram of an occultation of a star by the Earth is shown in Fig. 1. The satellite acquires the star in its telescopes prior to occultation above the absorbing atmosphere. As the satellite moves in its orbit, the source is ultimately occulted by the Earth's atmosphere and the geometry at two satellite positions is illustrated schematically in Fig. 1.

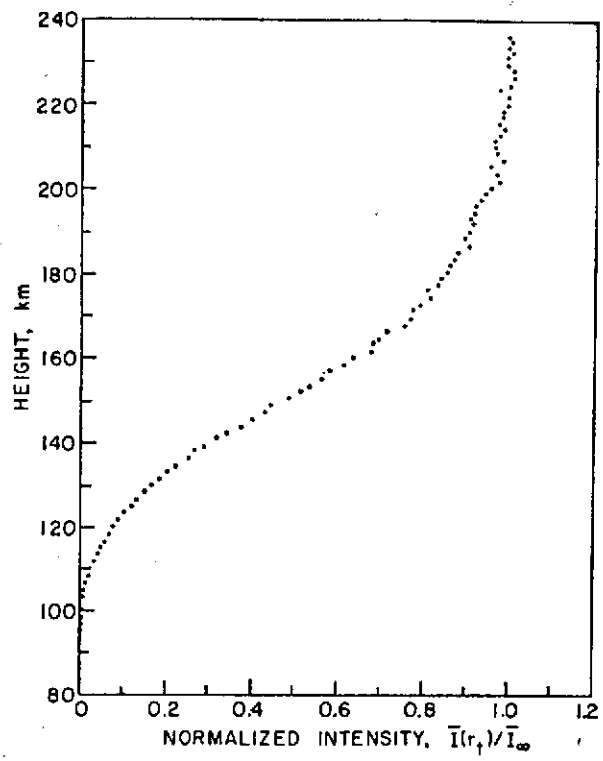

FIG. 4a. NORMALIZED STELLAR INTENSITY AS A FUNCTION OF TANGENT RAY HEIGHT DURING OCCULTATION.

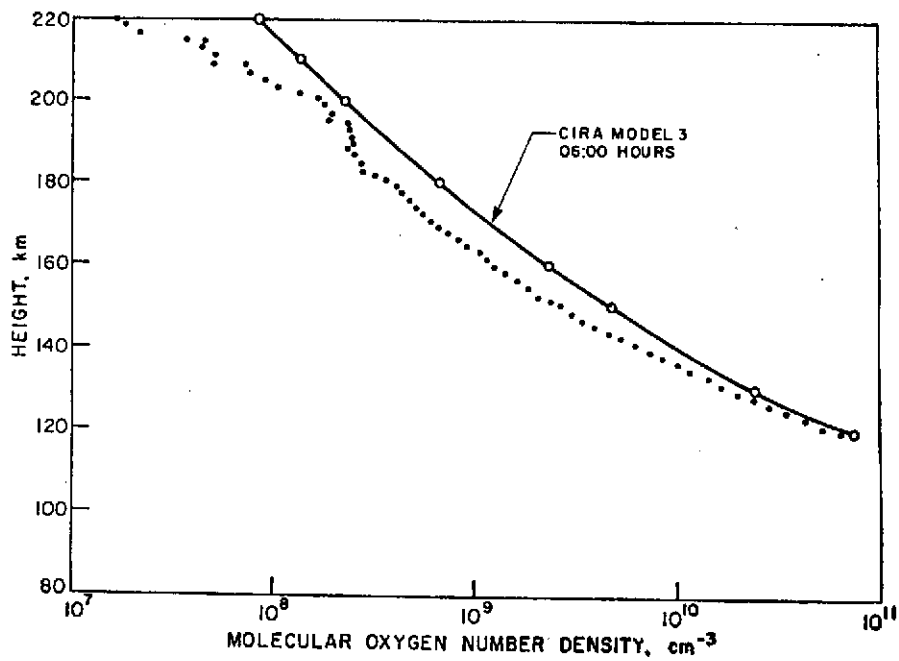

FIG. 4b. MOLECULAR OXYGEN DENSITY VS. HEIGHT FROM DATA SHOWN IN FIG. 4a.

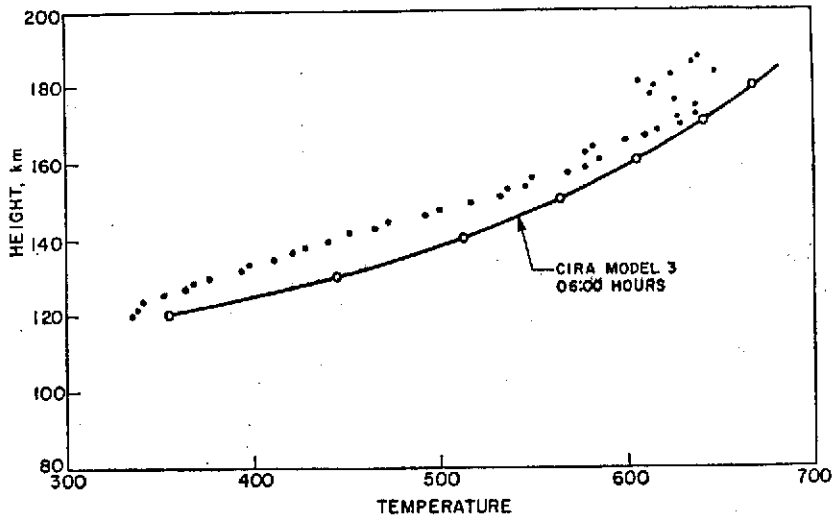

FIG. 4c. TEMPERATURE VS. HEIGHT DEDUCED FROM THE MOLECULAR OXYGEN NUMBER DENSITY DATA SHOWN IN FIG. 4b ASSUMING DIFFUSIVE EQUILIBRIUM.

The intensity of the star is measured as a function of time during occultation by the Earth. By knowing the satellite position as a function of time and the star's position, we can relate the star's intensity to the tangent ray height of the star during occultation. By also knowing the position of the star, satellite, and the time, we obtain from geometry the geographic position of the tangent ray point.

The intensity data are normalized to the intensity of the star above the atmosphere and the normalized data are related to the tangential column number density of the absorbing species, here O_3, by the integral relationships expressing Beer's law

$$I(r_t)/\bar{I}_\infty = \left\{\int_0^\infty T(\lambda)I_\infty(\lambda)\exp\left(-\sigma_{O_3}(\lambda)N_{O_3}(r_t)\,d\lambda\right)\right\}\left\{\int_0^\infty T(\lambda)I_\infty(\lambda)\,d\lambda\right\}^{-1} \tag{1}$$

where from the geometry in Fig. 1, assuming a spherically stratified atmosphere

$$N_{O_3}(r_t) = 2\int_{r_t}^\infty \frac{n_{O_3}(r)r\,dr}{\sqrt{r^2 - r_t^2}}. \tag{2}$$

Here $I(r_t)$ is the photometer count rate at tangent ray height r_t and $\bar{I}_\infty$ is the photometer count rate of the stellar signal above the atmosphere. $T(\lambda)$ is the filter transmission and $I_\infty(\lambda)$ is the intensity of the star at wavelength λ above the atmosphere determined by the spectrometer; $\sigma_{O_3}(\lambda)$ is the absorption cross-section of molecular oxygen shown in Fig. 2 (Ditchburn and Young, 1962; Hudson *et al.*, 1969; Ackerman, 1970) and $N_{O_3}(r_t)$ is the tangential column number density of molecular oxygen at tangent ray radius r_t; and $n_{O_3}(r)$ is the local number density at the radius r.

Molecular oxygen is the sole absorbing species in the wavelength interval determined by filter 4-1, therefore the normalized intensity data are converted to tangential column number density data using Equation (1). The basic measurements are thus converted to data giving the tangential column number density of molecular oxygen as a function of tangent ray height. Equation (2) for the tangential column number density is the Abel integral

equation (cf. Hays and Roble, 1968a, b) which is inverted to obtain the local number density at the tangent ray point assuming spherical symmetry,

$$n_{O_2}(r) = \frac{1}{2\pi}\frac{d}{dr}\left\{\int_r^\infty \frac{r}{r_t}\frac{N_{O_2}(r_t)\,dr_t}{\sqrt{r_t^2 - r^2}}\right\}. \tag{3}$$

The actual numerical techniques for accomplishing this inversion are described in detail in a paper by Roble and Hays (1972).

The neutral gas temperature is derived by assuming diffusive equilibrium above 130 km for the O_2 number density. Thus,

$$T_{O_2}(r) = \frac{m_{O_2}}{k n_{O_2}(r)}\int_r^\infty g(r')n_{O_2}(r')\,dr' \tag{4}$$

where m_{O_2} is the mass of molecular oxygen, k is Boltzmann's constant, and g is the acceleration of gravity.

3. RESULTS

A relatively large number of absorption profiles were obtained during the time period extending from January 1970 to August 1971. Of these, command errors and tracking errors have caused serious question about many profiles. The final result of carefully selecting only those profiles where altitude is accurately known and where there are no command interrupts during the occultation yields 14 useful occultations. Of these, approximately 6 are in geomagnetically quiet periods and one series of 8 profiles was obtained during the magnetic storm of August 1970. Almost all of these profiles were obtained in low latitudes due to the low inclination of the orbital plane of the OAO-2 satellite. In addition to the molecular oxygen occultation scans, measurements were also made with a filter located in the Hartley continuum of ozone. (Filters 2-5 and 3-2 shown in Fig. 2). A single nighttime ozone number density profile was presented by Hays *et al.* (1973) and the results of the other scans are presented by Hays and Roble (1973).

(a) Molecular oxygen profiles during geomagnetically quiet periods

The geographic position, date, and local time of all of the scans analyzed are given in Table 1. Six of these were taken during geomagnetically quiet conditions. The normalized intensity measurements obtained on orbit 8884 on 17 August 1970 are shown in Fig. 4a. In Figs. 4b and 4c the retrieved molecular oxygen number density and temperature are shown and they are compared with *CIRA* 1965 (model 3, 06:00 hr.). In general, the retrieved molecular oxygen number density distribution in the 140–180 km region is about a factor of two lower than the number densities predicted by the *CIRA* 1965 model atmosphere at the same local time as the measurements. The composite of all of our quiet time data is shown in Fig. 5 along with the results of Krankowsky *et al.* (1968), Weeks and Smith (1968), and Roble and Norton (1972). The envelope encompassing the ozone number density profiles obtained from Hays and Roble (1972) and the molecular oxygen number density given by the mean *CIRA* 1965 atmosphere are also shown. The small number of stellar occultation profiles makes detailed seasonal variations difficult to discern. However, there does appear to be a marked decrease in the molecular oxygen number density corresponding to the decrease in solar activity during the period from the beginning of 1970 to late 1971. The monthly mean of the solar F10·7 flux during this period decreased from 153 to 120 ($\times 10^{-22}$)W cm^{-2}. The daily solar F10·7 emission for each of the individual

TABLE 1

Orbit	Date	Universal time (hr)	Universal time (min)	Local time (hr)	Local time (min)	Long.* (deg)	Lat. (deg)	Daily solar F10·7 emission ($\times 10^{-22}$ W cm^{-2})
5778	1/13/70	5	28	23	52	−84	48	172·9
8884	8/17/70	4	55	5	55	15	4	151·6
8898	8/18/70	4	19	5	51	23	9	149·0
8913	8/19/70	5	22	5	54	8	11	145·4
8942	8/21/70	5	55	4	27	−22	24	142·8
8943	8/21/70	7	35	4	23	−48	24	142·8
8957	8/22/70	6	58	4	22	−39	25	141·7
8971	8/23/70	6	20	4	44	−24	27	146·2
8985	8/24/70	5	45	4	13	−23	24	140·2
8986	8/24/70	7	25	4	13	−48	24	140·2
9000	8/25/70	6	47	5	17	−32	27	136·5
10902	1/ 4/71	13	29	22	38	−223	−16	140·2
11795	3/ 7/71	15	59	0	33	128	−34	105·2
14580	9/17/71	6	22	1	50	−68	26	116·5

* Measured positive eastward from Greenwich.

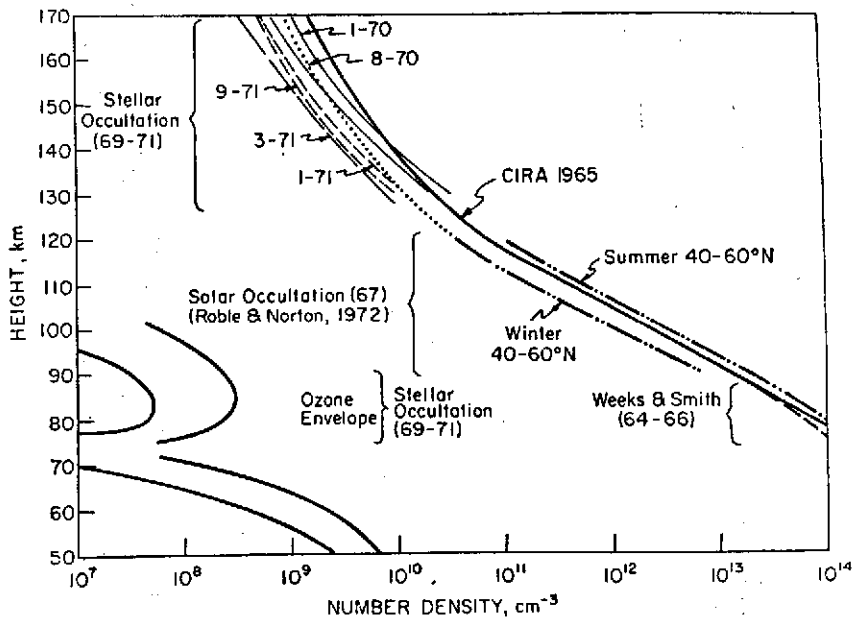

FIG. 5. COMPOSITE MOLECULAR OXYGEN DENSITY RESULTS FOR QUIET TIMES. .... Krankowsky *et al.*, 1968.

scans are given in Table 1. The apparent decrease in the thermospheric molecular oxygen at a fixed height probably implies that there is a general decrease in the altitude of the constant pressure surface at the base of the thermosphere as well as a decrease in the thermospheric temperature. This suggests a solar cycle influence in the lower thermosphere.

(b) Molecular oxygen profiles during geomagnetically disturbed periods

A series of observations was obtained during the magnetically disturbed period at the and of August 1970. These data are presented in Fig. 6 where density and temperature at

fixed heights are shown as a function of time. For comparison, we show the daily sum of magnetic K_p index on this same figure and give the latitude and longitude of the tangent ray point and local time of each occultation scan in Table 1. We note the marked decrease in the molecular oxygen number density following the storm at a time when the temperature was significantly enhanced. This is obviously in disagreement with the concept of a diffusively stable atmosphere. The decrease in the molecular oxygen density is apparently due to

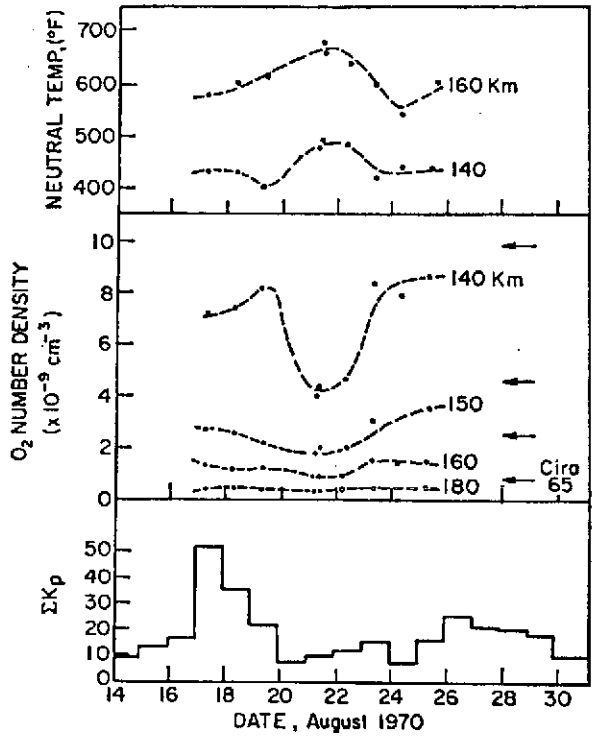

FIG. 6. MOLECULAR OXYGEN DENSITY AND TEMPERATURE VARIATIONS DURING THE MAGNETIC STORM OF AUGUST 1970.

the existence of a global-scale circulation system which upwells over the polar regions and subsides in the equatorial zone. Such a large horizontal scale overturning causes air with more atomic than molecular oxygen to move downward over the equator resulting in a change in the composition of the lower thermosphere. This result is consistent with the observation that energy deposited in the polar thermosphere is redistributed globally resulting in a global thermospheric temperature enhancement at low latitudes following a large magnetic storm (Hays *et al.*, 1972b). The daily solar F10·7 emission for the days on which occultation scans were made is given in Table 1. During the period the daily solar F10·7 emission decreased from 151·6 to 136·5 ($\times 10^{-22}$ W cm^{-2}). However, the molecular oxygen number density during this period first decreased, but then returned to pre-storm levels several days after the storm. This behavior also suggests an atmospheric response different from that expected from short term solar e.u.v. changes.

4. SUMMARY

The stellar occultation technique for measuring molecular oxygen in the Earth's thermosphere has demonstrated the following general behavior: (a) Thermospheric molecular oxygen decreases with decreasing solar activity. This may result from a general cooling of the lower thermosphere in addition to the cooling observed in the upper thermosphere.

(b) Magnetic storms result in strong global circulation systems which upwell in the polar regions and sink in equatorial regions. This results in a temporary decrease in the molecular constituents in the equatorial thermosphere.

Acknowledgement—We wish to acknowledge the support of Grant NGR 23-005-360, and NASA Contract Nas 1 9958. The National Center for Atmospheric Research is sponsored by the National Science Foundation. We wish to acknowledge the helpful support of Dr. Houk, and the O.A.O. Wisconsin and NASA experimental team.

REFERENCES

BRANNON, P. J. and HOFFMAN, J. M. (1971). Molecular oxygen density measurements from 80 to 140 kilometers. *J. geophys. Res.* **76**, 4630.

BYRAM, E. T., CHUBB, T. A. and FRIEDMAN, H. (1955). Dissociation of oxygen in the upper atmosphere. *Phys. Rev.* **98**, 1594.

CIRA, Cospar International Reference Atmosphere, (1965). 312 pp. North-Holland, Amsterdam.

DITCHBURN, R. W. and YOUNG, P. A. (1962). Absorption of molecular oxygen between 1850 and 2500 Å *J. atmos. terr. Phys.* **24**, 127.

FRIEDMAN, H., LICHTMAN, S. W. and BYRAM, E. T. (1951). Photon counter measurements of solar X-rays and extreme ultra-violet light. *Phys. Rev.* **83**, 1025.

HALL, L. A., SCHWEIZER, W. and HINTEREGGER, H. E. (1963). Diurnal variation of the atmosphere around 190 kilometers derived from solar extreme ultraviolet absorption measurements. *J. geophys. Res.* **68**, 6413.

HAYS, P. B. and ROBLE, R. G. (1968a). Stellar spectra and atmospheric composition. *J. atmos. Sci.* **25**, 1141.

HAYS, P. B. and ROBLE, R. G. (1968b). Atmospheric properties from the inversion of planetary occultation data. *Planet. Space Sci.* **16**, 1197.

HAYS, P. B., ROBLE, R. G. and SHAH, A. N. (1972). Terrestrial atmospheric composition from stellar occultations. *Science* **176**, 793.

HAYS, P. B., JONES, R. and REES, M. H. (1973). Auroral heating and the composition of the neutral atmosphere. *Planet. Space Sci.* in press.

HAYS, P. B. and ROBLE, R. G. (1973). Observations of mesospheric ozone at low latitudes. *Planet. Space Sci.*, **21**, 273.

HEDIN, A. E. and NIER, A. O. (1966). A determination of the neutral composition, number density, and temperature of the upper atmosphere from 120 to 200 kilometers with rocket-borne mass spectrometers. *J. geophys. Res.* **71**, 4121.

HINTEREGGER, H. E., HALL, L. A. and SCHMIDTKE, G. (1965). Solar XUV radiation and neutral particle distribution in July 1963 thermosphere. *Space Res. V*, 1175.

HUDSON, R. D., CARTER, V. C. and BREIG, E. L. (1969). Photodissociation in the Schumann-Runge Band system of O_2: Laboratory measurements and atmospheric effects. *J. geophys. Res.* **74**, 4079.

JURSA, A. S., NAKAMURA, M. and TANAKA, Y. (1963). Molecular oxygen distribution in the upper atmosphere. *J. geophys. Res.* **68**, 6145.

KRANKOWSKY, D., KASPRZAK, W. T. and NIER, A. O. (1968). Mass spectrometric studies of the composition of the lower thermosphere during summer 1967. *J. geophys. Res.* **73**, 7291.

KREPLIN, R. W. (1965). NRL solar radiation monitoring satellite: Description of instrumentation and preliminary results. *Space Res. V*, 951.

KUPPERIAN, J. E., JR., BYRAM, E. T. and FRIEDMAN, H. (1959). Molecular oxygen densities in the mesosphere at Fort Churchill. *J. atmos. terr. Phys.* **16**, 174.

LANDINI, M., RUSSO, D. and TAGLIAFERRI, G. L. (1965). Atmospheric density in the 120–190 Km region derived from the X-ray extinction measured by the U.S. Naval Research Laboratory Satellite 1964-01-D. *Nature* **206**, 173.

LANDINI, M., RUSSO, D. and TAGLIAFERRI, G. L. (1967). Atmospheric density measured by the attenuation of the solar X-rays monitored on the NRL 1965-16D satellite. *Icarus* **6**, 236.

LINK, R. (1969). *Eclipse in Astronomy*, 271 pp. Springer, New York.

LOCKEY, G. W., HORTON, B. H. and ROPE, B. (1969). Satellite measurement of upper atmospheric molecular oxygen density. *Nature, London* **223**, 387.

MAY, B. R. (1971). A method of determining the density of thermospheric gases from measurements of solar ultra-violet light absorption at grazing-ray and near-vertical incidence. *Planet. Space Sci.* **19**, 27.
NIER, A. O., HOFFMAN, J. H., JOHNSON, C. Y. and HOLMES, J. C. (1964). Neutral composition of the atmosphere in the 100 to 200 kilometer range. *J. geophys. Res.* **69**, 979.
NORTON, R. B. and WARNOCK, J. M. (1968). Seasonal variation of molecular oxygen near 100 kilometers. *J. geophys. Res.* **73**, 5798.
OPAL, C. B. and MOOS, H. W. (1969). Night-time molecular oxygen densities in the 100- to 130-km region from Schumann–Runge absorption. *J. geophys. Res.* **75**, 788.
QUESSETTE, J. A. (1970). On the measurement of molecular oxygen concentration by absorption spectroscopy. *J. geophys. Res.* **75**, 839.
REID, R. H. G. and WITHBROE, G. L. (1970). The density and vibrational distribution of molecular oxygen in the lower thermosphere. *Planet. Space Sci.* **18**, 1255.
ROBLE, R. G. and NORTON, R. B. (1972). Thermospheric molecular oxygen from solar EUV occultation measurements. *J. geophys. Res.* **77**, 3524.
ROBLE, R. G. and HAYS, P. B. (1972). A technique for recovering the vertical number density profile of atmospheric gases from planetary occultation data. Submitted to *Planet. Space Sci.* **20**, 1727.
SCHAEFER, E. J. and NICHOLS, M. H. (1964). Neutral composition obtained from a rocket-borne mass spectrometer. *Space Res. IV*, 205.
SCHAEFER, E. J. (1968). Temperature and composition of the lower thermosphere obtained from mass spectrometer measurements. *Space Res. VIII*, 959.
STEWART, K. H. and WILDMAN, P. J. L. (1969). Preliminary results of molecular oxygen observations from Ariel III satellite. *Proc. R. Soc.* **A311**, 591.
THOMAS, L. and NORTON, R. B. (1967). Absorption of solar X-rays and density changes between 140 and 160 kilometers. *J. geophys. Res.* **72**, 5552.
THOMAS, L., VENABLES, F. H. and WILLIAMS, K. M. (1965). Measurements of solar X-ray fluxes by the U.S. Naval Research Laboratory Satellite 1965-01-D.
VENABLES, F. H. (1967). Solar X-rays in the wavelength band 44-60A observed by the U.S. NRL satellite 1965-16D and atmospheric optical densities deduced from these observations. *Planet. Space Sci.* **15**, 681.
VON ZAHN, U. and GROSS, J. (1969). Mass spectrometric investigation of the thermosphere at high latitudes. *J. geophys. Res.* **74**, 4055.
WEEKS, L. H. and SMITH, L. G. (1968). Molecular oxygen concentrations in the upper atmosphere by absorption spectroscopy. *J. geophys. Res.* **73**, 4835.

APPENDIX VI.

Observation of Mesospheric Ozone at Low Latitudes

Planet. Space Sci. 1973, Vol. 21, pp. 273 to 279. Pergamon Press. Printed in Northern Ireland

OBSERVATION OF MESOSPHERIC OZONE AT LOW LATITUDES

P. B. HAYS
Departments of Aerospace Engineering, Meteorology and Oceanography, University of Michigan, Ann Arbor, Michigan 48104, U.S.A.

and

R. G. ROBLE
National Center for Atmospheric Research, Boulder, Colorado 80302, U.S.A.

(*Received in final form* 21 *August* 1972)

Abstract—Stellar ultraviolet light near 2500 Å is attenuated in the Earth's upper atmosphere due to strong absorption in the Hartley continuum of ozone. The intensity of stars in the Hartley continuum region has been monitored by the University of Wisconsin stellar photometers aboard the OAO-2 satellite during occultation of the star by the Earth's atmosphere. These data have been used to determine the ozone number density profile at the occultation tangent point. The results of approximately 12 stellar occultations, obtained in low latitudes, are presented, giving the nighttime vertical number density profile of ozone in the 60- to 100-km region. The nighttime ozone number density has a bulge in its vertical profile with a peak of 1 to 2 $\times 10^8$ cm^{-3} at approximately 83 km and a minimum near 75 km. The shape of the bulge in the ozone number density profile shows considerable variability with no apparent seasonal or solar cycle change. The ozone profiles obtained during a geomagnetic storm showed little variation at low latitudes.

1. INTRODUCTION

The first measurement of the ozone concentration in the upper atmosphere was made by Johnson *et al.* (1951) using u.v. absorption spectroscopy. The ozone number density distribution was determined from the u.v. absorption measurements made at various altitudes by a spectrometer aboard a rocket. Since then daytime measurements of the ozone number density distribution have been made from rockets using the Sun as the u.v. source (Van Allen and Hopfield, 1952; Johnson *et al.*, 1952; L'vova *et al.*, 1964; Poloskov *et al.*, 1966; Nagata *et al.*, 1967; Weeks and Smith, 1968; Krueger, 1969) and nighttime measurements have been made using the Moon as a source of u.v. light (Carver *et al.*, 1967; Carver *et al.*, 1972). The high altitude ozone number density distribution has also been determined from solar occultation measurements made from a satellite (Rawcliffe *et al.*, 1963; Miller and Stewart, 1965). These measurements have determined the ozone number density up to an altitude of about 70 km.

Several other techniques have been used to obtain the ozone number density distribution in the upper atmosphere which include (a) satellite eclipse photometry (Venkateswaren *et al.*, 1961; Fesenkov, 1967), (b) nighttime airglow spectral photometry (Reed, 1968), (c) spectral analysis of backscattered solar radiation as observed from a satellite (Rawcliffe and Elliot, 1966; Anderson *et al.*, 1969), (d) chemi-luminescent ozone sondes (Hilsenrath, 1971) and (e) rocket and ground based observations of the molecular oxygen emission $O_2(^1\Delta g)$ at 1·27 μ (Evans and Llewellyn, 1970; 1972; Evans *et al.*, 1970). In the latter technique, the ozone number density profile is calculated from the measured altitude profiles of the $O_2(^1\Delta g)$ emission at 1·27 μ using photochemical theory. Their results give the ozone number density profile at twilight up to 100 km and preliminary observations indicate a strong seasonal variation of the upper ozone layer at high latitudes. The peak ozone number density at 85 km varied between 1·3 $\times 10^8$ cm^{-3} in midwinter to less than 0·3 $\times 10^8$ cm^{-3} in midsummer.

Hays and Roble (1968a) suggested that the nighttime distribution of ozone in the upper mesosphere may be obtained from satellite measurements of the intensity of u.v. stars during occultation by the Earth's atmosphere. During the past few years, we have used the Orbiting Astronomical Observatory (OAO-2) to obtain u.v. stellar occultation data in various spectral regions. The data from the u.v. filters centered at 2390 and 2460 Å have been used to obtain the nighttime ozone number density distribution from 60 to 100 km at low latitudes. In this paper we describe the experimental technique and present the results which were obtained during quiet and disturbed geomagnetic conditions.

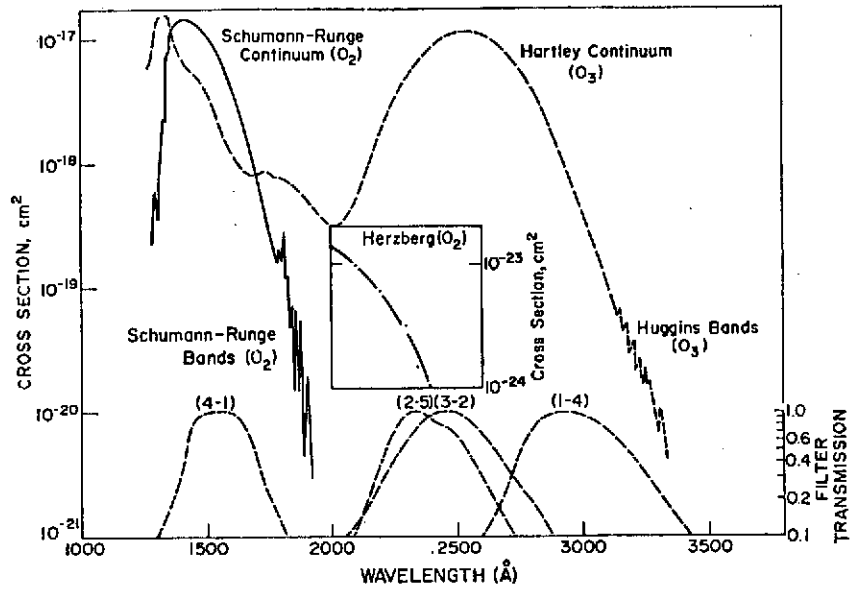

FIG. 1. ABSORPTION CROSS SECTIONS FOR MOLECULAR OXYGEN AND OZONE IN THE SPECTRAL REGION EXTENDING FROM 1000 TO 3500 Å.
Dashed curves are the OAO-2 stellar photometer filter transmission curves used in this study.

2. EXPERIMENTAL TECHNIQUE

The general details of the stellar occultation technique have been described by Hays and Roble (1968a, b; 1972), Hays *et al.* (1972) and Roble and Hays (1972). Here we describe the specifics of the occultation measurements made by the OAO-2 satellite as they apply to the determination of the nighttime ozone number density.

The OAO-2 satellite has one 16 in.-dia u.v. telescope and four 8 in.-dia u.v. telescopes and an u.v. spectrometer having a resolution of approximately 5 Å. Filter 2–5 and 3–2 shown in Fig. 1, are the two filters in the University of Wisconsin optical package that are used for the ozone stellar occultation measurements. The transmission function of these filters is located in the Hartley continuum of ozone (Fig. 1) with the peak transmission at 2380 and 2460 Å. The detection systems of the u.v. telescope have a maximum data acquisition rate of $\frac{1}{8}$ sec time integration resulting in a high altitude resolution at the tangent point. The intensity data are obtained as a function of time, and by knowing the star's position is orbital elements of the satellite, we can relate the intensity to the tangent ray heights during occultation by the Earth's atmosphere. Figure 2 shows the normalized intensity data as a function of tangent ray height for a typical occultation scan. Hays and Roble (1972) describe the technique used to relate the normalized intensity

data to the tangential column number density of the absorbing species along the ray path. This technique allows for the broadband characteristics of the u.v. transmission function and can be used as long as absorption is due to a single species. Hays and Roble (1968b) have calculated the u.v. transmission of the Earth's upper atmosphere and have shown that the stellar light in the wavelength regions covered by the filter transmission functions, shown in Fig. 1, is primarily absorbed by ozone. However, at

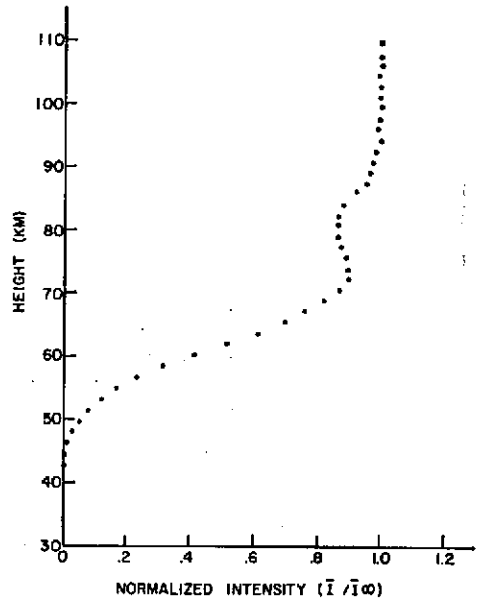

FIG. 2. NORMALIZED INTENSITY PROFILE FOR A TYPICAL OZONE OCCULTATION.

altitudes below about 70 km the stellar ultraviolet light is also absorbed by molecular oxygen in the Herzberg continuum. The absorption contribution in the Herzberg continuum is calculated using the molecular oxygen number density distribution obtained from the *CIRA* 1965 model atmosphere. This absorption contribution is removed from the stellar intensity data and the corrected normalized intensity is related to the ozone tangential column number density (Hays and Roble, 1972). Once the tangential column number density is known as a function of the tangent ray height, the data are inverted, using the technique described by Roble and Hays (1972), to obtain the local number density at the tangent ray point.

3. RESULTS

Stellar occultation measurements using the two filters centered in the Hartley continuum of ozone were made during the period extending from January 1970 through August 1971. From these data we have obtained 12 orbits on which one or both of the filters could be used to determine the ozone density in the mesosphere. These results, corrected for molecular oxygen absorption in the Herzberg continuum, and rayleigh scattering are presented in Figs. 3–5 where four separate profiles are illustrated in each figure. According to the analysis of Roble and Hays (1972), the ozone number density is best retrieved from the occultation data between tangent ray heights of 55 to 95 km. The retrieved ozone number density data above and below this altitude interval are less reliable.

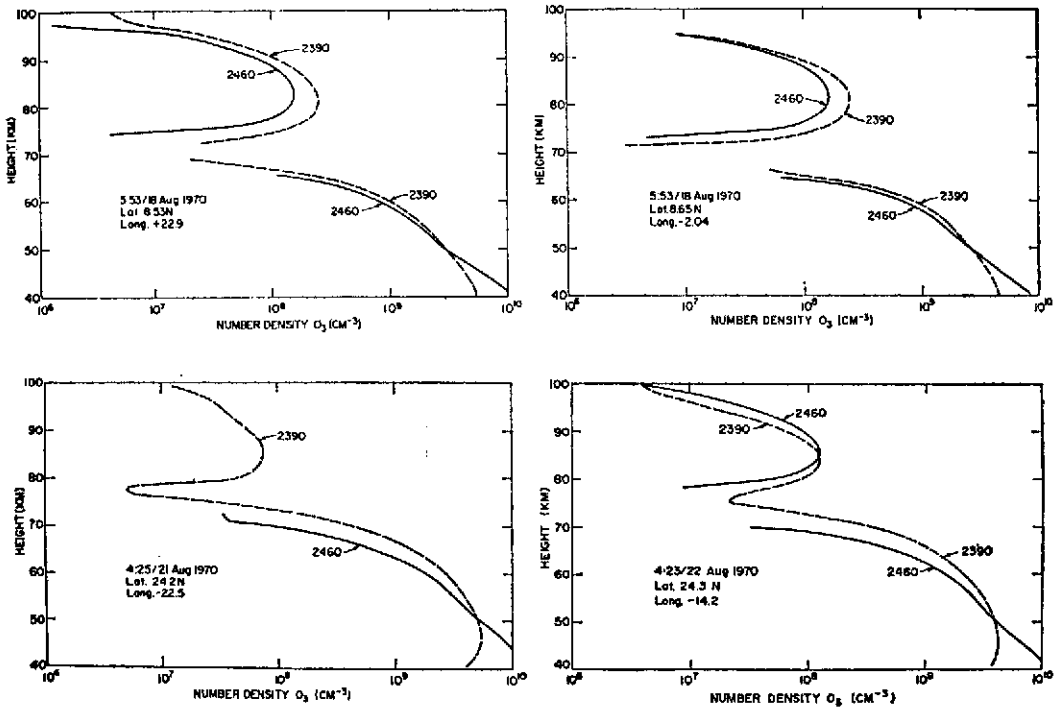

FIG. 3. ALTITUDE PROFILES FOR ATMOSPHERIC OZONE OBTAINED USING THE STELLAR OCCULTATION TECHNIQUE.
Geographic position refers to the tangent ray point of the occultation measurements (time as LMT; longitude measured positive eastward from Greenwich).

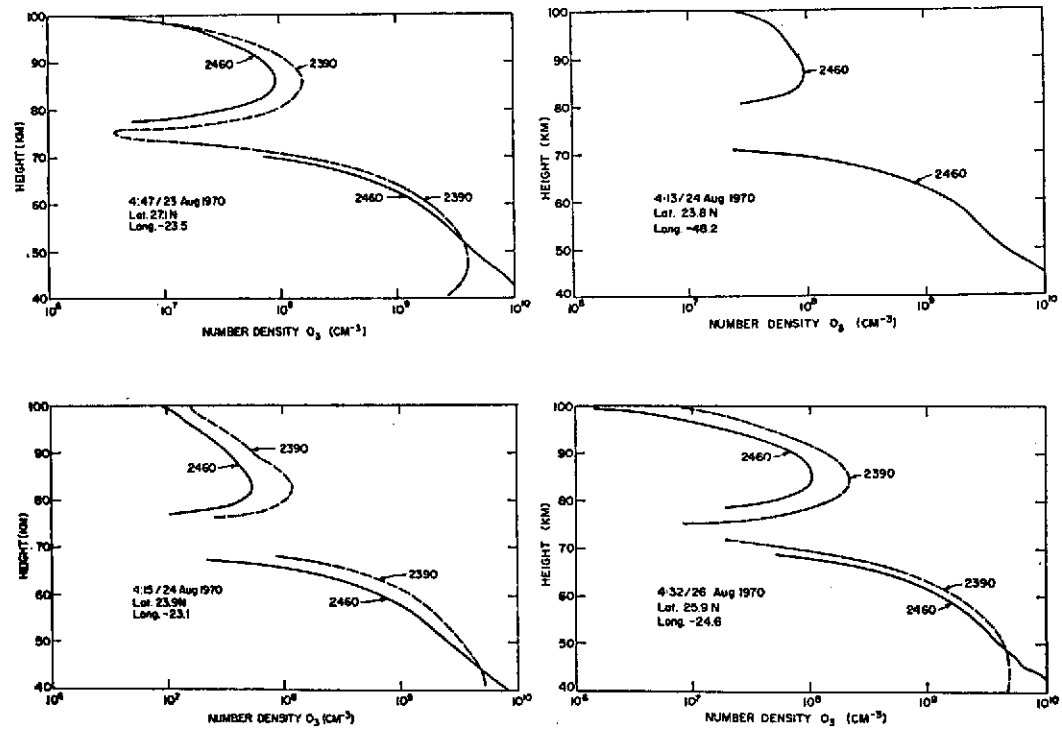

FIG. 4. SAME CAPTION AS IN FIG. 3.

A careful examination of these ozone profiles in the mesosphere does not show any striking systematic seasonal or diurnal pattern in the equatorial regions. There does appear to be a systematic increase in the altitude of the high altitude ozone bulge with increasing latitude. However, due to the small number of scans, which were made at nearly random local time, season, and latitude, it is difficult to place great weight on the

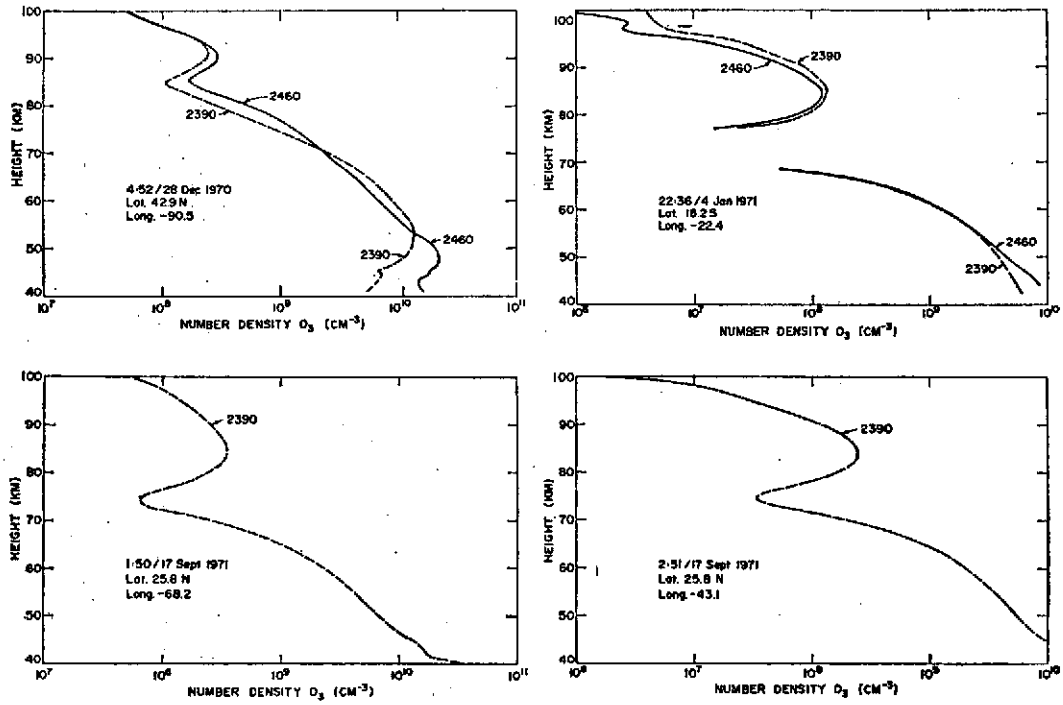

FIG. 5. SAME CAPTION AS IN FIG. 3.

slight variations observed. The major conclusion is that ozone varies very little between 55 and 100 km during the course of the night at low latitudes. The main feature is the expected bulge in density which occurs at approximately 85 km and the depletion of ozone just below that altitude. This behavior is predicted by most recent theoretical studies which incorporate the hydrogen chemistry in their model.

Numerous theoretical studies of the chemistry of ozone in a moist atmosphere have followed the early discussion of Bates and Nicolet (1950) of the influence of hydrogen compounds (Hampson, 1964; Hunt, 1966a; Hunt, 1966b; Hesstvedt, 1968; Leovy, 1969; Bowman *et al.*, 1970; Hunt, 1971; Shimazaki and Laird, 1972; Strobel, 1972). The result of these studies is somewhat confusing due to the large number of choices of possible rate coefficients, photodissociation rates, boundary conditions, and eddy mixing rates used by these authors. The theoretical results do indicate the general features observed in the OAO-2–A2 stellar occultation measurement. This is illustrated in Fig. 6 where three representative theoretical profiles (Hesstvedt, 1968; Shimazaki and Laird, 1970; Hunt, 1971) are compared with our envelope curve. Hunt (1971) appears to agree best with the observations, but it is difficult to assess whether this is fortuitous or the result of a correct choice of the multitude of possible variable factors.

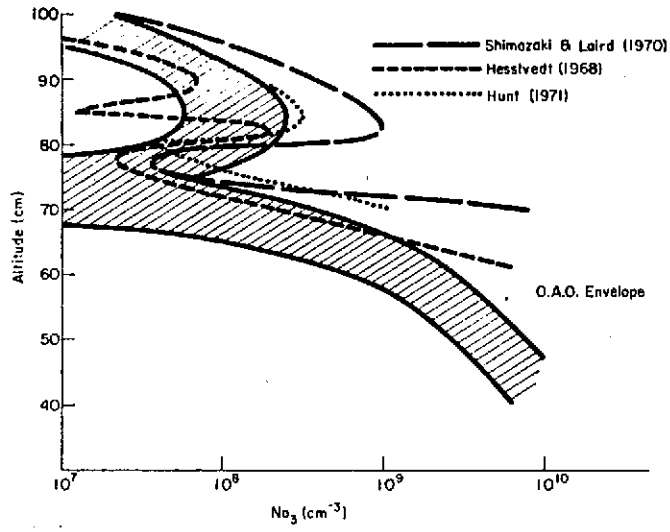

FIG 6. COMPARISON OF MEASURED OZONE ENVELOPE WITH THEORETICAL CALCULATIONS.

It should be pointed out that during the period of time in which these observations were taken one series of measurements was made while the large magnetic storm of August 1970 was in progress. There does not appear to be any significant correlation between the ozone density in the mesosphere and storm in agreement with the prediction of Maeda and Aiken (1968). This is not surprising, but relatively large variation in O_2 at higher altitudes was observed (Hays and Roble, 1972) at the same time.

SUMMARY

The stellar occultation measurements of ozone in the mesosphere indicate the following conclusions:

1. Mesospheric ozone varies by as much as a factor of 4 at high altitudes, but does not show any clear seasonal or diurnal nighttime pattern. A slight increase in the altitude of the 85 km bulge appears to be associated with increasing latitude.
2. The observations are generally in agreement with results of theoretical predictions which utilize a moist atmosphere in which hydrogen compounds are considered in the chemistry.
3. There is no apparent relationship between mesospheric ozone and geomagnetic activity at low latitudes.

Acknowledgement—This work was supported by NASA Grant NGR 23 005-360 and NASA Contract NAS 1 9958. The National Center for Atmospheric Research is sponsored by the National Science Foundation. We wish to acknowledge the helpful support of Dr. Houk, and the O.A.O. Wisconsin and NASA experimental team.

REFERENCES

ANDERSON, G. P., BARTH, C. A., CAYLA, F. and LONDON, J. (1969). Satellite observations of the vertical ozone distribution in the upper atmosphere. *Annls Géophys.* **25**, 341.

BATES, D. R. and NICOLET, M. (1950). The photochemistry of atmospheric water vapor. *J. geophys. Res.* **55**, 301.

BOWMAN, M. R., THOMAS, L. and GEISLER, J. E. (1970). The effect of diffusion processes on the hydrogen and oxygen constituents in the mesosphere and lower thermosphere. *J. atmos. terr. Phys.* **32**, 1661.

CARVER, J. H., HORTON, B. H. and BURGER, F. G. (1967). Rocket determination of the night ozone distribution and the lunar ultraviolet flux. *Space Research* VII, p. 1020.

CARVER, J. H., HORTON, B. H., O'BRIEN, R. S. and ROFE, B. (1972). Ozone determinations by lunar rocket photometry. *Planet. Space Sci.* **20**, 217.
EVANS, W. F. J., WOOD, H. C. and LLEWELLYN, E. J (1970). Ground-based photometric observations of the 1·27 μ band in the evening twilight. *Planet. Space Sci.* **18**, 1065.
EVANS, W. F. J. and LLEWELLYN, E. J. (1970). Molecular oxygen emissions in the airglow. *Annls Géophys.* **26**, 167
EVANS, W. F. J. and LLEWELLYN, E. J. (1972). Measurements of mesospheric ozone from observations of the 1·27 μ band. *Radio Sci.* **7**, 45.
FESENKOV, V. G. (1967). A satellite technique for sounding the optical properties of the atmosphere. *Soviet Astron* AJ, **11**, 1.
HAMPSON, J. (1964). Photochemical behavior of the ozone layer. *Can. Armament Res. Develop. Estab. Tech. Note 1627/64* Carde, Quebec, Canada.
HAYS, P. B. and ROBLE, R. G (1968a). Atmospheric properties from the inversion of planetary occultation data. *Planet. Space Sci.* **16**, 1197.
HAYS, P. B. and ROBLE, R. G. (1968b). Stellar spectra and atmospheric composition. *J. atmos. Sci.* **25**, 1141.
HAYS, P. B., ROBLE, R. G. and SHAH, A. N. (1972). Terrestrial atmospheric composition from stellar occultations. *Science*, **176**, 793.
HAYS, P. B. and ROBLE, R. G. (1972). Stellar occultation measurements of molecular oxygen in the lower thermosphere. *Planet. Space Sci.* In press.
HESSTVEDT, E. (1968). On the effect of vertical eddy transport on atmospheric composition in the mesosphere and lower thermosphere. *Geophys. Norv.* **27**, 1.
HILSENRATH, E. (1971). Ozone measurements in the mesosphere and stratosphere during two significant geophysical events. *J. atmos. Sci.* **28**, 295.
HUNT, B. G. (1966a) The need for a modified photochemical theory of the ozonosphere. *J. atmos. Sci.* **23**, 88.
HUNT, B. G. (1966b). Photochemistry of ozone in a moist atmosphere. *J. geophys. Res.* **71**, 1385.
HUNT, B. G. (1971). A diffusion photochemical study of the mesosphere and lower thermosphere and the associated conservation mechanism. *J. atmos. terr. Phys.* **33**, 1869.
JOHNSON, F. S., PURCELL, J. D. and TOUSEY, R. (1951). Measurements of the vertical distribution of atmospheric ozone from rockets. *J. geophys. Res.* **56**, 583.
JOHNSON, F. S. PURCELL, J. D., TOUSEY, R. and WATANABE, K. (1952). Direct measurements of the vertical distribution of atmospheric ozone to 70 km altitude. *J. geophys. Res.* **57**, 157.
KRUEGER, A. J. (1969). Rocket measurements of ozone over Hawaii *Annls Géophys.* **25**, 307.
LEOVY, C. B. (1969). Atmospheric ozone: An analytic model for photochemistry in the presence of water vapor. *J. geophys. Res.* **74**, 417.
L'VOVA, A. A., MIKIROV, A. Y. E. and POLOSKOV, S. M. (1964). Rocket investigation of the vertical ozone distribution above the level of maximum concentration during the total solar eclipse of February 15, 1961. *Geomagn. Aeron.* **4**, 839.
MAEDA, K. and AIKEN, A. C. (1968). Variations of polar mesospheric oxygen and ozone during auroral events. *Planet. Space Sci.* **16**, 371.
MILLER, D. E. and STEWART, K. H. (1965). Observations of atmospheric ozone from an artificial earth satellite. *Proc. R. Soc.* **A288**, 540.
NAGATA, T., TOHMATSU, T. and TSURUTA, H. (1967). Observations of mesospheric ozone density in Japan. *Space Research* VII, p. 639.
POLOSKOV, S. M., L'VOVA, A. A. and MIKIROV, A. E. (1966). Rocket measurements of ozone profiles above the level of maximum concentration. *Space Research* VII, p. 1009.
RAWCLIFFE, R. D., MELOY, G. E., FRIEDMAN, R. M. and ROGERS, E. H. (1963). Measurement of vertical distribution ozone from a polar orbiting satellite. *J. geophys. Res.* **68**, 6425.
RAWCLIFFE, R. D. and ELLIOT, D. D. (1966). Latitude measurement of ozone at high altitude deduced from a satellite measurement of the earth's radiance at 2840 Å. *J. geophys. Res.* **71**, 5077.
REED, E. I. (1968). A night measurement of mesospheric ozone by observations of ultraviolet airglow. *J. geophys. Res.* **73**, 2951.
ROBLE, R. G. and HAYS, P. B. (1972). A technique for recovering the vertical number density profile of atmospheric gases from planetary occultation data. *Planet. Space Sci.* **20**, 1727.
SHIMAZAKI, T. and LAIRD, A. R. (1972). Seasonal effects on distributions of minor neutral constituents in the mesosphere and lower thermosphere. *Radio Sci.* **7**, 23.
STROBEL, D. F. (1972). Minor neutral constituents in the mesosphere and lower thermosphere. *Radio Sci.* **7**, 1.
VAN ALLEN, J. A. and HOPFIELD, J. J. (1952). Preliminary report on atmospheric ozone measurements from rockets. *Mem Soc. R. Sci., Liège* **12**, 179.
VENKATESWARAN, S. V., MOORE, J. G. and KRUEGER, A. J. (1961). Determination of the distribution of ozone by satellite photometry. *J. geophys. Res.* **66**, 1751.
WEEKS, L. H. and SMITH, L. G. (1968). A rocket measurement of ozone near sunrise. *Planet. Space Sci.* **16**, 1189.

APPENDIX VII.

The Nighttime Distribution of Ozone in the Low-Latitude Mesosphere

THE NIGHTTIME DISTRIBUTION OF OZONE IN THE LOW-LATITUDE MESOSPHERE

R. G. Roble
National Center for Atmospheric Research[1]
Boulder, Colorado 80302

P. B. Hays
Department of Atmospheric & Oceanic Science
University of Michigan
Ann Arbor, Michigan 48104

---

[1]The National Center for Atmospheric Research is sponsored by the National Science Foundation.

In press, Pure and Applied Geophysics, 1973.

ABSTRACT

The intensity of stars at wavelengths in the Hartley continuum region of ozone has been monitored by the University of Wisconsin stellar photometers aboard the OAO-2 satellite during occultation of the star by the earth's atmosphere. These occultation data have been used to determine the ozone number density profile at the occultation tangent point. The nighttime ozone number density profile has a bulge in its vertical profile with a peak of 1 to $3 \times 10^8 \text{ cm}^{-3}$ at approximately 83 km and a minimum near 75 km. The ozone number density at high altitudes varies by as much as a factor of 4, but does not show any clear seasonal variation or nighttime variation. The retrieved ozone number density profiles define a data envelope that is compared with other nighttime observations of the ozone number density profile and also the results of theoretical models.

Calculations are also presented that illustrate the difference in retrieving the bulge in the ozone number density profile from stellar and solar occultation data.

1. Introduction

Stellar intensity measurements, in certain ultraviolet atmospheric absorption bands, made by a satellite during occultation of the star by the earth's atmosphere, can be used to obtain the local number density of the absorbing species at the occultation tangent point (Hays and Roble, 1968a;b). During the past few years the Orbiting Astronomical Observatory (OAO-2) has been used to make these occultation intensity measurements using bright ultraviolet stars (Hays, et al., 1972). The occultation technique is based on classical ultraviolet absorption spectroscopy. The star is the source of ultraviolet light and the stellar photometers aboard the OAO-2 satellite are the detectors. The atmosphere between the star and the detectors acts as the absorption cell. During the occultation process, the stellar light passes through progressively denser regions of the atmosphere and the ultraviolet light is absorbed due to the strong absorption features of certain atmospheric gases. The basic measurement is thus the stellar intensity as a function of time, but by knowing the star's position and the satellite orbital elements, the intensity is related to the tangent ray height of the occulting star. If absorption is due to a single species, the normalized stellar intensity is directly related to the tangential column number density of the absorbing species through Beer's Law (Hays and Roble, 1972a). The data giving the tangential column

number density as a function of tangent ray height are directly inverted, using the technique described by Roble and Hays (1972) to obtain the local number density profile of the absorbing species at the occultation tangent point.

Occultation measurements made in the Schumann - Runge continuum of molecular oxygen near 1500 Å have been used to obtain the molecular oxygen number density profile in the lower thermosphere. These measurements have been discussed by Hays and Roble (1972a). The nighttime number density profile of ozone in the mesosphere has also been determined from stellar intensity measurements made in the Hartley continuum region of ozone near 2500 Å. The results of these measurements are discussed by Hays and Roble (1972b).

In this paper, we compare the results of the OAO-2 ozone measurements with theory and other nighttime ozone measurements. We also present the results of a single occultation scan and discuss the difference in retrieving the ozone number density bulge near 80 km from solar and stellar occultation data.

2. Stellar occultation scan

The ozone and molecular oxygen absorption cross sections and the transmission function of the various ultraviolet filters used with the OAO-2 stellar photometers for the occultation measurements are shown in Fig. 1. Filter (4-1) is located in the Schumann - Runge continuum region of molecular oxygen and is used to obtain the molecular oxygen number density in the lower thermosphere. Filters (2-5) and (3-2) are in the Hartley continuum region of ozone and are used to obtain the ozone number density profile in the mesosphere. Filter (1-4) is used to measure the ozone number density in the stratosphere.

The results presented in this paper were determined from occultation data obtained by the OAO-2 stellar photometers using filters (2-5) and (3-2). Hays and Roble (1968b) have shown that stellar ultraviolet light near 2500 Å is primarily absorbed by ozone in the earth's atmosphere and stellar occultation measurements within this wavelength region can be used to obtain the ozone number density profile in the 60 to 100 km altitude interval. In the lower portion of the altitude interval rayleigh scattering and molecular oxygen absorption in the Hertzberg continuum have small contributions to the total attenuation. These contributions are eliminated from the data as discussed by Hays and Roble (1972a).

The intensity spectrum of the star above the earth's atmosphere

is measured by an ultraviolet spectrometer aboard the OAO-2 satellite. A typical star spectrum, obtained on orbit 12178 on April 3, 1971, is shown in Fig. 2. The solar spectrum is also shown in Fig. 2 for comparison. The normalized signal of this star, measured during occultation using the OAO-2 stellar photometer with filter (3-2), is shown in Fig. 3a. Below 100 km the signal decreases due to absorption by ozone. The decrease in the signal continues until an altitude of about 83 km, then a slight increase in the signal occurs reaching a maximum around 75 km. Below 75 km the signal decreases again until occultation near 45 km. The ozone number density profile at the occultation tangent point is obtained from the intensity data using the inversion scheme described by Roble and Hays (1972) and Hays and Roble (1972a) and is shown in Fig. 3b. The dip in the normalized intensity curve near 80 km, shown in Fig. 3a, is due to a bulge in the ozone number density distribution at that altitude. The peak ozone number density at the bulge is 3×10^8 cm^{-3} at 83 km. The minimum occurs near 73 km, however the magnitude of the number density at that altitude is difficult to determine. A complete discussion of accuracy of the inversion scheme and an analysis of errors in the occultation measurements have been given by Roble and Hays (1972).

3. Stellar vs. solar occultation

The ozone number density profile has also been determined from solar occultation measurements made from a satellite (Rawcliffe et al., 1963; Miller and Stewart, 1965). If the intensity from the entire solar disk is used during occultation, the effect of the finite size of the sun must be considered in analyzing the data. In this section we examine whether the bulge in the ozone number density near 80 km can be determined from solar occultation measurements when the entire solar disk is used as the source. For simplicity a model of the ozone number density profile is used in these calculations. The ozone profile is approximated by a sum of gaussian and exponential functions (Roble and Hays, 1972) and the profile is shown in Fig. 3b. The normalized intensity calculations for a stellar occultation, using OAO-2 filter (3-2), are shown in Fig. 3a. The intensity calculations for the broadband filter require a wavelength integration over the effective passband of the filter (Hays and Roble, 1972a). Therefore, we use the stellar spectrum, shown in Fig. 2, the ozone absorption cross-section and the filter transmission functions, shown in Fig. 1, to calculate the normalized occultation signal for the model ozone number density distribution. The calculated normalized intensity profile is shown in Fig. 3a and it has approximately the same shape as the OAO-2 occultation data. The dip in the intensity curve defines the bulge in the ozone number density profile.

For a solar occultation, the finite size of the sun must be considered because the solar energy emitted from different portions of the solar disk is transmitted through the earth's atmosphere at different tangent ray heights. The normalized intensity for a solar occultation is calculated using the technique of Roble and Norton (1972) and is shown in Fig. 3a. For these calculations, we used the solar energy spectrum, shown in Fig. 2, the ozone cross-section and the filter (3-2) transmission function shown in Fig. 1. The dip in the intensity curve that occurs in the stellar occultation case does not appear in the solar occultation case. From normal satellite altitudes the tangent ray heights of the upper and lower limb of the solar disk are separated by approximately 25 km. Therefore, a smearing of the intensity variation caused by the bulge in the ozone number density profile occurs when the entire solar disk is used during occultation and a dip in the intensity profile is not evident. The calculated normalized intensity variation across the solar disk at a tangent ray height of 83 km for the center of the solar disk is shown in Fig. 4. The tangent ray height of the upper limb is 95 km and the lower limb is 70 km. The intensity variation caused by the bulge in the ozone number density profile at 83 km occurs near the center of the solar disk. The intensity structure across the solar disk

is not evident when the overall intensity from the entire solar disk is measured during occultation. In theory, the structure in the ozone number density profile can be retrieved from solar occultation data using the entire solar disk, with an iterative technique. However, in practice, the iterative scheme is difficult to use especially in the presence of statistical noise. Better results would be obtained if a small portion of the solar disk is used for the solar occultation measurements.

4. Comparison of results

The ozone number density profiles from 12 stellar occultations have been presented by Hays and Roble (1972b). The measurements indicate that mesospheric ozone has a variation of as much as a factor of 4 at high altitudes, but does not show any clear seasonal or nighttime variation. A slight increase in the altitude of the bulge in the ozone number density profile appears to be associated with increasing latitude. These measurements plus a few additional ones are used to define an envelope representing the ozone number density profiles determined from the OAO-2 stellar occultation measurements. The envelope is shown in Fig. 5 along with nighttime and twilight ozone profiles determined by other experimenters. At high altitudes there is good agreement with the ozone number density profiles determined by the OAO-2 satellite and the profiles deduced by Evans and Llwellyn (1970; 1972). Between 60 and 75 km, the data of Evans and Llwellyn (1970; 1972), Evans et al. (1970), Weeks and Smith (1968), Miller and Stewart (1965), Tisone (1972) and Rawcliffe et al. (1963) are clustered along the upper limb of the OAO-2 ozone data envelope. Below 60 km, the OAO-2 ozone data envelope does not agree with the results of Carver, et al. (1967; 1972), Reed (1968) and Hilsenrath (1971). This departure from the other observations is probably due to the difficulty of retrieving the ozone number density at low signal levels in the presence of statistical noise.

Roble and Hays (1972) show that the ozone number density is best retrieved between normalized occultation data values of 0.1 - 0.9. Therefore, the ozone number density profile determined from the OAO-2 occultation measurements are limited to the 60 - 95 km altitude interval. In Fig. 6 the OAO-2 ozone data envelope is also compared with the ozone number density profile determined from various theoretical models. In general, there is a large variation between the various theoretical models. However, the general features of the OAO-2 ozone measurements appear to be present in the results of theoretical predictions which utilize a moist atmosphere in which hydrogen compounds are considered in the chemistry.

ACKNOWLEDGMENT

We thank K. S. Hansen for programming assistance and A. N. Shah for obtaining the data. This work was supported in part by NASA Grant NGR 23 005-360 and NASA contract NAS 19958. We wish to acknowledge the helpful support of Dr. Houk and the OAO Wisconsin and NASA experimental team.

REFERENCES

Ackerman, M., 1972: Ultraviolet solar radiation related to mesospheric processes. Aeron. Acta., A, No. 77.

Bowman, M. R., L. Thomas, and J. E. Geisler, 1970: The effect of diffusion processes on the hydrogen and oxygen constituents in the mesosphere and lower thermosphere. J. Atmos. Terr. Phys., 32, 1661.

Carver, J. H., B. H. Horton, and F. G. Burger, 1967: Rocket determination of the night ozone distribution and the lunar ultraviolet flux. Space Res., 7, 1020.

Carver, J. H., B. H. Horton, R. S. O'Brien, and B. Rofe, 1972: Ozone determinations by lunar rocket photometry. Planetary Space Sci., 20, 217.

Evans, W. F. J. and E. J. Llewellyn, 1970: Molecular oxygen emissions in the airglow. Ann. Geophys., 26, 167.

Evans, W. F. J. and E. J. Llewellyn, 1972: Measurements of mesospheric ozone from observations of the 1.27μ band. Radio Sci., 7, 45.

Evans, W. F. J., H. C. Wood, and E. J. Llewellyn, 1970: Ground-based photometric observations of the 1.27μ band in the evening twilight. Planetary Space Sci., 18, 1065.

Hays, P. B. and R. G. Roble, 1968a: Stellar spectra and atmospheric composition. J. Atmos. Sci., 25, 1141.

Hays, P. B. and R. G. Roble, 1968b: Atmospheric properties from the inversion of planetary occultation data. Planetary Space Sci., 16, 1197.

Hays, P. B. and R. G. Roble, 1972a: Stellar occultation measurements of molecular oxygen in the lower thermosphere. Planetary Space Sci., in press.

Hays, P. B. and R. G. Roble, 1972b: Observation of mesospheric ozone at low latitudes. Planetary Space Sci., in press.

Hays, P. B., R. G. Roble, and A. N. Shah, 1972: Terrestrial atmospheric composition from stellar occultations. Science, 176, 793.

Hesstvedt, E., 1968: On the effect of vertical eddy transport on atmospheric composition in the mesosphere and lower thermosphere. Geophys. Norv., 27, 1.

Hilsenrath, E., 1971: Ozone measurements in the mesosphere and stratosphere during two significant geophysical events. J. Atmos. Sci., 28, 295.

Hunt, B. G., 1966: Photochemistry of ozone in a moist atmosphere. J. Geophys. Res., 71, 1385.

Hunt, B. G., 1971: A diffusion photochemical study of the mesosphere and lower thermosphere and the associated conservation mechanism. J. Atmos. Terr. Phys., 33, 1869.

Leovy, C. B., 1969: Atmospheric ozone: An analytic model for photochemistry in the presence of water vapor. J. Geophys. Res., 74, 417.

Miller, D. E. and K. H. Stewart, 1965: Observations of atmospheric ozone from an artificial earth satellite. Proc. Roy. Soc. London, A288, 540.

Park, J., 1972: Ozone photochemistry and energy budget in the middle atmosphere. Ph. D. thesis, University of Colorado, Boulder, Colorado.

Rawcliffe, R. D., G. E. Meloy, R. M. Friedman, and E. H. Rogers, 1963: Measurement of vertical distribution of ozone from a polar orbiting satellite. J. Geophys. Res., 68, 6425.

Reed, E. I., 1968: A night measurement of mesospheric ozone by observations of ultraviolet airglow. J. Geophys. Res., 73, 2951.

Roble, R. G. and P. B. Hays, 1972: A technique for recovering the vertical number density profile of atmospheric gases from planetary occultation data. Planetary Space Sci., in press.

Roble, R. G. and R. B. Norton, 1972: Thermospheric molecular oxygen from solar EUV occultation measurements. J. Geophys. Res., 77, 3524.

Shimazaki, T. and A. R. Laird, 1972: Seasonal effects on distributions of minor neutral constituents in the mesosphere and lower thermosphere. Radio Sci., 7, 23.

Tisone, G. C., 1972: Measurements of the absorption of solar radiation by O_2 and O_3 in the 2150-A region. J. Geophys. Res., 77, 2971.

Weeks, L. H. and L. G. Smith, 1968: A rocket measurement of ozone near sunrise. Planetary Space Sci., 16, 1189.

FIGURE LEGENDS

Fig. 1. Absorption cross-sections for molecular oxygen and ozone. The dashed curves give the transmission functions for the filters used with the OAO-2 stellar photometers. Filter (4-1) is used to obtain the molecular oxygen number density in the lower thermosphere and Filters (2-5), (3-2) and (1-4) are used to determine the ozone number density in the mesosphere.

Fig. 2. Solid curve is the stellar intensity as a function of wavelength measured by the OAO-2 spectrometer prior to occultation on orbit 12178. This star was used to obtain the occultation data shown in Fig. 3. The dashed curve is the solar spectrum obtained from Ackerman (1970).

Fig. 3. a) The dots give the normalized intensity as a function of tangent ray height measured by the OAO-2 stellar photometers using the 2460 Å filter. The geographic position of the occultation tangent point is 35°N, 114°W and time is 22:33 LMT on April 3, 1971. The solid and dashed curves are the calculated normalized intensities for a stellar and solar occultation respectively using the model ozone profile in Fig. 3b. b) The dots give the retrieved ozone number density profile from the OAO-2 occultation data shown in Fig. 3a. The solid curve is the model ozone number density profile used to calculate the stellar and solar intensity profiles in Fig. 3a.

Fig. 4. The calculated normalized intensity distribution across the solar disk at a tangent ray height of 83 km. The satellite altitude at occultation is 715 km. The OAO-2 filter transmission function for the 2460 Å filter is used in the calculations. The tangent ray heights for the upper and lower solar limbs are also given in the figure.

Fig. 5. Comparison of the OAO-2 ozone data envelope with the nighttime ozone number density profiles determined by various observers.

Fig. 6. Comparison of the OAO-2 ozone data envelope with the ozone number density profile determined from various theoretical models.

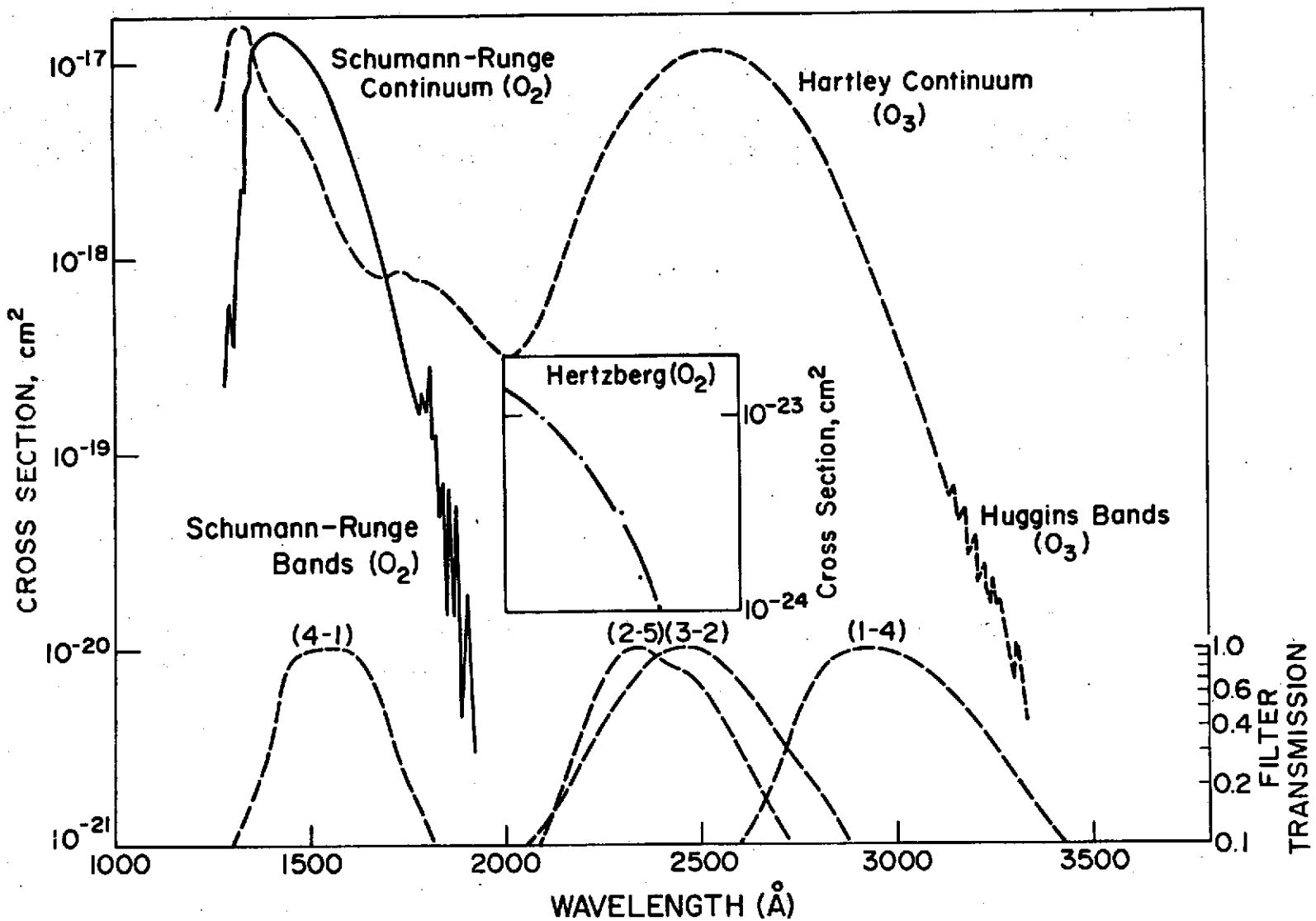
Schumann-Runge
Continuum (O_2)
Hartley Continuum
(O_3)
Hertzberg(O_2)
Schumann-Runge
Bands (O_2)
Huggins Bands
(O_3)
(4-1)
(2-5)(3-2)
(1-4)
CROSS SECTION, cm^2
Cross Section, cm^2
FILTER TRANSMISSION
WAVELENGTH (Å)
10^{-17}
10^{-18}
10^{-19}
10^{-20}
10^{-21}
10^{-23}
10^{-24}
1000
1500
2000
2500
3000
3500
1.0
0.6
0.4
0.2
0.1

Figure 1.

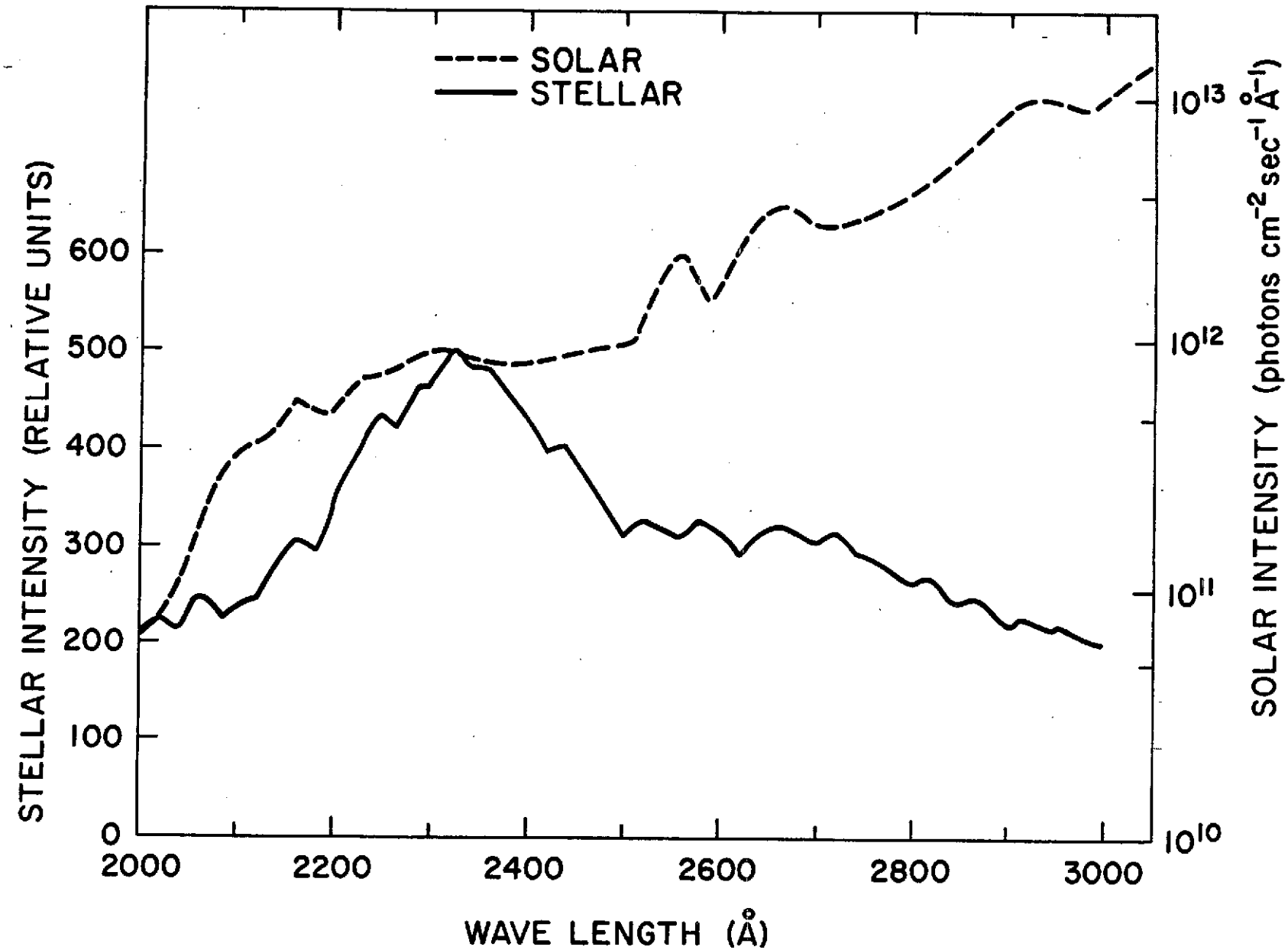
SOLAR
STELLAR
STELLAR INTENSITY (RELATIVE UNITS)
SOLAR INTENSITY (photons cm^{-2} sec^{-1} Å^{-1})
WAVE LENGTH (Å)
0
100
200
300
400
500
600
2000
2200
2400
2600
2800
3000
10^{10}
10^{11}
10^{12}
10^{13}

Figure 2.

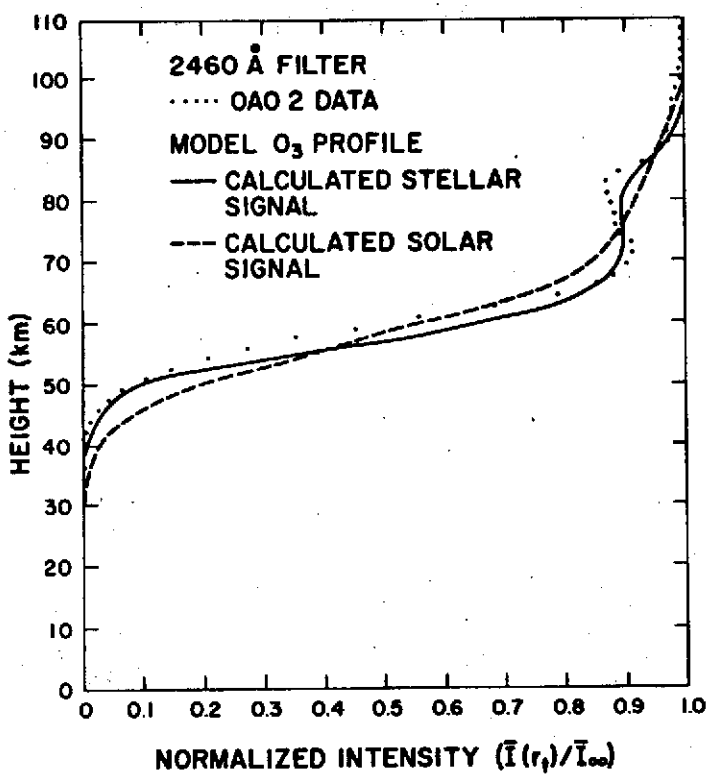

Figure 3a.

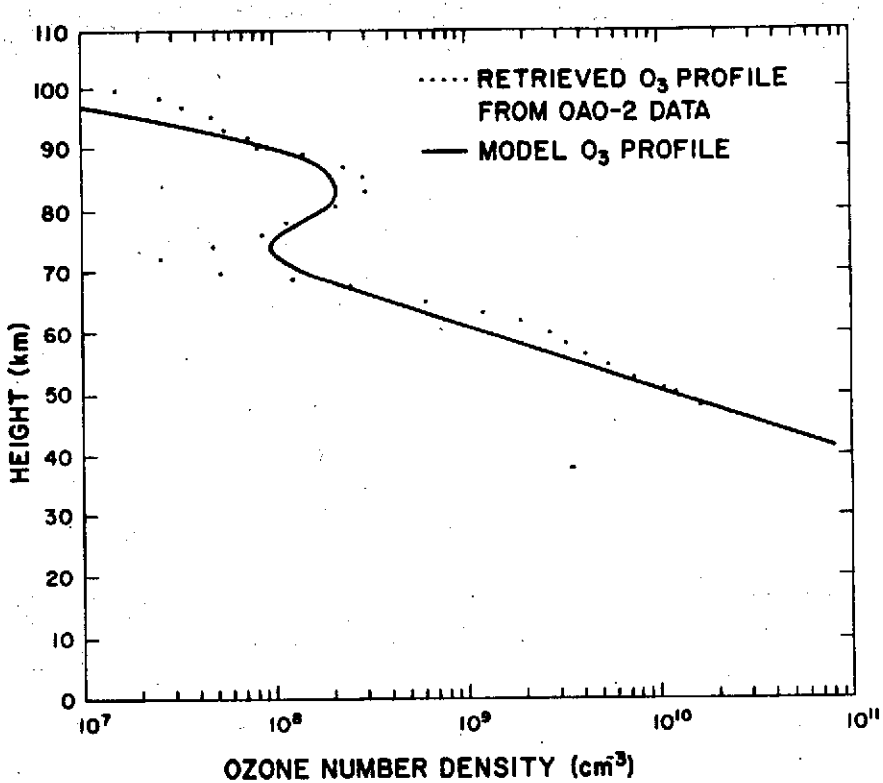

Figure 3b.

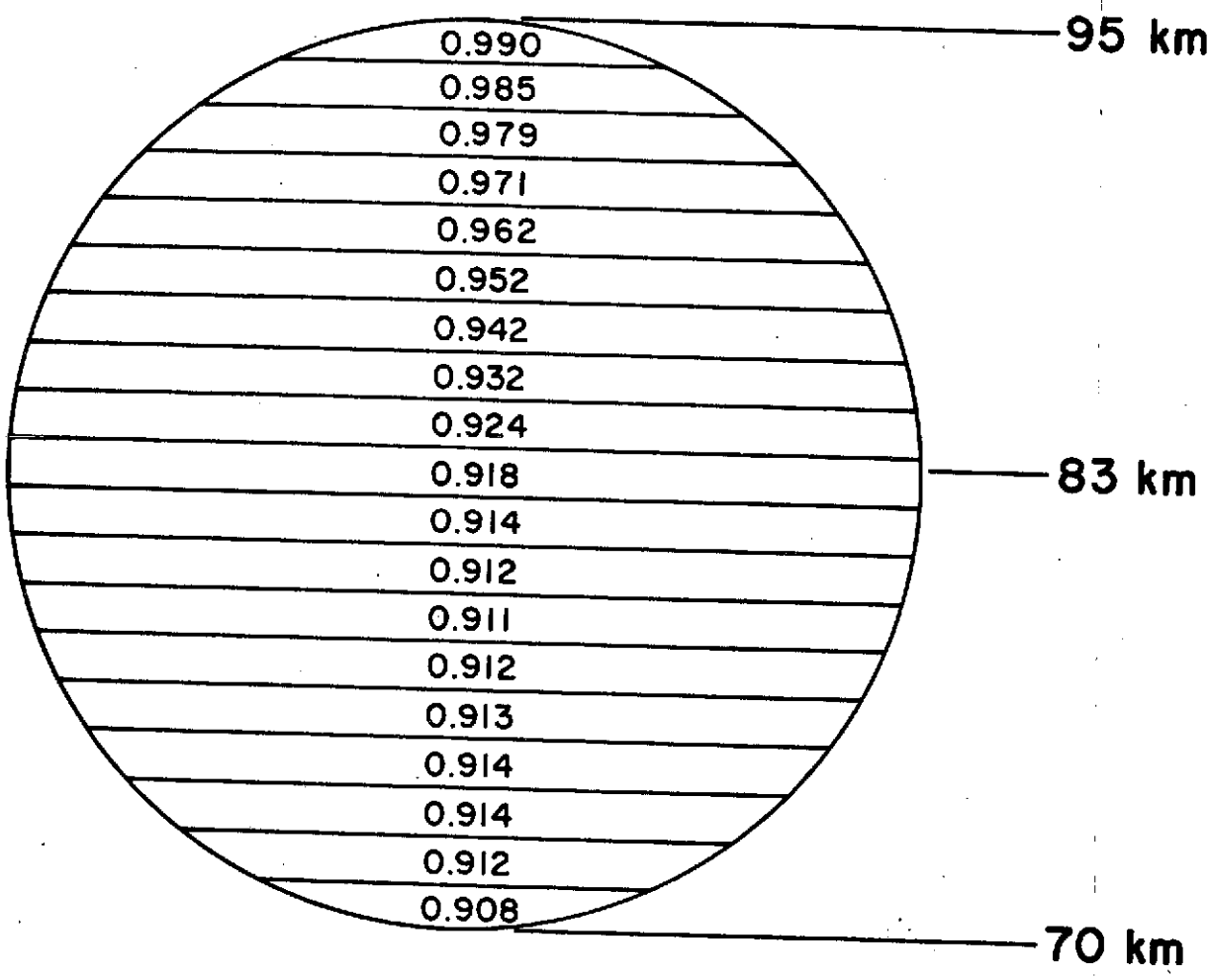
95 km
0.990
0.985
0.979
0.971
0.962
0.952
0.942
0.932
0.924
0.918
83 km
0.914
0.912
0.911
0.912
0.913
0.914
0.914
0.912
0.908
70 km

Figure 4.

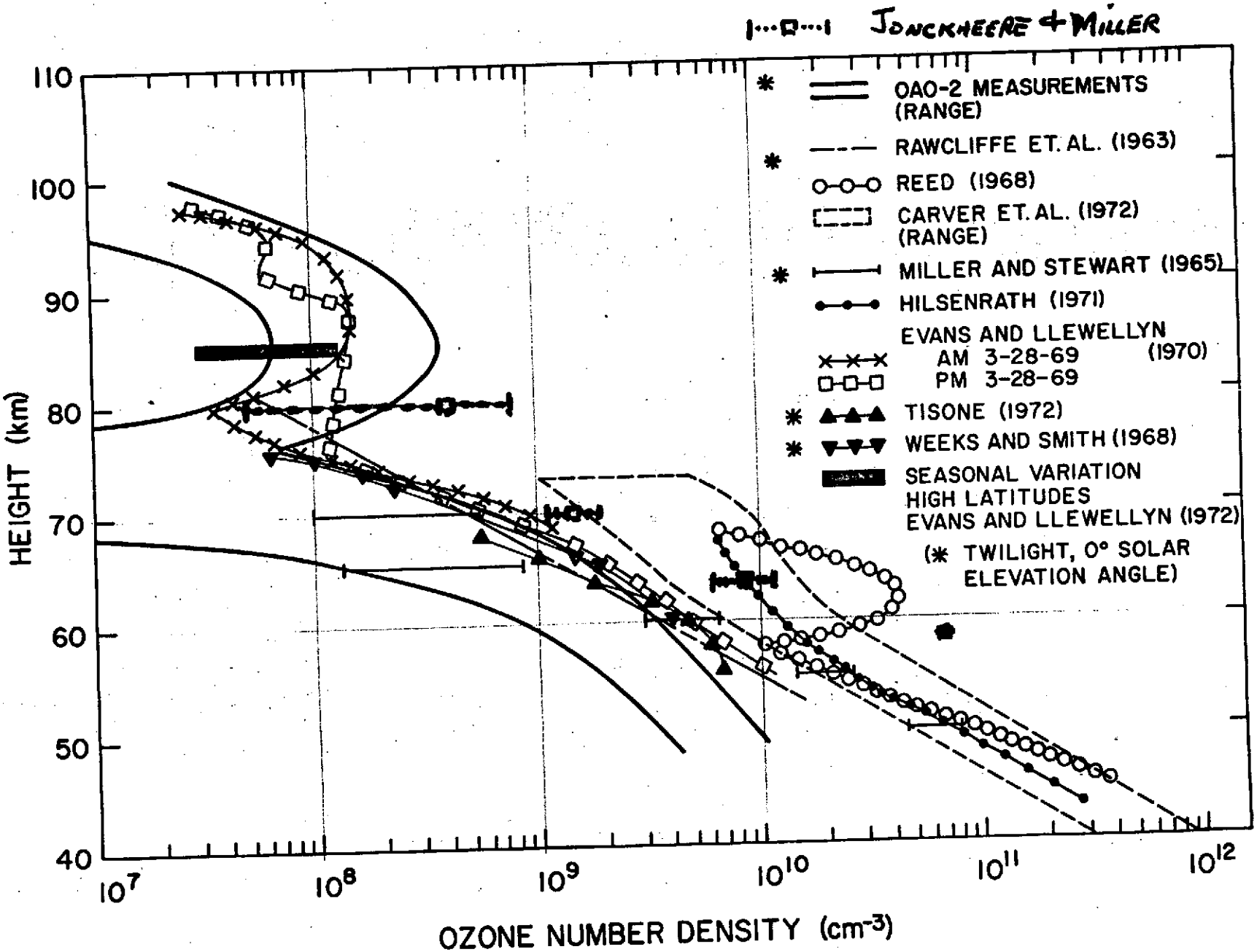
|···□···| JONCKHEERE + MILLER
110
100
90
80
70
60
50
40
HEIGHT (km)
10^7
10^8
10^9
10^{10}
10^{11}
10^{12}
OZONE NUMBER DENSITY (cm^{-3})
OAO-2 MEASUREMENTS (RANGE)
RAWCLIFFE ET. AL. (1963)
REED (1968)
CARVER ET. AL. (1972) (RANGE)
MILLER AND STEWART (1965)
HILSENRATH (1971)
EVANS AND LLEWELLYN (1970)
AM 3-28-69
PM 3-28-69
TISONE (1972)
WEEKS AND SMITH (1968)
SEASONAL VARIATION HIGH LATITUDES EVANS AND LLEWELLYN (1972)
(* TWILIGHT, 0° SOLAR ELEVATION ANGLE)

Figure 5.

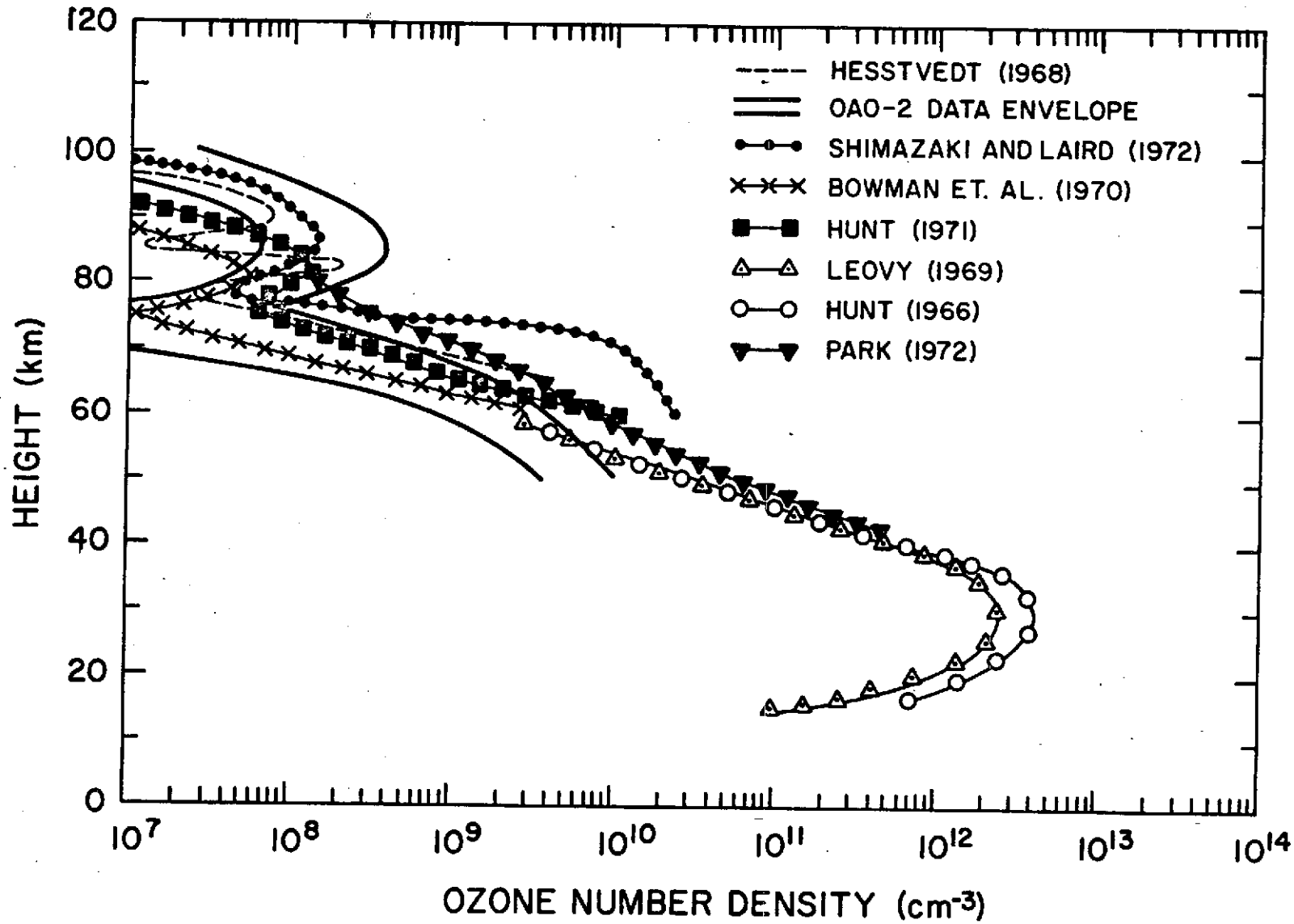
HESSTVEDT (1968)
OAO-2 DATA ENVELOPE
SHIMAZAKI AND LAIRD (1972)
BOWMAN ET. AL. (1970)
HUNT (1971)
LEOVY (1969)
HUNT (1966)
PARK (1972)
HEIGHT (km)
120
100
80
60
40
20
0
10^7
10^8
10^9
10^{10}
10^{11}
10^{12}
10^{13}
10^{14}
OZONE NUMBER DENSITY (cm^{-3})

Figure 6.